Impact of ion and neutron irradiation on the corrosion of the 6061-T6 aluminium alloy

Sarah L'haridon-Quaireau, Kimberly Colas, Bénédicte Kapusta, Bénédicte Verhaeghe, Marie Loyer-Prost, Gaëlle Gutierrez, Dominique Gosset, Sylvie Delpech

Journal of Nuclear Materials

Impact of ion and neutron irradiation on the corrosion of the 6061-T6 aluminium alloy

--Manuscript Draft--

Manuscript Number:	JNUMA-D-20-00259R1
Article Type:	Full Length Article
Section/Category:	Nuclear fuels and materials
Keywords:	Aluminium hydroxide; corrosion; microstructure; Ion irradiation; Neutron irradiation
Corresponding Author:	Sarah L'Haridon-Quaireau, Dr. Centre CEA de Saclay (Essonne): Commissariat a l'Energie Atomique et aux Energies Alternatives Centre de Saclay FRANCE
First Author:	Sarah L'Haridon-Quaireau, Dr.
Order of Authors:	Sarah L'Haridon-Quaireau, Dr.
	Kimberly Colas, Dr.
	Bénédicte Kapusta, Dr.
	Bénédicte Verhaeghe, Dr.
	Marie Loyer-Prost, Dr.
	Gaelle Gutierrez, Dr.
	Dominique Gosset, Dr.
	Sylvie Delpech, Dr.
Abstract:	In nuclear research reactors, aluminium alloys are corroded and aluminium hydroxide film covers their surface. Defects created by neutron can have a detrimental effect on this corrosion. In this study, two ion irradiations are performed on 6061-T6 aluminium alloy. The first irradiation experiment aims at studying the effect of metal matrix irradiation on aluminium corrosion. The second irradiation experiment aims at studying the effect of hydroxide irradiation on aluminium corrosion. The displacement per atom is at most 2.5 dpa in the hydroxide film irradiated with Al ions of 1.2 and 5 MeV and at most 8 dpa in the aluminium matrix irradiated with Al ions of 1.8 MeV (calculated with SRIM). The effects of ion irradiation are investigated by TEM and SEM observations. The crystalline structure of aluminium hydroxide is studied by electron diffraction, μ-Raman and X-rays diffraction. In the aluminium hydroxide film (composed of a mix of bayerite, α-Al(OH) 3 , and boehmite, γ-AlOOH, before irradiation), ion irradiation causes formation of voids and dehydrates aluminium hydroxide (nanocrystallites of η-Al 2 O 3 are observed in the irradiated film). In the aluminium matrix, irradiation increases density of dislocations and amorphizes dispersoids. After ion irradiation, samples are corroded at 70°C in 2.8L of demineralised water. The two irradiations increase aluminium corrosion. The second part of this study is about samples corroded in the Osiris nuclear research reactor, in water at 42°C, with a pH of 6 and for 18 months. The aluminium hydroxide film observed on these samples has a layered microstructure composed of a compact inner layer, a thick intermediate layer and an outer layer of cuboid microcrystals. Silicon enrichment is observed in the inner layer. The effect of ion and neutron irradiation on aluminium corrosion is compared in this study and similarities are observed between ion and neutron irradiations.
Suggested Reviewers:	Adrien Couet, Dr University of Wisconsin-Madison couet@wisc.edu Aluminium alloy specialist
	Karl Buchanan, Dr. Framatome Inc karl.g.buchanan@gmail.com irradiation specialist

	Nathalie Moncoffre, Dr. University of Lyon: Universite de Lyon n.moncoffre@ipnl.in2p3.fr corrosion specialist
Response to Reviewers:	We would like to thank the editor and the reviewers for their time and the quality of their comment. We have tried to answer as precisely as possible the reviewer's questions and improve the paper as suggested: Reviewer #1: This study focuses on the effect of irradiation on corrosion of aluminum alloys used in test reactors. This is an important research topic since the effect of irradiation on corrosion is still not well understood for structural materials. To investigate this ion irradiation of the Al matrix followed by corrosion is performed. Irradiation of the Al oxide in a pre-oxidized material followed by subsequent oxidation is also performed. Finally data on ion irradiated materials is compared to neutron irradiated specimen. The paper is relatively well written, although some typos are present and an English speaker should review the paper prior the re-submission. The conclusions are relatively well supported by the data and the reviewer would recommend publication of this study. However, there are a few points, highlighted below, that need revisions before the paper can be recommended for publication. 1. Large voids are observed in the oxide after ion irradiation. This is atypical in room temperature irradiation. The reviewer is concerned that the temperature in the oxide during irradiation maybe actually high than reported. The oxide acts as an insulator and the heat deposited by heavy-ion electronic stopping would not be easily transferred to the metal and cooling stage. This is reinforced by the fact that no voids are observed in the Al matrix, in similar conditions, which is expected. The authors need to discuss this in more details in a revised version of the manuscript. Response: The temperature is monitored at 20°C, and maximal variations of 2°C are observed when switching off the beam: the temperature in the oxide is hence close to 20°C. Voids are observed only at high dpa in metals, but are commonly observed at low dpa in oxides, even at room temperature. The reference [43] was added in which authors observe voids in zirconia after ion irradiation at 1 and 10 dpa at room temperature: the irradiation was done on FIB samples taken in corroded ZrNb. A few lines were added in the manuscript page 8 in the § 3.1 to explain this point. 2. It is written that ion irradiation dehydrates the oxide layer, but no mechanisms/evidence are proposed to support this argument. Considering the above issue of temperature control, would it be possible that a higher temperature of the oxide under ion irradiation is responsible for the dehydration of the oxide? Response: Irradiations of ceramic samples (insulators) with an energy deposit of 0,5 W/cm2 without sample cooling lead to temperatures under 80°C (from the Jannus feedback). In our case, the samples are cooled by a nitrogen circulation at the back of the sample holder, and the temperature of the alloy is monitored at 20°C by a thermocouple fixed on a sample. Moreover, the hydroxide film is only 4 µm thick on a 1 mm thick alloy sample : even with a low thermal conductivity of the hydroxide film, the temperature in the oxide film is very close to room temperature : this is confirmed by the maximal variations of 2°C indicated by the thermocouple when switching off the beam. Hence, the dehydration of the oxide cannot result from a local temperature increase. In addition, the reference [43] was added, showing that ion irradiations on zirconia formed on corroded ZrNb alloys (FIB samples) can lead to phase transformations of the oxide at room temperature. A few lines were added in the manuscript pages 9 and 10 in the §3.1 (Ion irradiation of aluminium hydroxide) to discuss this point. 3. While both ion and neutron irradiation result in an increase in corrosion rate, it is unclear if the mechanisms are the same. To the reviewer's opinion the mechanisms are clearly different. The authors should acknowledge that the ion irradiation did not provide insight on the increase in corrosion rate observed under neutron irradiation. The oxide layers of ion (followed by corrosion) and neutron irradiated oxides show a relatively similar structure, but that structure is actually similar to non-irradiated oxides… There is no evidence that the neutron irradiation induced increase in corrosion rate follow the same underlying mechanism than the ion irradiation induced increase in corrosion rate. Since the ion irradiation creates large voids and dehydration

in the oxide, which are not observed under neutron irradiation, the tow mechanisms should be clearly labelled as different.

Response: The authors agree with the reviewer that the mechanisms proposed in the paper apply to ion-irradiation and not directly to neutron- or in-core- irradiation. In order to make this point clearer, a sentence was added in section 4.2 as well as in the conclusion of the paper.

Reviewer #2:
The presented study compared the impact of ion and neutron irradiation on the corrosion of 6061-T6 alloy through microstructure characterization, and proposed a growth mechanism of aluminium hydroxide during corrosion tests coupled to ion irradiation. The study is comprehensive, and worthy to be published. However, more microstructure characterizations are suggested to make the study completed.

1. The authors stated "The objective of this paper is to compare neutron and ion irradiation effects on aluminium samples" on Page 2, and had a discussion section on page 16. However, the study presented SEM and TEM characterizations of ion-irradiated samples, but only SEM/EPMA on neutron irradiated samples. TEM characterization on neutron irradiated samples should be presented, so that the comparison will be completed and more sound.
Response: As suggested by the reviewer, TEM studies of neutron irradiated samples would indeed have been a valuable addition to the paper. However, preparation of such radioactive samples is a very costly and complex process that was not performed at the time of the study presented here. This is however a study that is envisioned for the future. As such, a sentence was added in the conclusion to address this point.

2. Page 6, "Scattering Electron Microscopy (SEM)" should be "Scanning Electron Microscopy (SEM)".
As suggested, correction was done.

3. Page 6, "length camera" should be "camera length".
As suggested, correction was done.

4. Pages 11-12, section 3.2, Fig. 7. The authors stated in Fig. 7b, region 2, "it is difficult to discern one grain from another and the grain size cannot be measured". However, Fig. 7b gives information on the contrary, i.e., grain boundaries are clearly seen and grain size can be measured. In fact, there are no much different on grain boundary and grain size between regions 1 and 2, except some grains in region 2 show stronger diffraction contrast which typically related to grain orientations.
Response: The grains are not necessarily easy to measure in our sample due to the presence of many dislocations, in particular for the irradiated sample. By observation of the figures presented in the paper, it can indeed be seen that the grain size for the unirradiated sample and area 1 of the irradiated sample are similar. Due to the high number of dislocations in area 2 of the irradiated sample, it seems difficult to identify properly grains and in particular define an average grain size.

a. How did the authors define the boundary between regions 1 and 2?
Response: The boundary was placed using SRIM calculation as the peak of implantation of the irradiating ions. A sentence was added in section 3.2 and in the key for Fig. 7 to make this point clearer.

b. The authors stated "voids are not observed in the irradiated matrix". However, did the authors characterized the sample using through focus (large defocus in both under and over focus ranges) technique to verify whether nanosized voids in the irradiated region?
Response: The technique used to verify the presence of nanosized voids is:
1.When the sample is observed to a high magnitude, the focus is done on default (grains boundary, nanometric precipitate …) present in the aluminium matrix.
2.Then, defocus is done in both under and over focus ranges, outline of voids become clear with defocus.
This technique is the one described by the reviewers and was indeed applied in this study.
In addition, this technique is also used in the irradiated aluminium hydroxide in order to

	characterize the samples and as reported in the manuscript, nanosized voids were observed in hydroxide, contrary to what was observed in the irradiated aluminium matrix. Addition details are added in the article. c. Lower magnification images of both Figs. 7 a and b would be better to show the microstructure difference between the two samples, as well as different regions in Fig. 7b. As suggested by the reviewer, lower magnification image of the irradiated aluminium matrix is presented in Fig. 7. 5. Page 12. The authors verified the dispersoid is crystalline and amorphous in unirradiated and irradiated regions, respectively, by tilting the sample in TEM. This is correct in most cases, however, convergence beam electron diffraction (CBED) is recommended, which provides direct, more accurate evidence, and also easier to do. Precipitates have the same size than grains of the aluminium matrix. As a result, electron diffraction pattern show a constellation of spots were circles could be seen with great difficulties. This fact also come from that the litter diaphragm of the used TEM does not allow to select only the precipitates, a lot of grain of the aluminium matrix are taken in the electron diffraction pattern. As a result, the authors choose the technique described in [35].

Cover Letter

DE LA RECHERCHE À L'INDUSTRIE

www.cea.fr

Sarah L'Haridon-Quaireau
Corresponding author
sarah.quaireau@laposte.net

Saclay, France, 02/09/2020

Dear Editors,

I am pleased to submit an original research article entitled "***Impact of ion and neutron irradiation on the corrosion of the 6061-T6 aluminium alloy***" for consideration for publication in **Journal of Nuclear Materials**. The authors of this paper are Dr. Sarah L'haridon-Quaireau, Dr. Kimberly Colas, Dr. Bénédicte Kapusta, Dr. Bénédicte Verhaeghe, Dr. Marie Loyer-Prost, Dr. Gaelle Gutierrez and Dr. Dominique Gosset from the Commissariat à l'Energie Atomique and Professor Sylvie Delpech from IJCLab.

This manuscript describes a study about the effect of ion and neutron irradiation on the aqueous corrosion of an aluminium alloy used in nuclear research reactors and the characterisation of the aluminium hydroxide. The highlights of this study are:

- Ion irradiation dehydrates aluminium hydroxide (boehmite and bayerite).
- Ion irradiation induces microstructure changes and voids in aluminium hydroxide.
- Neutron and ion irradiations increase aluminium alloy corrosion.
- Neutron irradiation causes silicon enrichment of aluminium hydroxide.

We believe that this manuscript is appropriate for publication by Journal of Nuclear Materials because the results presented in our manuscript allow to better understand the impact of neutron irradiation on the hydroxide growth at the surface of aluminium alloy.

This manuscript has not been published and is not under consideration for publication elsewhere. We have no conflicts of interest to disclose.

Thank you for your consideration.

Sarah L'Haridon-Quaireau

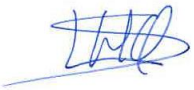

afaq ISO 9001 ISO 14001 Qualité Environnement AFNOR CERTIFICATION

Commissariat à l'énergie atomique et aux énergies alternatives
Centre de Saclay – Bât 625P - pc 123 | 91191 Gif-sur-Yvette Cedex
T. +33 (0)1 69 08 46 24 | F. +33 (0)1 69 08 90 73
mail :catherine.allenou@cea.fr
Etablissement public à caractère industriel et commercial | RCS Paris B 775 685 019

Direction de l'Energie Nucléaire
Direction déléguée aux Activités Nucléaires de Saclay
Département des Matériaux pour le Nucléaire
Service d'Etudes des Matériaux Irradiés
LABORATOIRE DE MICROSCOPIE ET D'ETUDES DE L'ENDOMMAGEMENT

HIGHLIGHTS:

- Ion irradiation dehydrates aluminium hydroxide (boehmite and bayerite).
- Ion irradiation induces microstructure changes and voids in aluminium hydroxide.
- Neutron and ion irradiations increase aluminium alloy corrosion.
- Neutron irradiation causes silicon enrichment of aluminium hydroxide.

Reponses to reviewers:

We would like to thank the editor and the reviewers for their time and the quality of their comment. We have tried to answer as precisely as possible the reviewer's questions and improve the paper as suggested:

Reviewer #1:

This study focuses on the effect of irradiation on corrosion of aluminum alloys used in test reactors. This is an important research topic since the effect of irradiation on corrosion is still not well understood for structural materials. To investigate this ion irradiation of the Al matrix followed by corrosion is performed. Irradiation of the Al oxide in a pre-oxidized material followed by subsequent oxidation is also performed. Finally data on ion irradiated materials is compared to neutron irradiated specimen. The paper is relatively well written, although some typos are present and an English speaker should review the paper prior the re-submission. The conclusions are relatively well supported by the data and the reviewer would recommend publication of this study. However, there are a few points, highlighted below, that need revisions before the paper can be recommended for publication.

1. Large voids are observed in the oxide after ion irradiation. This is atypical in room temperature irradiation. The reviewer is concerned that the temperature in the oxide during irradiation maybe actually high than reported. The oxide acts as an insulator and the heat deposited by heavy-ion electronic stopping would not be easily transferred to the metal and cooling stage. This is reinforced by the fact that no voids are observed in the Al matrix, in similar conditions, which is expected. The authors need to discuss this in more details in a revised version of the manuscript.

Response: The temperature is monitored at 20°C, and maximal variations of 2°C are observed when switching off the beam: the temperature in the oxide is hence close to 20°C. Voids are observed only at high dpa in metals, but are commonly observed at low dpa in oxides, even at room temperature. The reference [43] was added in which authors observe voids in zirconia after ion irradiation at 1 and 10 dpa at room temperature: the irradiation was done on FIB samples taken in corroded ZrNb. A few lines were added in the manuscript page 8 in the § 3.1 to explain this point.

2. It is written that ion irradiation dehydrates the oxide layer, but no mechanisms/evidence are proposed to support this argument. Considering the above issue of temperature control, would it be possible that a higher temperature of the oxide under ion irradiation is responsible for the dehydration of the oxide?

Response: Irradiations of ceramic samples (insulators) with an energy deposit of 0,5 W/cm2 without sample cooling lead to temperatures under 80°C (from the Jannus feedback). In our case, the samples are cooled by a nitrogen circulation at the back of the sample holder, and the temperature of the alloy is monitored at 20°C by a thermocouple fixed on a sample. Moreover, the hydroxide film is only 4 µm thick on a 1 mm thick alloy sample : even with a low thermal conductivity of the hydroxide film, the temperature in the oxide film is very close to room temperature : this is confirmed by the maximal variations of 2°C indicated by the thermocouple when switching off the beam. Hence, the dehydration of the oxide cannot result from a local temperature increase. In addition, the reference [43] was added, showing that ion irradiations on zirconia formed on corroded ZrNb alloys (FIB samples) can lead to phase transformations of the oxide at room temperature. A few lines were added in the manuscript pages 9 and 10 in the §3.1 (Ion irradiation of aluminium hydroxide) to discuss this point.

3. While both ion and neutron irradiation result in an increase in corrosion rate, it is unclear if the mechanisms are the same. To the reviewer's opinion the mechanisms are clearly different. The authors should acknowledge that the ion irradiation did not provide insight on the increase in corrosion rate observed under neutron irradiation. The oxide layers of ion (followed by corrosion) and neutron irradiated oxides show a relatively similar structure, but that structure is actually similar to non-irradiated oxides… There is no evidence that the neutron irradiation induced increase in corrosion rate follow the same underlying mechanism than the ion irradiation induced increase in corrosion rate. Since the ion irradiation creates large voids and dehydration in the oxide, which are not observed under neutron irradiation, the tow mechanisms should be clearly labelled as different.

Response: The authors agree with the reviewer that the mechanisms proposed in the paper apply to ion-irradiation and not directly to neutron- or in-core- irradiation. In order to make this point clearer, a sentence was added in section 4.2 as well as in the conclusion of the paper.

Reviewer #2:

The presented study compared the impact of ion and neutron irradiation on the corrosion of 6061-T6 alloy through microstructure characterization, and proposed a growth mechanism of aluminium hydroxide during corrosion tests coupled to ion irradiation. The study is comprehensive, and worthy to be published. However, more microstructure characterizations are suggested to make the study completed.

1. The authors stated "The objective of this paper is to compare neutron and ion irradiation effects on aluminium samples" on Page 2, and had a discussion section on page 16. However, the study presented SEM and TEM characterizations of ion-irradiated samples, but only SEM/EPMA on neutron irradiated samples. TEM characterization on neutron irradiated samples should be presented, so that the comparison will be completed and more sound.

Response: As suggested by the reviewer, TEM studies of neutron irradiated samples would indeed have been a valuable addition to the paper. However, preparation of such radioactive samples is a very costly and complex process that was not performed at the time of the study presented here. This is however a study that is envisioned for the future. As such, a sentence was added in the conclusion to address this point.

2. Page 6, "Scattering Electron Microscopy (SEM)" should be "Scanning Electron Microscopy (SEM)".

As suggested, correction was done.

3. Page 6, "length camera" should be "camera length".

As suggested, correction was done.

4. Pages 11-12, section 3.2, Fig. 7. The authors stated in Fig. 7b, region 2, "it is difficult to discern one grain from another and the grain size cannot be measured". However, Fig. 7b gives information on the contrary, i.e., grain boundaries are clearly seen and grain size can be measured. In fact, there are no

much different on grain boundary and grain size between regions 1 and 2, except some grains in region 2 show stronger diffraction contrast which typically related to grain orientations.

Response: The grains are not necessarily easy to measure in our sample due to the presence of many dislocations, in particular for the irradiated sample. By observation of the figures presented in the paper, it can indeed be seen that the grain size for the unirradiated sample and area 1 of the irradiated sample are similar. Due to the high number of dislocations in area 2 of the irradiated sample, it seems difficult to identify properly grains and in particular define an average grain size.

a. How did the authors define the boundary between regions 1 and 2?

Response: The boundary was placed using SRIM calculation as the peak of implantation of the irradiating ions. A sentence was added in section 3.2 and in the key for Fig. 7 to make this point clearer.

b. The authors stated "voids are not observed in the irradiated matrix". However, did the authors characterized the sample using through focus (large defocus in both under and over focus ranges) technique to verify whether nanosized voids in the irradiated region?

Response: The technique used to verify the presence of nanosized voids is:

1. When the sample is observed to a high magnitude, the focus is done on default (grains boundary, nanometric precipitate …) present in the aluminium matrix.
2. Then, defocus is done in both under and over focus ranges, outline of voids become clear with defocus.

This technique is the one described by the reviewers and was indeed applied in this study.

In addition, this technique is also used in the irradiated aluminium hydroxide in order to characterize the samples and as reported in the manuscript, nanosized voids were observed in hydroxide, contrary to what was observed in the irradiated aluminium matrix. Addition details are added in the article.

c. Lower magnification images of both Figs. 7 a and b would be better to show the microstructure difference between the two samples, as well as different regions in Fig. 7b.

As suggested by the reviewer, lower magnification image of the irradiated aluminium matrix is presented in Fig. 7.

5. Page 12. The authors verified the dispersoid is crystalline and amorphous in unirradiated and irradiated regions, respectively, by tilting the sample in TEM. This is correct in most cases, however, convergence beam electron diffraction (CBED) is recommended, which provides direct, more accurate evidence, and also easier to do.

Precipitates have the same size than grains of the aluminium matrix. As a result, electron diffraction pattern show a constellation of spots were circles could be seen with great difficulties. This fact also come from that the litter diaphragm of the used TEM does not allow to select only the precipitates, a lot of grain of the aluminium matrix are taken in the electron diffraction pattern. As a result, the authors choose the technique described in [35].

Impact of ion and neutron irradiation on the corrosion of the 6061-T6 aluminium alloy

Sarah L'HARIDON-QUAIREAU, Kimberly COLAS, Bénédicte KAPUSTA, Bénédicte VERHAEGHE
DES-Service d'Etude des Matériaux Irradiés, CEA, Université Paris-Saclay
F-91191, Gif-sur-Yvette – France

Marie LOYER-PROST, Gaëlle GUTIERREZ
DES-Service de Recherche de Métallurgies Physiques, CEA, Université Paris-Saclay
F-91191, Gif-sur-Yvette - France

Dominique GOSSET
DES-Service de Recherche de Métallurgies Appliquées, CEA, Université Paris-Saclay
F-91191, Gif-sur-Yvette – France

Sylvie DELPECH
IJCLab, Paris-Saclay University
Paris – France

Corresponding author: S. L'HARIDON-QUAIREAU, sarah.quaireau@laposte.net

HIGHLIGHTS:

- Ion irradiation dehydrates aluminium hydroxide (boehmite and bayerite).
- Ion irradiation induces microstructure changes and voids in aluminium hydroxide.
- Neutron and ion irradiations increase aluminium alloy corrosion.
- Neutron irradiation causes silicon enrichment of aluminium hydroxide.

ABSTRACT: (300 MOTS MAX)
In nuclear research reactors, aluminium alloys are corroded and an aluminium hydroxide film covers their surface. Defects created by neutron irradiation can have a detrimental effect on this corrosion. In this study, two ion irradiations are performed on a 6061-T6 aluminium alloy. The first irradiation experiment aims at studying the effect

of metal matrix irradiation on aluminium corrosion. The second irradiation experiment aims at studying the effect of hydroxide irradiation on aluminium corrosion. The displacement per atom is at most 2.5 dpa in the hydroxide film irradiated with Al ions of 1.2 and 5 MeV and at most 8 dpa in the aluminium matrix irradiated with Al ions of 1.8 MeV (calculated with SRIM). The effects of ion irradiation are investigated by TEM and SEM observations. The crystalline structure of aluminium hydroxide is studied by electron diffraction, μ-Raman and X-rays diffraction. In the aluminium hydroxide film (composed of a mix of bayerite, α-$Al(OH)_3$, and boehmite, γ-AlOOH, before irradiation), ion irradiation causes formation of voids and dehydrates the aluminium hydroxide (nanocrystallites of η-Al_2O_3 are observed in the irradiated film). In the aluminium matrix, irradiation increases density of dislocations and amorphizes dispersoids. After ion irradiation, samples are corroded at 70°C in 2.8L of demineralised water. The two irradiations increase aluminium corrosion.
The second part of this study is about samples corroded in the Osiris nuclear research reactor, in water at 42°C, with a pH of 6 and for 18 months. The aluminium hydroxide film observed on these samples has a layered microstructure composed of a compact inner layer, a thick intermediate layer and an outer layer of cuboid microcrystals. Silicon enrichment is observed in the inner layer. The effect of ion and neutron irradiation on aluminium corrosion is compared in this study and similarities are observed between ion and neutron irradiations.

KEYWORDS:
Aluminium hydroxide; Corrosion; Microstructure; Ion irradiation; Neutron irradiation.

1. INTRODUCTION

Aluminium alloys are used in Materials Testing Reactors (MTRs, nuclear research reactors) because of low activation, good mechanical properties and good neutron transparency. In particular, the aluminium alloy AA-6061-T6 is used for core structures and for fuel cladding [1–3]. In the aqueous coolant of reactor, aluminium alloys are corroded and an aluminium hydroxide film covers their surface. The thermal conduction of this aluminium hydroxide is sufficiently low (~2 W/m/K [4]) to degrades the heat exchange between the core components and the coolant, it could lead to a local overheating of core components. As a result, the study of aluminium alloys corrosion is important for safe operation of MTRs. In this regard, aluminium alloy corrosion tests were performed in MTRs in the literature [3,5–12]. In these studies, the authors characterised the crystalline structure of the aluminium hydroxide by X-Ray Diffraction (XRD) and measured the thickness of the hydroxide film developed under neutron irradiation. The objective of this paper is to compare neutron and ion irradiation effects on aluminium samples.

The ion irradiation experiments are performed at the JANNuS platform (Joint Accelerators for Nanoscience and Nuclear Simulation), in CEA Paris-Saclay, in France. Contrary to tests performed in MTRs, ion irradiation allows to perform corrosion tests in various conditions, and thus to lead parametric studies, without dealing with the problems of radioactive samples (the matter is not activated by low energy ion irradiation). In addition, ion irradiation allows to obtain high irradiation doses in a very short time.

In this study, we perform corrosion tests coupled to ion irradiation in order to irradiate the aluminium hydroxide film and the aluminium matrix. After ion irradiation, the irradiated film and the irradiated aluminium matrix are characterized and observed by SEM and TEM. Their crystalline structure is studied using Selected Area Electron Diffraction (SAED) performed in a TEM, µ-Raman, and X-rays diffraction (XRD). The neutron irradiation is realized in the Osiris reactor in CEA Saclay, in France (French Atomic Energy Commission). The microstructure of the film is observed by SEM, its chemical composition is investigated using Electron Probe Micro-Analysis (EPMA) and its thickness is measured on a cross-section of the samples. These results are compared to the samples corroded in a corrosion loop with no irradiation in order to highlight the effect of neutron irradiation on aluminium corrosion. Finally, the samples after ion irradiation are compared to the neutron-irradiated samples in order to assess the relevance of using ion irradiation to study aluminium corrosion for nuclear reactor application.

2. EXPERIMENTAL METHODS AND SAMPLES

In order to compare ion and neutron irradiations, three studies are leaded in this paper. These studies are summarized in Fig. 1.

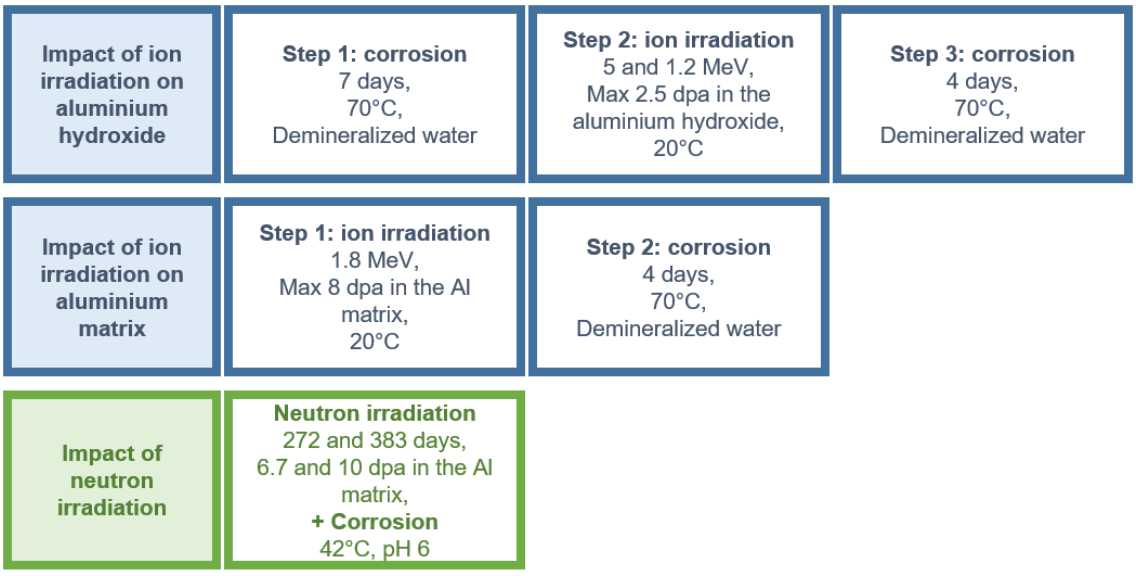

Figure 1: Purpose, step and conditions of irradiation of the three studies performed in this paper.

Samples and preparation:

The samples are in AA-6061-T6 aluminium alloy. The chemical composition of this alloy is presented in Table 1. The T6 treatment was obtained by solution annealing at 550°C for 4h

following by water quenching and tempering at 175°C for 4h. This thermal treatment is performed to improve the mechanical properties of the material [18]. The samples are coupon-shaped with dimensions of 10 mm x 10 mm x 1 mm. They have a non-finished surface: the samples are obtained by milling and they are not polished in order to have a representative surface such as the one Material Testing Reactors components would have [19].

Table 1: Chemical composition of the 6061-T6 aluminium alloy used.

Element	Mg	Si	Cu	Fe	Cr	Mn	Al
Content (wt.%)	1.15	0.61	0.25	0.2	0.2	0.03	Balance

Ion irradiation experiments:

The conditions of the ion irradiations are described in Table 2.

Table 2: Conditions of the ion irradiations.

Irradiation N°	Target	Al ions energy	Flux	Dose	Time	Temperature
		MeV	Ions/cm²/s	ions/cm²	Hours	°C
1	Aluminium hydroxide	5	$5.3\pm1.2*10^{11}$	$9.5\pm2.3*10^{15}$	5h	20
		1.2	$5.3\pm1.2*10^{11}$	$7.6\pm2.3*10^{15}$	4h	20
2	6061-T6 metal matrix	1.8	$6\pm1.5*10^{11}$	$7.6\pm1.9*10^{15}$	4h	20

The ion irradiation experiments are performed at the JANNuS platform (Joint Accelerators for Nanoscience and Nuclear Simulation), in CEA Paris-Saclay, in France. The first ion irradiation is performed on aluminium hydroxide. Prior to irradiation, aluminium alloy samples are corroded in autoclave at 70°C, for 7 days and in 2.8L of demineralised water (Fig. 1). The temperature of 70°C is chosen because this is relevant of core structures in MTRs. The thickness of the obtained hydroxide film is about 4 µm. After the corrosion test, ion irradiation is performed: the hydroxide film is irradiated with Al ions under vacuum. The energy of the Al ions used is 5 MeV and then 1.2 MeV in order to irradiate the hydroxide film on all its thickness. A SRIM calculation (using the Stopping and Range of Ions in Matter software [21] with the mode “full damage cascade”) indicates the damage is at most 2.5 dpa (displacement per atom) and 1.5 dpa on average in the aluminium hydroxide film (Fig. 2.a). For the SRIM calculation, the threshold displacement energies used are 20 eV and 50 eV for the aluminium and oxygen sublattice,

respectively [22]. After ion irradiation experiment, the irradiated samples are corroded a second time in autoclave in order to study the impact of ion irradiation on the corrosion kinetics. For this corrosion experiment, the conditions are: 4 days, 70°C and 2.8 L of demineralised water.
The second ion irradiation is performed on the metal aluminium matrix. Metal samples are irradiated with Al ions with an energy of 1.8 MeV. A SRIM calculation indicates the damage is at most 8 dpa in the aluminium matrix (Fig. 2.b, obtained with the mode “full damage cascade”). For the SRIM calculation, the aluminium threshold displacement energy used is 16 eV [23,24]. After the ion irradiation, the samples are corroded at 70°C, for 4 days and in 2.8L of demineralised water in order to evaluate the influence of the irradiation on aluminium alloy corrosion. During the two irradiations, the temperature is monitored using a thermocouple in contact with a sample, the maximum temperature is 20°C for the two irradiation experiments. For each irradiation, four samples are irradiated together on one face and for each corrosion condition, three samples are used.

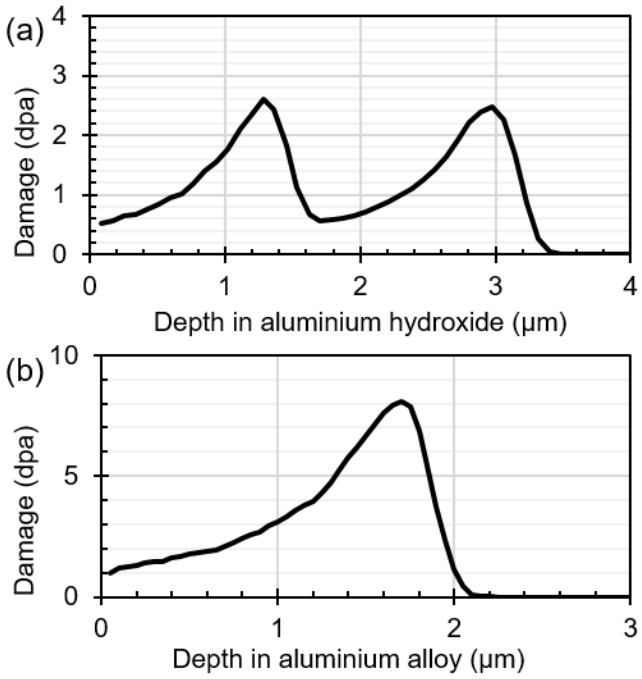

Figure 2: Damage profiles (dpa: displacement per atom) created by (a) Al ions with successive energies of 5 MeV and then 1.2 MeV irradiating the aluminium hydroxide film and by (b) Al ions with an energy of 1.8 MeV irradiating the aluminium matrix, profiles calculated by SRIM with the mode “full damage cascade” [21].

Autoclave:

Coupled to ion irradiations, corrosion tests are performed using an autoclave made of 316L steel. The inside of the autoclave is covered with polytetrafluoroethylene in order to avoid contamination of the samples surface by iron from the autoclave. The sample holder is in zirconium alloy in order to limit galvanic coupling between aluminium alloy samples and the

sample holder. Before performing the corrosion tests, helium is injected in the autoclave in order to deoxygenate the corrosive media. The pressure in the autoclave is imposed by the vapour pressure (i.e. the pressure is 0.5 bar relative at 70°C).

Characterization techniques:

The aluminium hydroxide is characterized using Scannring Electron Microscopy (SEM, measurements of the film thickness in particular), Transmission Electron Microscopy (TEM, observation of the microstructure and analyses of its crystal structure by electrons diffraction), X-rays Diffraction analyses (XRD) and µ-Raman spectroscopy. In order to observe a cross section of the aluminium hydroxide film using a SEM, samples are embedded in a conductive resin and polished down to a 1 µm finish with diamond pastes. The thickness of the film is measured on a cross-section of the samples. For each sample, five micrographs of the film are taken at different locations with a SEM (*iT300* model from *JEOL)*. The thickness of the film is measured on these micrographs using the *ANALYSIS*™ software: 100 measurements are made on each micrograph. The average of these 500 measurements is taken as a result.

To characterize the samples at the nanoscale, Transmission Electron Microscopy is used (TEM: *TECNAI 3042* model from *FEI*, with an acceleration voltage of 200 kV and a camera length of 865 mm for diffraction). TEM samples of the corroded materials are prepared with conventional Focused Ion Beam methods (FIB: *Auriga 40* model from *ZEISS*). A Pt deposit is added to the samples' surface to protect the hydroxide film during the TEM thin film preparation.

The crystalline phases of the aluminium hydroxide are studied using low-incidence X-ray diffraction (XRD) and µ-Raman spectroscopy. The X-rays diffractometer (*CPS120 –Curved Position Sensitive- detector from INEL*) is used with Cu-Kα1 radiation (Ge(111) monochromator, wavelength: 1.5406 angstrom) in an asymmetric configuration. The incident angle of the X-ray beam is 2°: in this configuration, the analysed depth is about 4 µm in Al metal and 4 µm in the hydroxides. The µ-Raman spectrometer (*InVia Reflex* from *Reinshaw)* is used with a green laser (wavelength: 532 nm) and at 5% of the spectrometer power (5% of 100mW, to limit hydroxide damage during the analyses). The µ-Raman analyses are performed on the cross-section of the embedded samples with an optical microscope with a magnification of 50x.

Corrosion in Materials Testing Reactor:

Samples in 6061-T6 are placed in the centre of the nuclear core of Osiris reactor (reactor located in CEA Saclay, in France) and they are corroded by the water circulating thought the core. The corrosion conditions are thus imposed by the nominal operating conditions of the reactor: temperature is 42°C, pH is 6 and coolant flow rate is 0.9 m /s. Samples are corroded for 272 and 383 days in total (the test is interrupted several times to perform analyses). The maximum received dose of fast neutrons is 10^{22} n_f/cm^2 (E > 1 MeV) and the one of thermal neutrons is $6.5*10^{22}$ n_{th}/cm^2 (E = 0.025 eV) [25]. After corrosion in the reactor, the microstructure of the film is observed by SEM in a shielded cell in the LECI of the CEA Saclay, its chemical composition is investigated using Electron Probe Micro-Analysis (EPMA) and its

thickness is measured on the cross-section of the samples observed with an optical microscope.

3. RESULTS

In this part, the effects of ion and neutron irradiations are described (microstructure, crystalline structure and evolution of thickness of the aluminium hydroxide film).

3.1 ION IRRADIATION OF ALUMINIUM HYDROXIDE

In this section, the effects of ion irradiation on aluminium hydroxide are studied. Samples are corroded at 70°C for 7 days and in 2.8L of demineralised water. Fig. 3.a presents a TEM micrograph of the unirradiated aluminium hydroxide film obtained on the samples surface. The film is composed of two main layers, an inner and an outer. The inner layer in contact with the aluminium matrix is compact. According to µ-Raman analyses, this layer is composed of nanometric boehmite (γ-AlOOH, the data from [26,27] are used to identify this phase). The outer layer in contact with the aqueous solution is composed of cuboid microcrystals. These microcrystals are observed on the samples surface as illustrated in Fig. 4.a. According to µ-Raman analyses, these microcrystals are well-crystallised bayerite (α-$Al(OH)_3$, the data from [26] are used to identify this phase. The µ-Raman analyses performed on the inner and the outer layers are compared to XRD analyses: the film is composed of a mix of boehmite and bayerite as seen by both techniques. A thin intermediate layer is present between the two main layers. This layer is composed of needle-like nanocrystallites as seen in Fig 3.a.

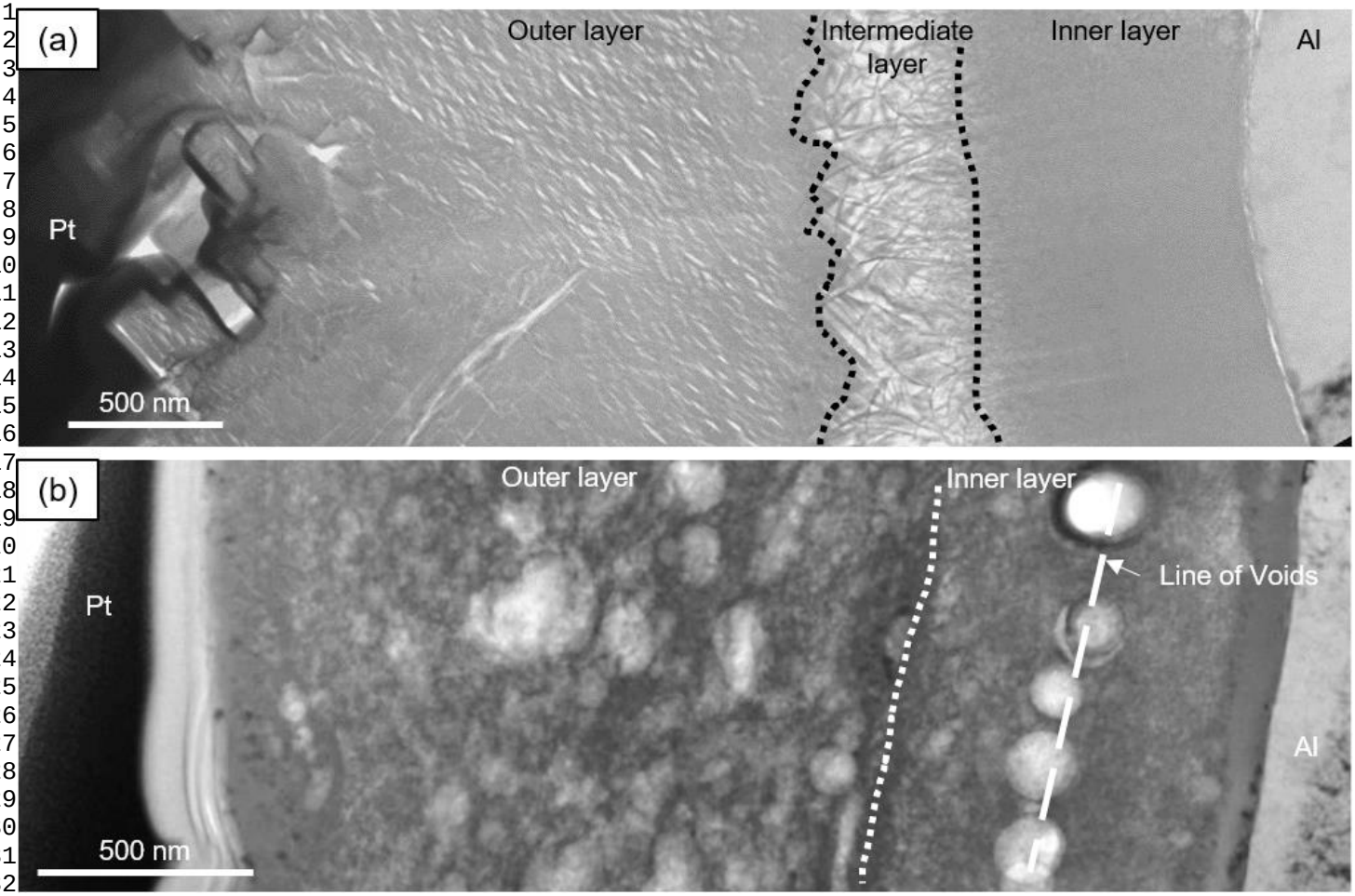

Figure 3: TEM micrographs of (a) a unirradiated film of aluminium hydroxide (obtained on samples corroded at 70°C, in 2.8L of demineralised water and for 7 days), (b) a film irradiated with Al ions of successive energies 5 MeV then 1.2 MeV.

After corrosion experiment, the aluminium hydroxide film is irradiated with Al ions of energies 5 MeV and 1.2 MeV, the two energies are used in order to irradiate the two main layers of the film. The damages are at most 2.5 dpa and 1.5 dpa on average (Fig. 2.a). Fig. 3.b presents a TEM micrograph of the irradiated film. The aluminium hydroxide is between the Pt deposit and the aluminium matrix. After ion irradiation, the distinction between the two former layers (inner and outer layers) is difficult to make and the thin intermediate layer cannot be observed as seen in Fig. 3.b. Voids are present in all the irradiated film. In particular, a line of voids is observed in the middle of the former inner layer. This line likely corresponds to the peak damage done by the Al ions in the inner layer. The presence of voids in ion irradiated oxides at room temperature was already observed [43] : the zirconia film present on ZrNb FIB samples presents some voids after irradiation at 1 and 10 dpa. In addition, a change of microstructure is observed in the hydroxide outer layer of our samples. After ion irradiation, cuboid microcrystals are not observed on the samples surface: as illustrated in Fig. 4.b, the former microcrystal are globular. This change of microstructure is similar to the observations done by Nabhan [10]: a film of boehmite (γ-AlOOH) was obtained during corrosion tests performed with samples in AlFeNi aluminium

alloy in 0.065L of solution at pH 5.2 for 11 days and at 140°C. The samples were then irradiated with Al ions of 1.6 MeV for 36 dpa. Before irradiation, needle-like nanocrystallites (size inferior to 0.5 µm) were observed on the samples surface. After ion irradiation, only spheroids were present on the samples surface (SEM observation).

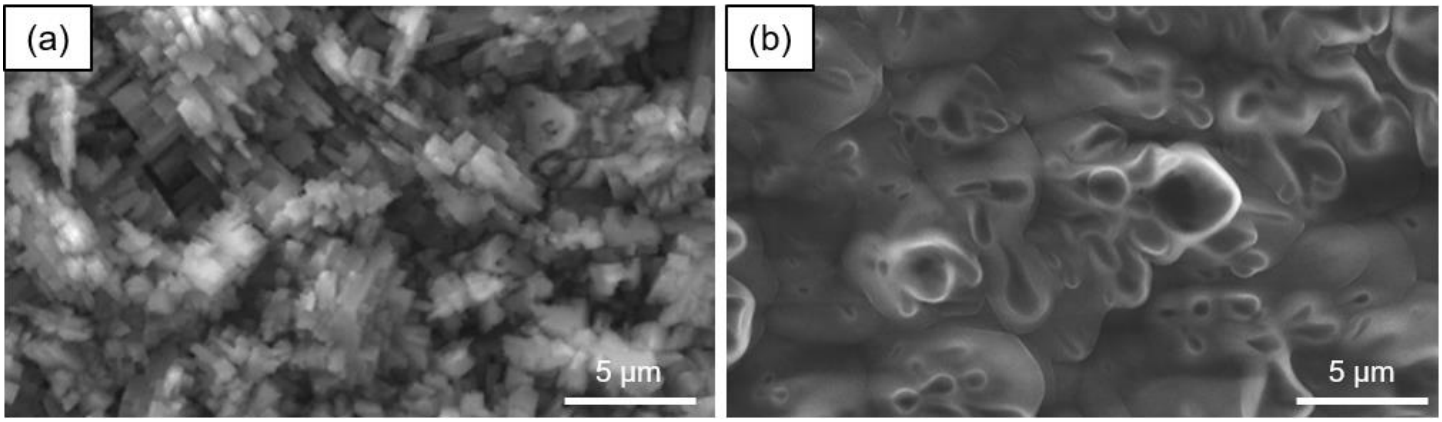

Figure 4: SEM micrographs of the samples surface: (a) unirradiated (obtained on samples corroded at 70°C, in 2.8L of demineralised water and for 7 days) and (b) irradiated with Al ions of successive energies 5 MeV then 1.2 MeV.

Selected Area Electron Diffractions (SAED) are performed on the inner layer and on the outer layer of the irradiated film. Similar diffraction patterns are observed in all the irradiated film, one of these patterns is presented in Fig. 5.a. Rings observed in Fig. 5.a indicate the presence of nanocrystallites. A dark field performed on a part of the ring of 1.40 Å is presented in Fig. 5.b: the nanocrystallites that have diffracted are in white. The electron diffraction pattern on Fig. 5.a can be attributed to a nanometric η-Al_2O_3 phase [28,29]. In the literature [29], this oxide phase comes from the thermal decomposition of bayerite and pseudo-boehmite at 200-650°C in vacuum. During irradiation, the thermal flux is low (0.2W/cm² for 1.2 MeV Al^+ and 0,8 W/cm² for 5 MeV Al^{2+}) and the maximal measured temperature of samples is 20°C. Considering the low oxide thickness (4 µm) on the 1mm thick alloy samples, even with the low thermal conductivity of the oxide, the temperature in the oxide is close to 20°C : this is confirmed by the 2°C thermocouple variation when switching off the ion beam. As a result, the presence of η-Al_2O_3 cannot be attributed to a high temperature. In addition, analyses are performed on the aluminium hydroxide exposed to the vacuum but protected from the irradiation: µ-Raman analyses and electron diffraction indicates the aluminium hydroxide is not dehydrated (traces of η-Al_2O_3 are not observed). As a result, the dehydration is not due to the vacuum but to the ion irradiation. In addition, when the irradiation starts, the pressure of the vacuum in the accelerator increases immediately from $133*10^{-8}$ Pa to $133*10^{-7}$ Pa: due to the ion beam, the former aluminium hydroxide is possibly decomposed into η-Al_2O_3 by releasing water. Unfortunately, the presence of η-Al_2O_3 could not be confirmed by a µ-Raman analysis: after irradiation, the laser light is strongly diffused by the oxide, which makes impossible to realize an accurate measurement. This type of problem is common with this aluminium oxide [30]. Also, phase

transitions in zirconium oxides under ion flux were already observed at room temperature on FIB samples taken in a corroded ZrNb alloy [43]. Therefore, the identified damages created by ion irradiation in the aluminium hydroxide are: creation of voids, change of microstructure and formation of η-Al_2O_3 nanocrystallites.

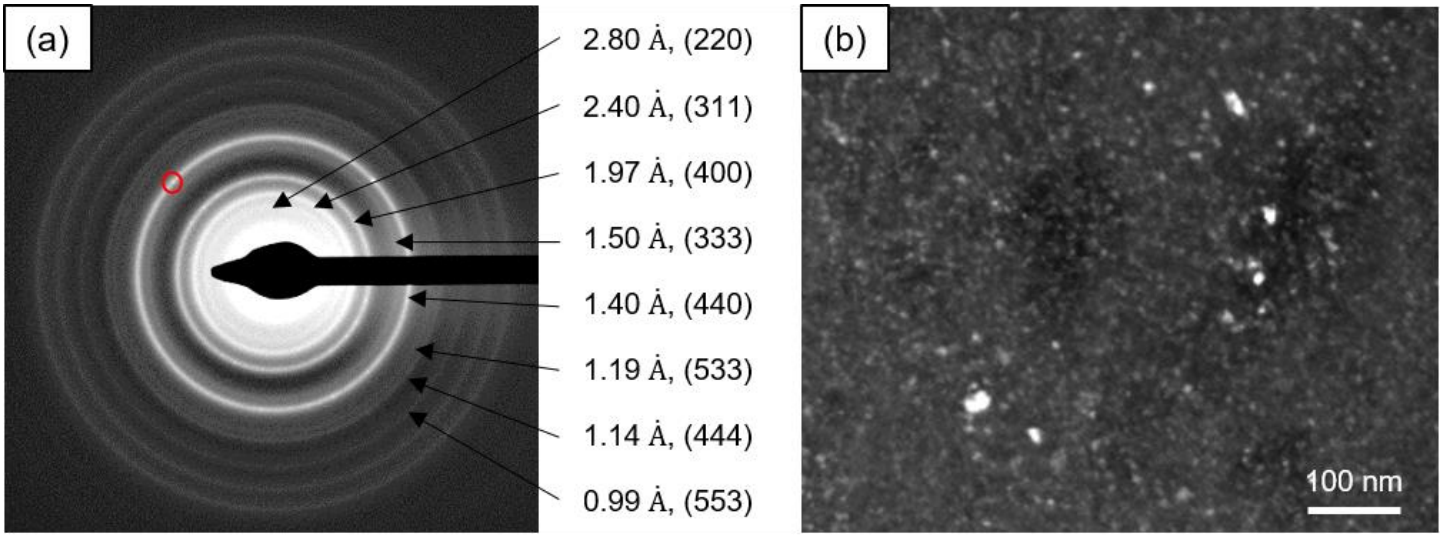

Figure 5: (a) SAED pattern obtained on the film irradiated with Al ions of successive energies 5 MeV then 1.2 MeV (the planes corresponding to the d-spacing come from [28,29]) and (b) Dark Field micrograph of the nanocrystallites which have diffracted in the red circle in Fig 5.a(TEM).

Irradiated samples are re-corroded at 70°C, for 4 days and in 2.8L of demineralised water in order to follow the evolution of the damage in an aqueous medium. After ion irradiation and re-corrosion, the aluminium hydroxide film has the same microstructure than the unirradiated film presented in Fig. 3.a: it is composed of a compact inner layer of boehmite and an outer layer of cuboid microcrystals (similar to the ones observed in Fig. 4.a). A thin intermediate layer of needle-like nanocrystallites is present between these two main layers and voids are not observed (TEM observation). The crystalline structure, analysed by µ-Raman, is also the same for the unirradiated samples and for the irradiated and re-corroded samples: the inner layer is composed of boehmite (γ-AlOOH) and the outer layer, of bayerite (α-$Al(OH)_3$. Traces of η-Al_2O_3 are not detected by SAED. As a result, the film is fully rehydrated and the damage due to ion irradiation is not still present in the aluminium hydroxide film. However, ion irradiation has an influence on the thickness of the film. Fig. 6.a presents the thickness of the inner and outer layers and Fig. 6.b is about the mass gain of samples. The points on the curves represent the average of measurements performed on the three samples. For 11 days (which is the total corrosion time, 7 days before irradiation and 4 days after), the total average thickness of the film and the average mass gain are the most important on irradiated samples: ion irradiation increases aluminium corrosion. In addition, for 11 days, the inner layer composed of boehmite is thicker and the outer layer composed of bayerite is thinner on irradiated samples than on un-irradiated samples. Thus, ion irradiation facilitates the formation of boehmite (γ-AlOOH) to the detriment of bayerite (α-$Al(OH)_3$). This observation is due to the process of rehydration of the

irradiated aluminium hydroxide: according to Aad [31], at a temperature above 50°C (this is 70°C in this study), alumina obtained from dehydrated aluminium hydroxide is rehydrated in water to form boehmite. As a result, after irradiation and re-corrosion, the new inner layer contains, in part, the two former layers. In order to compete this study on the effect of ion irradiation on aluminium corrosion, the metal aluminium matrix is irradiated and then corroded as described in the following section.

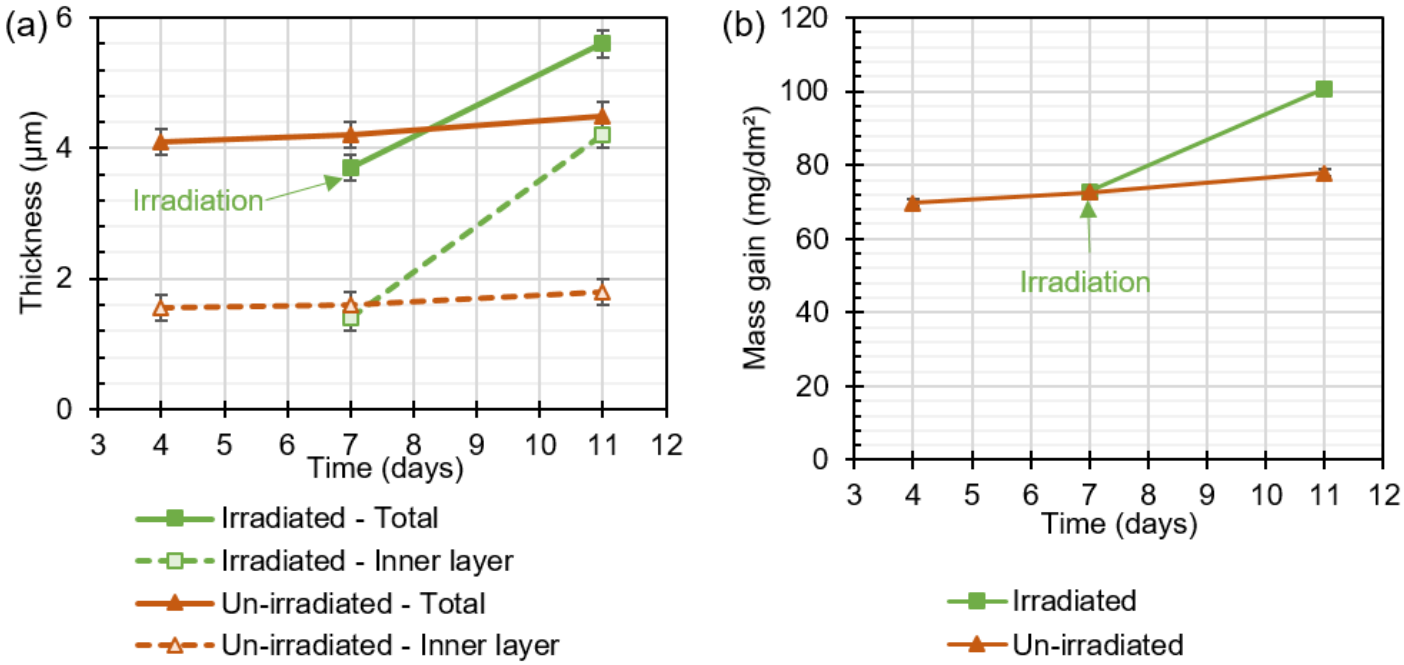

Figure 6: (a) Average thickness of the aluminium hydroxide film and (b) average mass gain of the samples unirradiated and irradiated with Al ions of successive energies 5 MeV then 1.2 MeV (the term “irradiation” on the graphics indicates when the ion irradiation occurs).

3.2 Ion irradiation of the aluminium matrix

Uncorroded samples in 6061-T6 aluminium alloy are irradiated with Al ions of an energy 1.8 MeV. Samples are then corroded in order to evaluate the impact of the damage created in the aluminium matrix on its corrosion behaviour. Fig. 7 presents two micrographs of un-irradiated matrix (Fig. 7.a) and irradiated matrix (Fig. 7.b). In the unirradiated matrix (Fig. 7.a), the grain size is between 100 and 200 nm on average, the minimum size is ~50 nm and the maximal is ~300 nm. In the irradiated matrix (Fig. 7.b), two areas are observed. The boundary between area 1 and area 2 is placed from SRIM calculations (as described in Fig. 2) as the start of the implantation peak. In area ❶, where the damage is between 1 dpa and 5 dpa, the grain boundaries are well defined and the grain size is the same than in the unirradiated matrix presented in Fig. 7.a. In area ❷, at the maximum damage zone of 8 dpa, it is difficult to discern one grain from another and the grain size cannot be measured. This observation is due to a

high dislocation density: the ion irradiation increases the number of dislocations in the material. This observation has already been described in the literature [10]: samples in AlFeNi aluminium alloy were irradiated with Al ions at 18 dpa, the number of dislocations increased in the irradiated zone of the aluminium alloy. In addition, using the defocus technique (large defocus in both under and over focus ranges) with a high magnitude, voids are not observed in the irradiated matrix. This observation agrees with the literature for ion irradiations on 6061-T6 alloy up to 30 dpa [32].

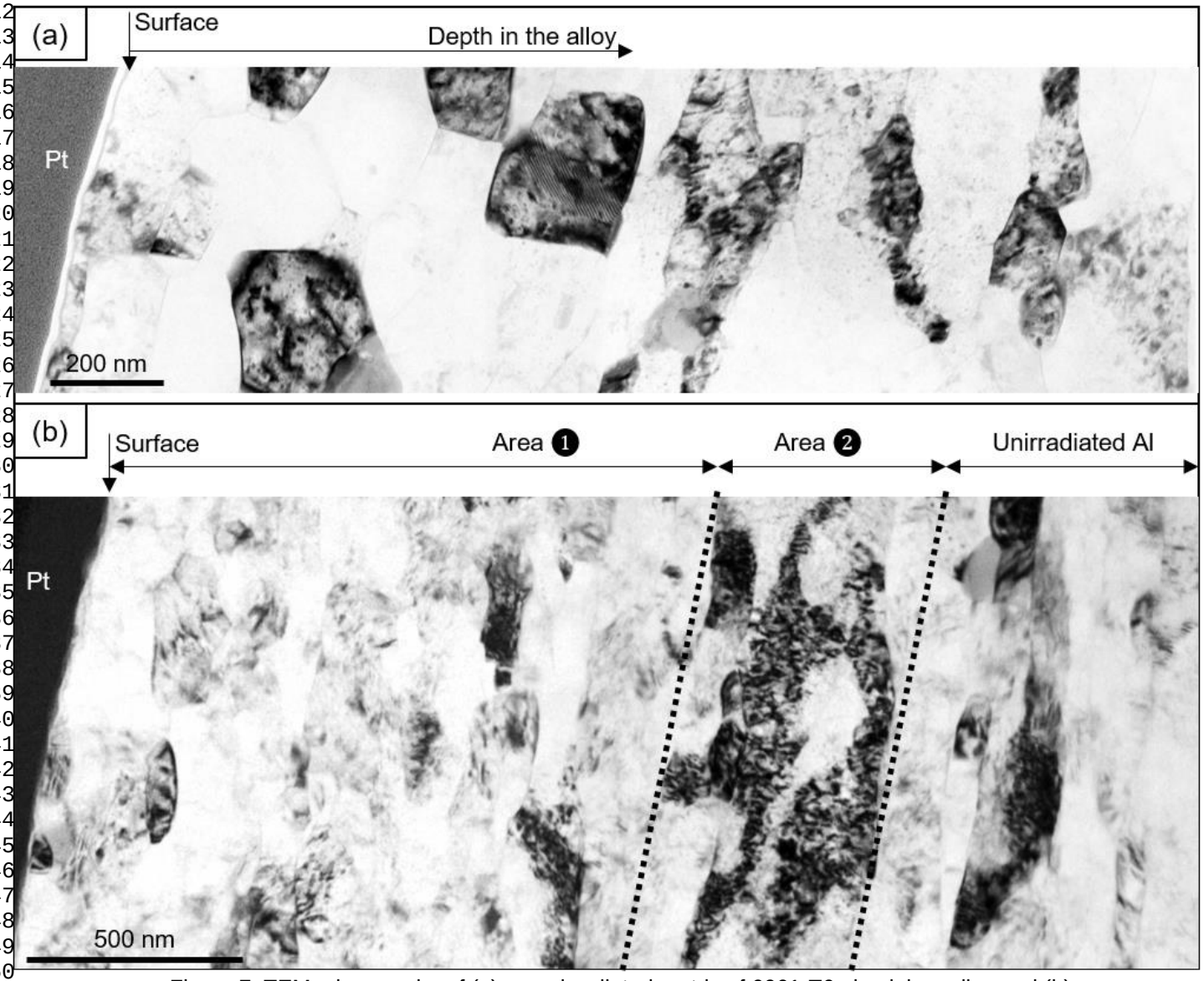

Figure 7: TEM micrographs of (a) an unirradiated matrix of 6061-T6 aluminium alloy and (b) irradiated matrix with Al ions of 1.8 MeV. The areas ❶ and ❷ correspond respectively to the area irradiated at 1-5 dpa (displacement per atom) and to the most irradiated area at 8 dpa. The boundary between area 1 and 2 is the start of the implantation peak (peak calculated with SRIM in Fig. 2.b).

Additional TEM observations are performed on the dispersoids present in the 6061-T6 aluminium alloy. The dispersoids size is between 50 and 200 nm. There are two families of dispersoids depending on their chemical composition: the first one is composed of iron, manganese and chromium, the second is composed of silicon and magnesium (chemical analyses performed with an EDX during the TEM observations). These two types of dispersoids are common in 6061-T6 aluminium alloy: they are Mg_2Si and Al(Cr,Mn,Fe)Si [33,34]. Fig. 8 presents a dispersoid observed from two angles in the unirradiated matrix (Fig. 8.a and b) and two dispersoids observed from different angles in the matrix irradiated at 14 dpa (Fig. 8.c and b, dispersoids located in the area ❷ in Fig. 7.b). In the unirradiated matrix, the contrast of the dispersoid changes with the tilt angle: the dispersoid is transparent with an observation angle of α=0° (Fig. 8.a) and it is grey/black with α=10° (Fig. 8.b). This contrast variation indicates the dispersoid is crystalline. In the matrix irradiated at 14 dpa, the contrast of the dispersoids does not change with the observation angle (Fig. 8.c and d, the dispersoids are observed from several angles between 0 and 20° and variation of contrast is not observed with any angle). The absence of variation of contrast indicates the dispersoids are amorphous [35]. Ion irradiation thus causes an amorphisation of the dispersoids for the conditions used in this study. This observation agrees with the literature for similar ion irradiations [32]: an amorphisation of dispersoids is observed during ion irradiation performed on 6061-T6 aluminium alloy with W ions for 10-30 dpa at 20°C. In addition to the dispersoids, other nanometric phases are present in the 6061-T6 aluminium alloy, the influence of ion irradiation on these phases are the subjects for several studies [32,36] and are not studied during this work.

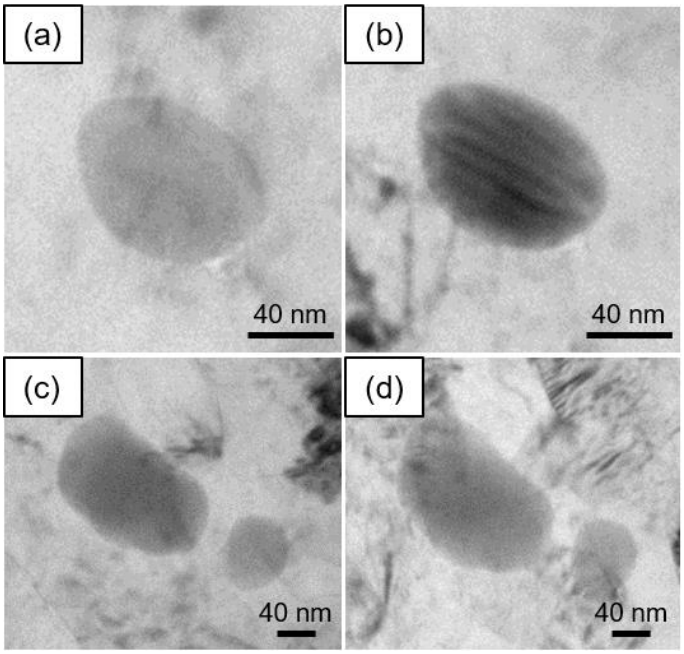

Figure 8: TEM micrographs: dispersoid observed in the unirradiated matrix from two different tilt angles: (a) α=0° and (b) α=10°, and two dispersoids observed in the matrix irradiated at 14 dpa from two different tilt angles: (c) α=0° and (d) α=10°.

After the ion irradiation, the samples are corroded at 70°C, for 4 days and in 2.8L of demineralised water. A film of aluminium hydroxide is present on the corroded samples. Microstructure of the film is the same on unirradiated samples and on irradiated samples: the film is composed of two main layers, an inner and an outer, similar to the ones described in Fig. 3.a and in Section 3.1. The film has also the same crystalline composition on un-irradiated and irradiated samples (mix of bayerite and boehmite, analyses performed by XRD). Thicknesses of the inner layer and the outer layer of the film are respectively 1.63 ± 0.2 µm and 2.65 ± 0.2 µm on average on un-irradiated samples, and 1.98 ± 0.2 µm and 3.06 ± 0.2 µm on average on irradiated samples. Ion irradiation causes thus an increase of thickness of the aluminium hydroxide film: the irradiated samples are more corroded than the unirradiated ones. This increase of aluminium corrosion could be due to the amorphisation of dispersoids and to the increase of dislocation density. Similar observations have been made in corroded irradiated AlFeNi aluminium alloy [10]: uncorroded samples were irradiated with Al ions for 18 dpa and were then corroded at 140°C, for 16 days in 0.065L of solution at pH 5.2. The irradiated samples were more corroded. In order to compete this study about the effect of irradiation on aluminium corrosion, samples are corroded in a MTR under neutron irradiation.

3.3 Corrosion of the 6061-T6 aluminium alloy in Materials Testing Reactor

Samples in 6061-T6 aluminium alloy have been irradiated and corroded in the Osiris nuclear reactor of the French Atomic Energy Commission (CEA) in Saclay, in France. After irradiation experiments in the Osiris reactor, the film obtained on the samples surface is characterised in hot cells. Fig. 9.a presents an SEM observation of the film. For this observation, a sample is broken in two pieces and the film is observed on the fractured side of the sample in order to highlight the layered microstructure of the film. The film is composed of three layers. The inner layer is brittle (Fig. 9.a and c): numerous cracks are present in all the layer. The thickness of this layer is ~5 µm. The intermediate layer is the thickest of the three, its thickness is ~13 µm. This layer looks micro-porous (Fig. 9.a, b and c). The outer layer is composed of cuboid microcrystals (Fig. 9.a and b). These microcrystals are similar to the ones observed on the samples surface during unirradiated corrosion tests (Fig. 4.a). The outer layer is not observed on all the samples surface: desquamations of the hydroxide film are observed (SEM observation of the film surface).

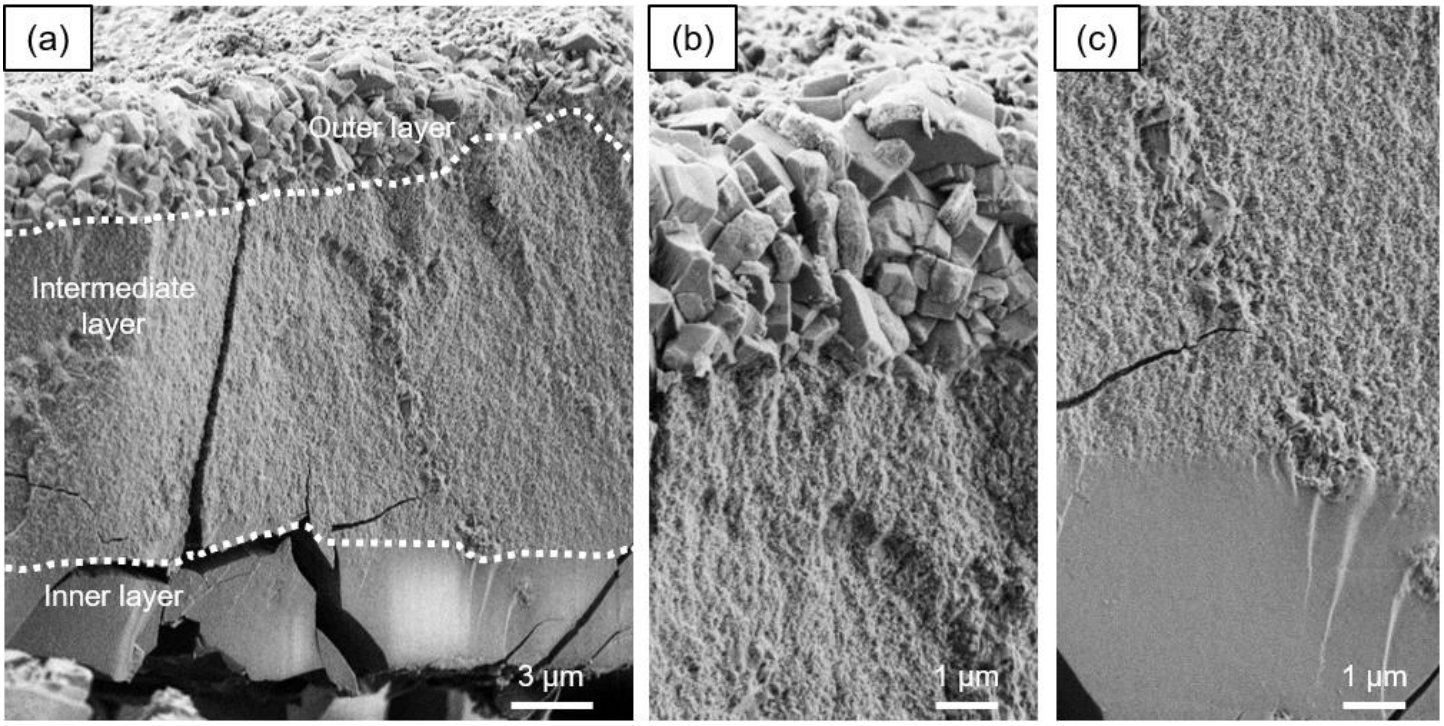

Figure 9: SEM micrographs of (a) the film obtained on sample corroded for 560 days at pH 6 and at 42°C in the reactor Osiris and zoom on (b) the outer and intermediate layers and on (c) the intermediate and inner layers.

The chemical composition of the film is analysed by EPMA. For this analysis, a sample is embedded in a tin-bismuth mixture and then polished down to a 1 µm finish with diamond past. The film is composed on average of 50-55 wt. % of aluminium and 40-45 wt. % of oxygen. Silicon and magnesium are also observed in the film (Fig. 10). In particular, the film is enriched in silicon on a depth of 5/6 µm near the aluminium matrix. This depth corresponds to the thickness of the inner layer: this indicates that only the inner layer of the film is enriched with silicon. Silicon enrichment is not observed for unirradiated samples. This enrichment could be due to the transmutation of aluminium in silicon due to thermal neutrons following the reactions (2) and (3) [37,38]:

$$^{27}_{13}Al + {}^{1}_{0}n \xrightarrow{(n,\gamma)} {}^{28}_{13}Al \quad (2)$$

$$^{28}_{13}Al \rightarrow {}^{28}_{14}Si + e^{-} \quad (3)$$

Silicon enrichment of the film had already been observed during corrosion tests performed in MTR [10,39]. Magnesium content decreases from 0.9 wt. % in the alloy to 0.1 wt. % from a depth of 5/6 µm in the film. Magnesium is thus present only in the inner layer of the film and the decreasing profile of magnesium content indicates a release of this chemical element in solution after a diffusion through the film. This profile agrees with the literature: during corrosion of Mg-containing aluminium alloy, a magnesium release in solution had already been observed during unirradiated corrosion tests [3,20,39] and in an aqueous medium at a pH of 6, the stable form of

the oxidised magnesium is the aqueous ion Mg^{2+} according to the corresponding Pourbaix diagram [40].

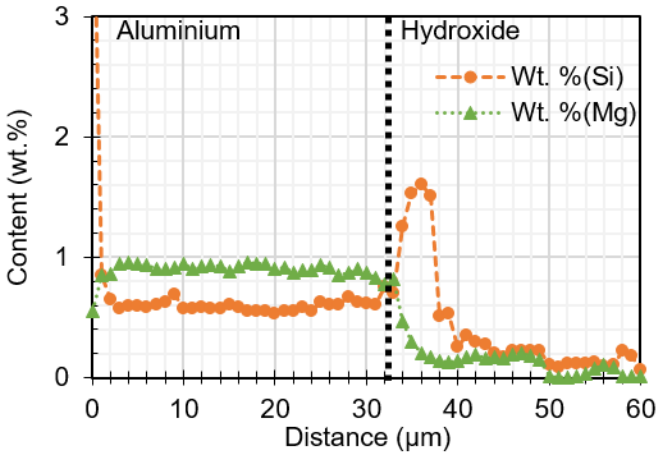

Figure 10: Chemical evolution of magnesium and silicon by EMPA in the aluminium matrix and in the aluminium hydroxide film obtained on a sample corroded for 560 days at pH 6 and at 42°C in the Osiris reactor.

In order to follow the thickness of the film during corrosion test in the Osiris reactor, samples are embedded in an epoxy resin and then polished down to a 1 µm finish with diamond past. The thickness of the film is measured on a cross section of the samples observed with an Optical Microscope. Table 3 summarizes the results of this examination performed on two samples (the displacements per atom due to the fast neutrons flux in the aluminium matrix are calculated based on the formula and the observation of Farrell et al. [6]). In addition, in order to highlight the effect of neutron irradiation on aluminium corrosion, these results are compared to samples corroded in a corrosion loop with recirculating water [41]. The loop allowed a renewal of the aqueous solution: after a passage in front of the sample at very low flow rate, the water was cleaned by filters and then reinjected in the loop. The film is five time thicker on samples corroded in the Osiris reactor than in the corrosion loop: neutron irradiation increases aluminium corrosion. The effect of neutron irradiation on aluminium corrosion is thus very strong. The observations performed on samples corroded in the Osiris rector (layered microstructure of the film, silicon enrichment and increase of aluminium corrosion) allows us to compare neutron and ion irradiations.

Table 3: Thickness of the film measured on samples corroded in the reactor Osiris and in a corrosion loop [41]

Sample id	Corroded in	Time	Temperature	pH	Flow rate	Dose of fast neutrons	Displacement per atom in the aluminium matrix	Dose of thermal neutrons	Thickness of the film

		days	°C		m/s	n/cm² (E > 1 MeV)	Dpa	n/cm² (E = 0.025 eV)	µm
N°1-Osi	Osiris reactor	272	42	6	0.9	$4.65*10^{21}$	6.7	$3.2*10^{22}$	13.5 ± 2.0
N°2-Osi	Osiris reactor	383	42	6	0.9	$6.8*10^{21}$	10	$4.0*10^{22}$	14.0 ± 1.4
N°1-Loop [41]	Corrosion loop	279	50	5.7	-	-	-	-	2.1 ± 0.3
N°2-Loop [41]	Corrosion loop	346	50	5.7	-	-	-	-	2.5 ± 0.3

4. DISCUSSION

Corrosion tests coupled with ion irradiations and corrosion experimentations performed in nuclear reactor are compared in this section. In addition, the observations performed on the ion irradiated samples allow us to propose corrosion mechanisms associated to ion irradiation.

4.1 COMPARISON BETWEEN ION IRRADIATION AND NEUTRON IRRADIATION

Some similarities are observed between ion and neutron irradiations. Films formed in nuclear reactor and obtained after ion irradiation and re-corrosion have similar crystalline structure. Indeed, at 70°C, the aluminium hydroxide film irradiated with Al ions and then re-corroded is composed of a mix of boehmite (γ-AlOOH) and bayerite (α-$Al(OH)_3$), and the main crystalline phase is boehmite. For a similar temperature (70/90°C), the film obtained in Materials Testing Reactors (MTRs) has the same crystalline structure (i.e. the main crystalline phase in the XRD patterns is boehmite with traces of bayerite) [5,9,39]. In addition, the film has a similar layered microstructure after ion irradiation and re-corrosion (cf. Section 3.1), and during corrosion tests with neutron irradiation (Fig. 9). The two types of irradiation increase aluminium corrosion and accelerate the aluminium hydroxide growth on the samples surface (cf. Fig. 6 and Section 3.3). Because of these similarities, ion irradiation can be used during un-activated corrosion tests in corrosion loops or in autoclave in order to be closer to the conditions found in MTRs. However, silicon enrichment is observed in the film obtained in nuclear reactor (cf. Fig. 10), this enrichment is not observed during unirradiated corrosion tests. Silicon ions can be used during ion irradiation in order to simulate the silicon enrichment in the film.

Nevertheless, in this study, we can observe some limitations to the use of ion irradiation to simulate the damage created by the fast neutron flux in reactor. Ion irradiation leads to a dehydration of the aluminium hydroxide. The damage due to this dehydration (nanocrystallites of η-Al_2O_3) may not be observed in aluminium hydroxide irradiated in a nuclear core (SAED should be performed in the samples corroded in the Osiris reactor to answer to this incertitude). In addition, to irradiate the aluminium hydroxide film, the corrosion tests are interrupted, the samples are exposed to air during the break of corrosion tests. Wintergerst observed an effect of breaks during corrosion test: the hydroxide thickness is less important during corrosion tests with breaks than without break [3]. It means the thickness measured in this study may be underestimated because of the interruptions to irradiate the aluminium hydroxide (cf. Section 3.1).

4.2 GROWTH MECHANISMS OF ALUMINIUM HYDROXIDE DURING CORROSION TESTS COUPLED TO ION IRRADIATION (IRRADIATION OF THE ALUMINIUM HYDROXIDE FILM)

Mechanisms of aluminium corrosion have been studied in the literature without irradiation [39,42]. Based on these mechanisms and with the observations done in Section 3.1, the following mechanisms associated with ion irradiation are proposed below and summarized in Fig. 11. It should be noted that the proposed mechanisms apply to ion irradiation and not to neutron irradiation or to in-core irradiation in general.

1. Before ion irradiation, due to corrosion tests, aluminium matrix is oxidised at the interface hydroxide-metal, this oxidation reaction is accompanied by the reduction of water and dioxygen, and the production of OH hydroxide groups. A part of this oxidised aluminium reacts with the OH hydroxide groups to form boehmite (γ-AlOOH), the inner layer, at the hydroxide-metal interface (internal growth). The rest of the oxidised aluminium diffuses through the film and is released as ions Al(III) in the corrosive solution. These ions then precipitate on the samples surface to form bayerite (α-$Al(OH)_3$), the outer layer (external growth). (Fig. 11.a).
2. During ion irradiation, the former aluminium hydroxide is dehydrated and change of microstructure is observed (Fig. 11.b).
3. After irradiation, during the re-corrosion of the samples, the irradiated film is a part of the new inner layer: at 70°C, alumina obtained from dehydrated aluminium hydroxide is rehydrated by water to form boehmite [31], the crystalline phase of the inner layer. Due to the non protective quality of this irradiated film, the matrix is oxidised and aluminium is released in solution. A new outer layer is formed by the precipitation of aluminium ions in solution on the samples surface (Fig. 11.c). The proposed global reactions are :

   $2AlO(OH) \rightarrow Al_2O_3 + H_2O$ and

   $2Al(OH)_3 \rightarrow Al_2O_3 + 3H_2O$

   When the samples are reintroduced in the autoclave containing water for the corrosion test after irradiation, the Al_2O_3 layer is firstly hydrated to AlO(OH) (formation of boehmite, the most thermodynamically stable specie) and the corrosion is observed

again with the formation of $Al(OH)_3$ at the interface AlO(OH)/solution following the mechanism previously described (Figure 11).

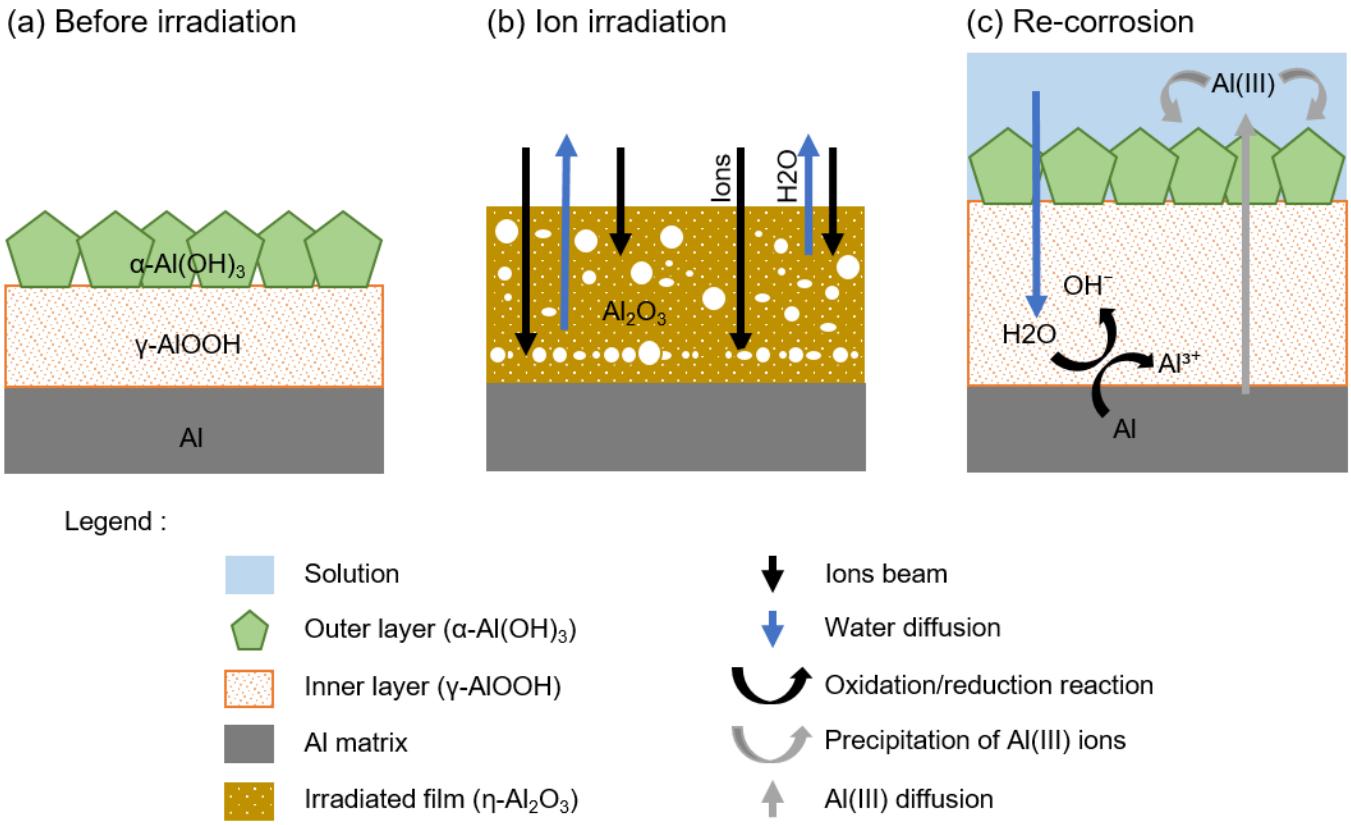

Figure 11: Schematic of the three steps of the proposed mechanisms of aluminium corrosion during corrosion tests coupled with ion irradiation.

5. CONCLUSIONS

In this study, two ion irradiations are performed in order to highlight the effect of ion irradiation on aluminium corrosion. Ion irradiation is performed on an aluminium hydroxide film Before irradiation, this film is composed of three layers: an compact inner layer of boehmite (γ-AlOOH), a thin intermediate layer of needle-like nanocristallites and an outer layer of parallelepiped microcrystals composed of bayerite (α-$Al(OH)_3$). After irradiation, voids are present in the film and a change of microstructure is observed: former cuboid microcrystals become spheroids on the samples surface and the thin intermediate layer is not observed. In addition, ion irradiation causes dehydration of the aluminium hydroxide: nanocrystallites of η-Al_2O_3 are present in all the film. The irradiated samples are then re-corroded. Damage is not observed in the new aluminium hydroxide film and this film is fully rehydrated. However, an effect of ion irradiation persists: ion irradiation increases aluminium corrosion. This observation is attributed to the damages observed in the irradiated film which possibly decrease the passivation properties of the film.

A second ion irradiation is performed on aluminium matrix, on uncorroded samples in 6061-T6 aluminium alloy (Al ions with an energy of 1.8 MeV in order to create at most 14 dpa in the

matrix). This irradiation increases the dislocation density and amorphizes the dispersoids. After irradiation, the samples are corroded. The ion irradiation increases aluminium corrosion. Samples are corroded in the Osiris nuclear reactor (located in CEA Saclay in France), at 42 °C, at a pH of 6 and for 18 months in total. The film has a layered microstructure on the samples surface composed of a brittle inner layer, a thick intermediate layer and an outer layer of cuboid microcrystals. Silicon enrichment is observed in the inner layer, this enrichment is possibly due to the transmutation of aluminium in silicon due to thermal neutron irradiation. Similarities are observed between ion and neutron irradiations: the film has a similar crystalline structure and a similar layered microstructure for the two types of irradiation. In addition, ion and neutron irradiations increase aluminium corrosion and accelerate the aluminium hydroxide growth on the samples surface. Because of these similarities, ion irradiation can be used for corrosion tests in corrosion loops or in autoclave in order to perform parametric studies and bring some relevant information on corrosion in MTRs. However, the corrosion mechanisms proposed in this paper apply specifically to ion-irradiation. In particular, ion irradiation dehydrates the aluminium hydroxide. This dehydration is one of the limitation of the use of ion irradiation as well as damage flux. As a result, in further studies, ion irradiation coupled to corrosion tests in corrosion loop could be performed in order to increase the application range of the empirical models used in the literature to estimate the thickness of the film depending on the nominal operating conditions of MTRs. Finally, conducting fine TEM characterizations on neutron irradiated samples would be very interesting to observe the particular oxide phases created during irradiation. These studies could be envisioned in future work on this subject.

ACKNOWLEDMENTS

This work received assistance from the “Agence Nationale de la Recherche” program GENESIS referenced as ANR-11-EQPX-0020. The ion irradiation experiments were performed at JANNuS-Saclay (Joint Accelerators for Nanoscience and Nuclear Simulation), CEA Paris-Saclay, France. The nuclear corrosion experiments were performed in the Materials Testing Reactor Osiris, CEA Paris-Saclay, France.

DATA AVAILABILITY STATEMENT

The raw/processed data required to reproduce these findings cannot be shared at this time as the data also forms part of an ongoing study.

REFERENCES

[1] S.J. Pawel, G.L. Yoder, C.D. West, B.H. Montgomery, The development of a preliminary correlation of data on oxide groth on 6061 aluminium under ANS thermal-hydraulic conditions, ORNLTM-11517. (1990).

[2] J.C. Griess, H.C. Savage, T.H. Mauney, J.L. English, Effect of heat flux on the corrosion of aluminium by water. Part I : Experimental equipment and preliminary results, Oak Ridge, TN, USA, 1960.

[3] M. Wintergerst, N. Dacheux, F. Datcharry, E. Herms, B. Kapusta, Corrosion of the AlFeNi alloy used for the fuel cladding in the Jules Horowitz research reactor, J. Nucl. Mater. 393 (2009) 369–380. https://doi.org/10.1016/j.jnucmat.2009.06.003.
[4] C. Vargel, Corrosion de l'aluminium, Dunod, 1999.
[5] A.E. Richt, R.W. Knight, G.M. Adamson, Postirradiation examination and evalution of the performance of HFIR fuel elements, 1971. https://doi.org/10.2172/4698779.
[6] K. Farrell, R.T. King, A. Jostsons, Examination of the irradiated 6061 aluminum HFIR target holder, 1973. https://doi.org/10.2172/4490342.
[7] G.H. Hanson, G.W. Gribson, J.C. Griess, Report of the ANS aluminium cladding corrosion workshop, in: Oak Ridge National Laboratory, Idaho, 1988.
[8] S. Gosmain, Examens par diffraction des rayons X d'échantillons en alliage d'aluminium 6061-T6 provenant du réacteur BR2 de Mol, CEA Saclay, 2005.
[9] B. Kapusta, Synthèse des caractérisations du casier aléolé en AG3-NET irradié de 1966 à 1996 dans Osiris, CEA Saclay, 2006.
[10] D. Nabhan, Etude de la corrosion aqueuse de l'alliage d'aluminium AlFeNi utilisé comme gainage de combustible nucléaire : effet de l'état de surface, du pH et d'une irradiation aux ions, Thèse de doctorat, Collège Doctoral du Languedoc-Rousillon, Université Montpellier 2, 2014.
[11] Y.S. Kim, H.T. Chae, S.V. den Berghe, A. Leenaers, V. Kuzminov, A.M. Yacout, Aluminum cladding oxide growth prediction for high flux research reactors, J. Nucl. Mater. 529 (2020) 151926. https://doi.org/https://doi.org/10.1016/j.jnucmat.2019.151926.
[12] Y.S. Kim, G.L. Hofman, A.B. Robinson, J.L. Snelgrove, N. Hanan, Oxidation of aluminum alloy cladding for research and test reactor fuel, J. Nucl. Mater. 378 (2008) 220–228. https://doi.org/10.1016/j.jnucmat.2008.06.032.
[13] J.C. Griess, H.C. Savage, T.H. Mauney, J.L. English, J.G. Rainwater, Effect of heat flux on the corrosion of aluminium by water. Part II : Influence of water temperature, velocity and pH on corrosion-product formation, Oak Ridge, TN, USA, 1961.
[14] J.C. Griess, H.C. Savage, T.H. Mauney, J.L. English, J.G. Rainwater, Effect of heat flux on the corrosion of aluminium by water. Part III : Final report on tests relative ot the high-flux isotop reactor, Oak Ridge, TN, USA, 1961.
[15] S.J. Pawel, G.L. Yoder, D.K. Felde, B.H. Montgomery, M.T. McFee, The corrosion of 6061 aluminium under heat transfer conditions in the ANS corrosion test loop, Oxid. Met. 36 (1991) 175–194.
[16] S.J. Pawel, D.K. Felde, R.E. Pawel, Influence of coolant pH on corrosion of 6061 aluminium under reactor heat transfer conditions, Oak Ridge, TN, USA, 1995.
[17] J.C. Griess, H.C. Savage, J.L. English, Effect of heat flux on the corrosion of alumnium by water. Part IV : Tests relative to the advanced test reactor and correlation with previous results, Oak Ridge, TN, USA, 1964.
[18] T. Petit, J. Besson, C. Ritter, K. Colas, L. Helfen, T.F. Morgeneyer, Effect of hardening on toughness captured by stress-based damage nucleation in 6061 aluminum alloy, Acta Mater. 180 (2019) 349–365. https://doi.org/10.1016/j.actamat.2019.08.055.
[19] D. Nabhan, B. Kapusta, P. Billaud, K. Colas, D. Hamon, N. Dacheux, Effects of pH, surface finish and thermal treatment on the corrosion of AlFeNi aluminum alloy. Characterization of oxide layers, J. Nucl. Mater. 457 (2015) 196–204. https://doi.org/10.1016/j.jnucmat.2014.10.023.
[20] S. L'Haridon-Quaireau, M. Laot, K. Colas, B. Kapusta, S. Delpech, D. Gosset, Effects of temperature and pH on uniform and pitting corrosion of aluminium alloy 6061-T6 and characterisation of the hydroxide layers, J. Alloys Compd. (2020) 155146. https://doi.org/10.1016/j.jallcom.2020.155146.
[21] J.F. Ziegler, M.D. Ziegler, J.P. Biersack, SRIM – The stopping and range of ions in matter (2010), 19th Int. Conf. Ion Beam Anal. 268 (2010) 1818–1823. https://doi.org/10.1016/j.nimb.2010.02.091.
[22] S.. Zinkle, G.. Pells, Microstructure of Al2O3 and MgAl2O4 irradiated at low temperatures, J. Nucl. Mater. 253 (1998) 120–132. https://doi.org/10.1016/S0022-3115(97)00323-1.
[23] H.H. Neely, W. Bauer, Electron-Irradiation Damage-Rate Measurements in Aluminum, Phys Rev. 149 (1966) 535–539. https://doi.org/10.1103/PhysRev.149.535.
[24] P. Jung, Average atomic-displacement energies of cubic metals, Phys Rev B. 23 (1981) 664–670. https://doi.org/10.1103/PhysRevB.23.664.
[25] F. Rozeblum, Floréal : Résultats et interprétation des mesures obtenues par intégrateurs de dose, CEA Saclay, 2006.

[26] C.J. Doss, R. Zallen, Raman studies of sol-gel alumina: Finite-size effects in nanocrystalliine AlO(OH), Phys Rev B. 48 (1993) 626–637.
[27] H.D. Ruan, R.L. Frost, J.T. Kloprogge, Comparison of Raman spectra in characterizing gibbsite, bayerite, diaspore and boehmite, J. Raman Spectrosc. 32 (2001) 745–750. https://doi.org/10.1002/jrs.736.
[28] D.B. Tilley, R.A. Eggleton, The Natural Occurrence of Eta-Alumina (eta-Al2O3) in Bauxite, Clays Clay Miner. 44 (1996). http://explore.bl.uk/primo_library/libweb/action/display.do?tabs=detailsTab&gathStatTab=true&ct=display&fn=search&doc=ETOCRN613373549&indx=1&recIds=ETOCRN017880329 (accessed January 14, 2019).
[29] K. Wefers, C. Misra, Oxides and hydroxides of aluminium, ALCOA Laboratories, 1987.
[30] Y. Chen, J. Hyldtoft, C.J.. Jacobsen, O.F. Nielsen, NIR FT Raman spectroscopic studies of η-Al2O3 and Mo/η-Al2O3 catalysts, Spectrochim. Acta. A. Mol. Biomol. Spectrosc. 51 (1995) 2161–2169. https://doi.org/10.1016/0584-8539(95)01495-4.
[31] J. Aad, Dégradation chimique et mécanique de l'alumine en phase aqueuse : mécanisme et inhibition en conditions ambiantes et hydrothermales, Thèse de doctorat, Université pierre et Marie Curie - Paris VI, 2016. https://tel.archives-ouvertes.fr/tel-01913067/document.
[32] V. Garric, Etude du gonflement par cavités d'un alliage d'aluminium irradié sous faiseau d'ions, Thèse de doctorat, Université Grenoble Alpes, 2019.
[33] C. Flament, J. Ribis, J. Garnier, T. Vandenberghe, J. Henry, A. Deschamps, Electron irradiation-enhanced core/shell organization of Al(Cr, Fe, Mn)Si dispersoids in Al–Mg–Si alloys, Philos. Mag. 95 (2015) 1–12. https://doi.org/10.1080/14786435.2015.1009959.
[34] Y. Shen, Comportement et endommagement des alliages d'aluminium 6061-T6 : approche micrométrique, Thèse de doctorat, Ecole Nationale Supérieure des Mines de Paris, 2012.
[35] M. Tupin, R. Verlet, K. Colas, M. Jublot, G. Baldacchino, K. Wolski, Effect of ion irradiation of the metal matrix on the oxidation rate of Zircaloy-4, Corros. Sci. 136 (2018) 28–37. https://doi.org/ 10.1016/j.corsci.2018.02.023.
[36] C. Flament, J. Ribis, J. Garnier, Y. Serruys, F. Leprêtre, A. Gentils, C. Baumier, M. Descoins, D. Mangelinck, A. Lopez, K. Colas, K. Buchanan, P. Donnadieu, A. Deschamps, Stability of β″ nano-phases in Al-Mg-Si(-Cu) alloy under high dose ion irradiation, Acta Mater. 128 (2017) 64–76. https://doi.org/10.1016/j.actamat.2017.01.044.
[37] D. Zuili, Comportement en corrosion des alliages d'aluminium des séries 5000 et 6000 sous flux de neutrons, CEA Saclay, Saclay, 2000.
[38] B. Kapusta, RCC-MX - Annexe X3.1A et X3.2A, CEA Saclay, Saclay, 2005.
[39] M. Wintergerst, Etude des mécanismes et des cinétiques de corrosion aqueuse de l'alliage d'aluminium AlFeNi utilisé comme gainage du combustible nucléaire de réacteurs expérimentaux., Thèse de doctorat, Université Paris XI, U.F.R Scientifique d'orsay, 2010.
[40] M. Pourbaix, Atlas d'équilibres électrochimiques, Villars, 1963.
[41] S. Cathalau, R. Mombellet, A. Vivet, P. Schindler, Programme expérimental erosion/corrosion de l'aluminium 6061-T6 pour le RJH, résultats de la 3ème et 4ème phase de 2000 heures et synthèse de l'essai 6, CEA Cadarache, 2009.
[42] R.K. Hart, The formation of films on aluminium immersed in water, Trans Faraday Soc. 53 (1956) 1020–1025.
[43] J. Liu, A.H. Mir, G. He, M. Danaye, J. Hinks, S. Donnelly, H. Nordin, S. Lozano-Perez, C. R.M. Grovenor, In-situ TEM study of irradiation-induced damage-mechanisms in monoclinic ZrO_2, Acta Materialia 199 (2020) 429-442 https://doi.org/10.1016/j.actamat.2020.08.064.

Figure captions:

Fig. 1: Purpose, step and conditions of irradiation of the three studies performed in this paper.

Fig. 2: Damage profiles (dpa: displacement per atom) created by (a) Al ions with successive energies of 5 MeV and then 1.2 MeV irradiating the aluminium hydroxide film and by (b) Al ions with an energy of 1.8 MeV irradiating the aluminium matrix, profiles calculated by SRIM with the mode "full damage cascade" [21].

Fig. 3: TEM micrographs of (a) a unirradiated film of aluminium hydroxide (obtained on samples corroded at 70°C, in 2.8L of demineralised water and for 7 days), (b) a film irradiated with Al ions of successive energies 5 MeV then 1.2 MeV.

Fig. 4: SEM micrographs of the samples surface: (a) unirradiated (obtained on samples corroded at 70°C, in 2.8L of demineralised water and for 7 days) and (b) irradiated with Al ions of successive energies 5 MeV then 1.2 MeV.

Fig. 5: (a) SAED pattern obtained on the film irradiated with Al ions of successive energies 5 MeV then 1.2 MeV (the planes corresponding to the d-spacing come from [28,29]) and (b) Dark Field micrograph of the nanocrystallites which have diffracted in the red circle in Fig 5.a(TEM).

Fig. 6: (a) Average thickness of the aluminium hydroxide film and (b) average mass gain of the samples unirradiated and irradiated with Al ions of successive energies 5 MeV then 1.2 MeV (the term “irradiation” on the graphics indicates when the ion irradiation occurs).

Fig. 7: TEM micrographs of (a) an unirradiated matrix of 6061-T6 aluminium alloy and (b) irradiated matrix with Al ions of 1.8 MeV. The areas ❶ and ❷ correspond respectively to the area irradiated at 1-5 dpa (displacement per atom) and to the most irradiated area at 8 dpa.

Fig. 8: TEM micrographs: dispersoid observed in the unirradiated matrix from two different tilt angles: (a) α=0° and (b) α=10°, and two dispersoids observed in the matrix irradiated at 14 dpa from two different tilt angles: (c) α=0° and (d) α=10°.

Fig. 9: SEM micrographs of (a) the film obtained on sample corroded for 560 days at pH 6 and at 42°C in the reactor Osiris and zoom on (b) the outer and intermediate layers and on (c) the intermediate and inner layers.

Fig. 10: Chemical evolution of magnesium and silicon by EMPA in the aluminium matrix and in the aluminium hydroxide film obtained on a sample corroded for 560 days at pH 6 and at 42°C in the Osiris reactor.

Fig. 11: Schematic of the three steps of the proposed mechanisms of aluminium corrosion during corrosion tests coupled with ion irradiation.

Impact of ion and neutron irradiation on the corrosion of the 6061-T6 aluminium alloy

Sarah L'HARIDON-QUAIREAU, Kimberly COLAS, Bénédicte KAPUSTA, Bénédicte VERHAEGHE
DES-Service d'Etude des Matériaux Irradiés, CEA, Université Paris-Saclay
F-91191, Gif-sur-Yvette – France

~~Sylvie DELPECH~~
~~IJCLab, Paris-Saclay University~~
~~Paris – France~~

Marie LOYER-PROST, Gaëlle GUTIERREZ
DES-Service de Recherche de Métallurgies Physiques, CEA, Université Paris-Saclay
F-91191, Gif-sur-Yvette - France

Dominique GOSSET
DES-Service de Recherche de Métallurgies Appliquées, CEA, Université Paris-Saclay
F-91191, Gif-sur-Yvette – France

Sylvie DELPECH
IJCLab, Paris-Saclay University
Paris – France

Corresponding author: S. L'HARIDON-QUAIREAU, sarah.quaireau@laposte.net

HIGHLIGHTS:

- Ion irradiation dehydrates aluminium hydroxide (boehmite and bayerite).
- Ion irradiation induces microstructure changes and voids in aluminium hydroxide.
- Neutron and ion irradiations increase aluminium alloy corrosion.
- Neutron irradiation causes silicon enrichment of aluminium hydroxide.

ABSTRACT: (300 MOTS MAX)

In nuclear research reactors, aluminium alloys are corroded and an aluminium hydroxide film covers their surface. Defects created by neutron irradiation can have a detrimental effect on this corrosion. In this study, two ion irradiations are performed on a 6061-T6 aluminium alloy. The first irradiation experiment aims at studying the effect of metal matrix irradiation on aluminium corrosion. The second irradiation experiment aims at studying the effect of hydroxide irradiation on aluminium corrosion. The displacement per atom is at most 2.5 dpa in the hydroxide film irradiated with Al ions of 1.2 and 5 MeV and at most 8 dpa in the aluminium matrix irradiated with Al ions of 1.8 MeV (calculated with SRIM). The effects of ion irradiation are investigated by TEM and SEM observations. The crystalline structure of aluminium hydroxide is studied by electron diffraction, µ-Raman and X-rays diffraction. In the aluminium hydroxide film (composed of a mix of bayerite, α-$Al(OH)_3$, and boehmite, γ-AlOOH, before irradiation), ion irradiation causes formation of voids and dehydrates the aluminium hydroxide (nanocrystallites of η-Al_2O_3 are observed in the irradiated film). In the aluminium matrix, irradiation increases density of dislocations and amorphizes dispersoids. After ion irradiation, samples are corroded at 70°C in 2.8L of demineralised water. The two irradiations increase aluminium corrosion.
The second part of this study is about samples corroded in the Osiris nuclear research reactor, in water at 42°C, with a pH of 6 and for 18 months. The aluminium hydroxide film observed on these samples has a layered microstructure composed of a compact inner layer, a thick intermediate layer and an outer layer of cuboid microcrystals. Silicon enrichment is observed in the inner layer. The effect of ion and neutron irradiation on aluminium corrosion is compared in this study and similarities are observed between ion and neutron irradiations.

KEYWORDS:
Aluminium hydroxide; Corrosion; Microstructure; Ion irradiation; Neutron irradiation.

1. INTRODUCTION

Aluminium alloys are used in Materials Testing Reactors (MTRs, nuclear research reactors) because of low activation, good mechanical properties and good neutron transparency. In particular, the aluminium alloy AA-6061-T6 is used for core structures and for fuel cladding [1–3]. In the aqueous coolant of reactor, aluminium alloys are corroded and an aluminium hydroxide film covers their surface. The thermal conduction of this aluminium hydroxide is sufficiently low (~2 W/m/K [4]) to degrades the heat exchange between the core components and the coolant, it could lead to a local overheating of core components. As a result, the study of aluminium alloys corrosion is important for safe operation of MTRs. In this regard, aluminium alloy corrosion tests were performed in MTRs in the literature [3,5–12]. In these studies, the authors characterised the crystalline structure of the aluminium hydroxide by X-Ray Diffraction

(XRD) and measured the thickness of the hydroxide film developed under neutron irradiation. The objective of this paper is to compare neutron and ion irradiation effects on aluminium samples.

The ion irradiation experiments are performed at the JANNuS platform (Joint Accelerators for Nanoscience and Nuclear Simulation), in CEA Paris-Saclay, in France. Contrary to tests performed in MTRs, ion irradiation allows to perform corrosion tests in various conditions, and thus to lead parametric studies, without dealing with the problems of radioactive samples (the matter is not activated by low energy ion irradiation). In addition, ion irradiation allows to obtain high irradiation doses in a very short time.

In this study, we perform corrosion tests coupled to ion irradiation in order to irradiate the aluminium hydroxide film and the aluminium matrix. After ion irradiation, the irradiated film and the irradiated aluminium matrix are characterized and observed by SEM and TEM. Their crystalline structure is studied using Selected Area Electron Diffraction (SAED) performed in a TEM, µ-Raman, and X-rays diffraction (XRD). The neutron irradiation is realized in the Osiris reactor in CEA Saclay, in France (French Atomic Energy Commission). The microstructure of the film is observed by SEM, its chemical composition is investigated using Electron Probe Micro-Analysis (EPMA) and its thickness is measured on a cross-section of the samples. These results are compared to the samples corroded in a corrosion loop with no irradiation in order to highlight the effect of neutron irradiation on aluminium corrosion. Finally, the samples after ion irradiation are compared to the neutron-irradiated samples in order to assess the relevance of using ion irradiation to study aluminium corrosion for nuclear reactor application.

2. EXPERIMENTAL METHODS AND SAMPLES

In order to compare ion and neutron irradiations, three studies are leaded in this paper. These studies are summarized in Fig. 1.

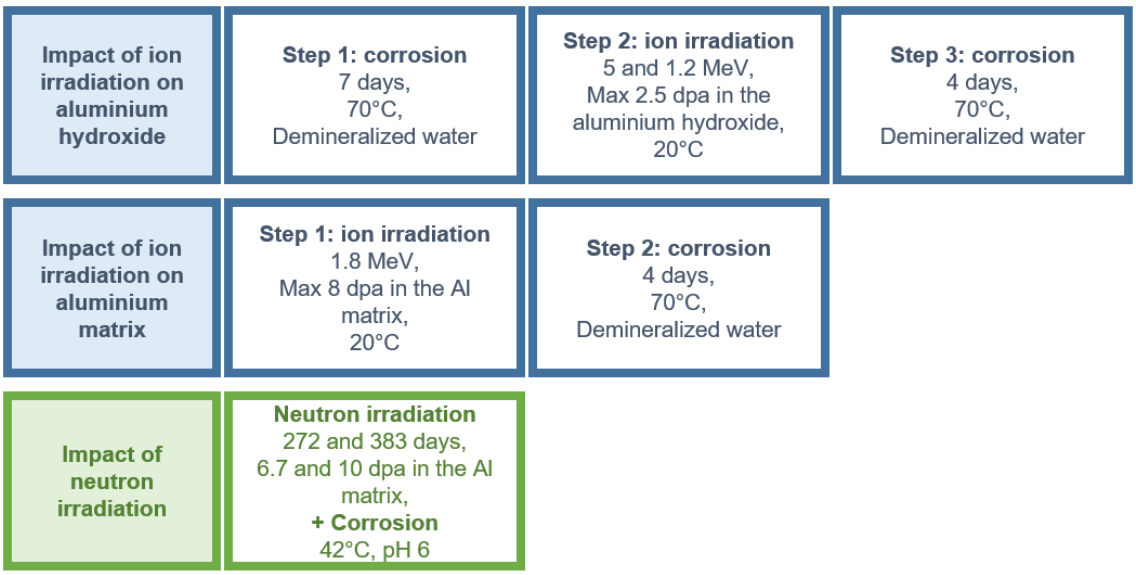

Figure 1: Purpose, step and conditions of irradiation of the three studies performed in this paper.

Samples and preparation:

The samples are in AA-6061-T6 aluminium alloy. The chemical composition of this alloy is presented in Table 1. The T6 treatment was obtained by solution annealing at 550°C for 4h following by water quenching and tempering at 175°C for 4h. This thermal treatment is performed to improve the mechanical properties of the material [18]. The samples are coupon-shaped with dimensions of 10 mm x 10 mm x 1 mm. They have a non-finished surface: the samples are obtained by milling and they are not polished in order to have a representative surface such as the one Material Testing Reactors components would have [19].

Table 1: Chemical composition of the 6061-T6 aluminium alloy used.

Element	Mg	Si	Cu	Fe	Cr	Mn	Al
Content (wt.%)	1.15	0.61	0.25	0.2	0.2	0.03	Balance

Ion irradiation experiments:

The conditions of the ion irradiations are described in Table 2.

Table 2: Conditions of the ion irradiations.

Irradiation N°	Target	Al ions energy	Flux	Dose	Time	Temperature
		MeV	Ions/cm²/s	ions/cm²	Hours	°C
1	Aluminium hydroxide	5	$5.3\pm1.2*10^{11}$	$9.5\pm2.3*10^{15}$	5h	20
		1.2	$5.3\pm1.2*10^{11}$	$7.6\pm2.3*10^{15}$	4h	20
2	6061-T6 metal matrix	1.8	$6\pm1.5*10^{11}$	$7.6\pm1.9*10^{15}$	4h	20

The ion irradiation experiments are performed at the JANNuS platform (Joint Accelerators for Nanoscience and Nuclear Simulation), in CEA Paris-Saclay, in France. The first ion irradiation is performed on aluminium hydroxide. Prior to irradiation, aluminium alloy samples are corroded in autoclave at 70°C, for 7 days and in 2.8L of demineralised water (Fig. 1). The temperature of 70°C is chosen because this is relevant of core structures in MTRs. The thickness of the obtained hydroxide film is about 4 µm. After the corrosion test, ion irradiation is performed: the hydroxide film is irradiated with Al ions under vacuum. The energy of the Al ions used is 5 MeV and then 1.2 MeV in order to irradiate the hydroxide film on all its thickness. A SRIM calculation (using the Stopping and Range of Ions in Matter software [21] with the mode “full damage

cascade") indicates the damage is at most 2.5 dpa (displacement per atom) and 1.5 dpa on average in the aluminium hydroxide film (Fig. 2.a). For the SRIM calculation, the threshold displacement energies used are 20 eV and 50 eV for the aluminium and oxygen sublattice, respectively [22]. After ion irradiation experiment, the irradiated samples are corroded a second time in autoclave in order to study the impact of ion irradiation on the corrosion kinetics. For this corrosion experiment, the conditions are: 4 days, 70°C and 2.8 L of demineralised water.
The second ion irradiation is performed on the metal aluminium matrix. Metal samples are irradiated with Al ions with an energy of 1.8 MeV. A SRIM calculation indicates the damage is at most 8 dpa in the aluminium matrix (Fig. 2.b, obtained with the mode "full damage cascade"). For the SRIM calculation, the aluminium threshold displacement energy used is 16 eV [23,24]. After the ion irradiation, the samples are corroded at 70°C, for 4 days and in 2.8L of demineralised water in order to evaluate the influence of the irradiation on aluminium alloy corrosion. During the two irradiations, the temperature is monitored using a thermocouple in contact with a sample, the maximum temperature is 20°C for the two irradiation experiments. For each irradiation, four samples are irradiated together on one face and for each corrosion condition, three samples are used.

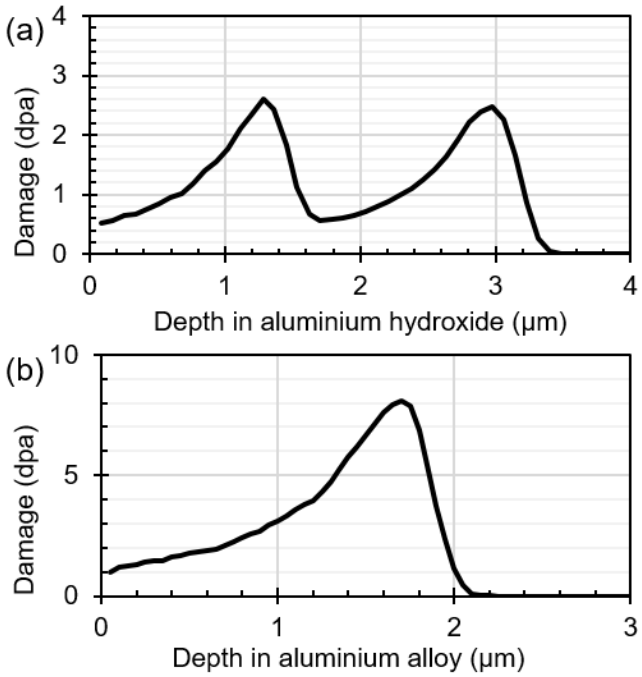

Figure 2: Damage profiles (dpa: displacement per atom) created by (a) Al ions with successive energies of 5 MeV and then 1.2 MeV irradiating the aluminium hydroxide film and by (b) Al ions with an energy of 1.8 MeV irradiating the aluminium matrix, profiles calculated by SRIM with the mode "full damage cascade" [21].

Autoclave:

Coupled to ion irradiations, corrosion tests are performed using an autoclave made of 316L steel. The inside of the autoclave is covered with polytetrafluoroethylene in order to avoid contamination of the samples surface by iron from the autoclave. The sample holder is in zirconium alloy in order to limit galvanic coupling between aluminium alloy samples and the sample holder. Before performing the corrosion tests, helium is injected in the autoclave in order to deoxygenate the corrosive media. The pressure in the autoclave is imposed by the vapour pressure (i.e. the pressure is 0.5 bar relative at 70°C).

Characterization techniques:

The aluminium hydroxide is characterized using Scannttering Electron Microscopy (SEM, measurements of the film thickness in particular), Transmission Electron Microscopy (TEM, observation of the microstructure and analyses of its crystal structure by electrons diffraction), X-rays Diffraction analyses (XRD) and µ-Raman spectroscopy. In order to observe a cross section of the aluminium hydroxide film using a SEM, samples are embedded in a conductive resin and polished down to a 1 µm finish with diamond pastes. The thickness of the film is measured on a cross-section of the samples. For each sample, five micrographs of the film are taken at different locations with a SEM (*iT300* model from *JEOL)*. The thickness of the film is measured on these micrographs using the *ANALYSIS*™ software: 100 measurements are made on each micrograph. The average of these 500 measurements is taken as a result.
To characterize the samples at the nanoscale, Transmission Electron Microscopy is used (TEM: *TECNAI 3042* model from *FEI*, with an acceleration voltage of 200 kV and a length camera length of 865 mm for diffraction). TEM samples of the corroded materials are prepared with conventional Focused Ion Beam methods (FIB: *Auriga 40* model from *ZEISS*). A Pt deposit is added to the samples' surface to protect the hydroxide film during the TEM thin film preparation.
The crystalline phases of the aluminium hydroxide are studied using low-incidence X-ray diffraction (XRD) and µ-Raman spectroscopy. The X-rays diffractometer (*CPS120 –Curved Position Sensitive- detector from INEL*) is used with Cu-Kα1 radiation (Ge(111) monochromator, wavelength: 1.5406 angstrom) in an asymmetric configuration. The incident angle of the X-ray beam is 2°: in this configuration, the analysed depth is about 4 µm in Al metal and 4 µm in the hydroxides. The µ-Raman spectrometer (*InVia Reflex* from *Reinshaw)* is used with a green laser (wavelength: 532 nm) and at 5% of the spectrometer power (5% of 100mW, to limit hydroxide damage during the analyses). The µ-Raman analyses are performed on the cross-section of the embedded samples with an optical microscope with a magnification of 50x.

Corrosion in Materials Testing Reactor:

Samples in 6061-T6 are placed in the centre of the nuclear core of Osiris reactor (reactor located in CEA Saclay, in France) and they are corroded by the water circulating thought the core. The corrosion conditions are thus imposed by the nominal operating conditions of the reactor: temperature is 42°C, pH is 6 and coolant flow rate is 0.9 m /s. Samples are corroded for 272 and 383 days in total (the test is interrupted several times to perform analyses). The

maximum received dose of fast neutrons is 10^{22} n_f/cm^2 (E > 1 MeV) and the one of thermal neutrons is $6.5*10^{22}$ n_{th}/cm^2 (E = 0.025 eV) [25]. After corrosion in the reactor, the microstructure of the film is observed by SEM in a shielded cell in the LECI of the CEA Saclay, its chemical composition is investigated using Electron Probe Micro-Analysis (EPMA) and its thickness is measured on the cross-section of the samples observed with an optical microscope.

3. RESULTS

In this part, the effects of ion and neutron irradiations are described (microstructure, crystalline structure and evolution of thickness of the aluminium hydroxide film).

3.1 ION IRRADIATION OF ALUMINIUM HYDROXIDE

In this section, the effects of ion irradiation on aluminium hydroxide are studied. Samples are corroded at 70°C for 7 days and in 2.8L of demineralised water. Fig. 3.a presents a TEM micrograph of the unirradiated aluminium hydroxide film obtained on the samples surface. The film is composed of two main layers, an inner and an outer. The inner layer in contact with the aluminium matrix is compact. According to µ-Raman analyses, this layer is composed of nanometric boehmite (γ-AlOOH, the data from [26,27] are used to identify this phase). The outer layer in contact with the aqueous solution is composed of cuboid microcrystals. These microcrystals are observed on the samples surface as illustrated in Fig. 4.a. According to µ-Raman analyses, these microcrystals are well-crystallised bayerite (α-$Al(OH)_3$, the data from [26] are used to identify this phase. The µ-Raman analyses performed on the inner and the outer layers are compared to XRD analyses: the film is composed of a mix of boehmite and bayerite as seen by both techniques. A thin intermediate layer is present between the two main layers. This layer is composed of needle-like nanocrystallites as seen in Fig 3.a.

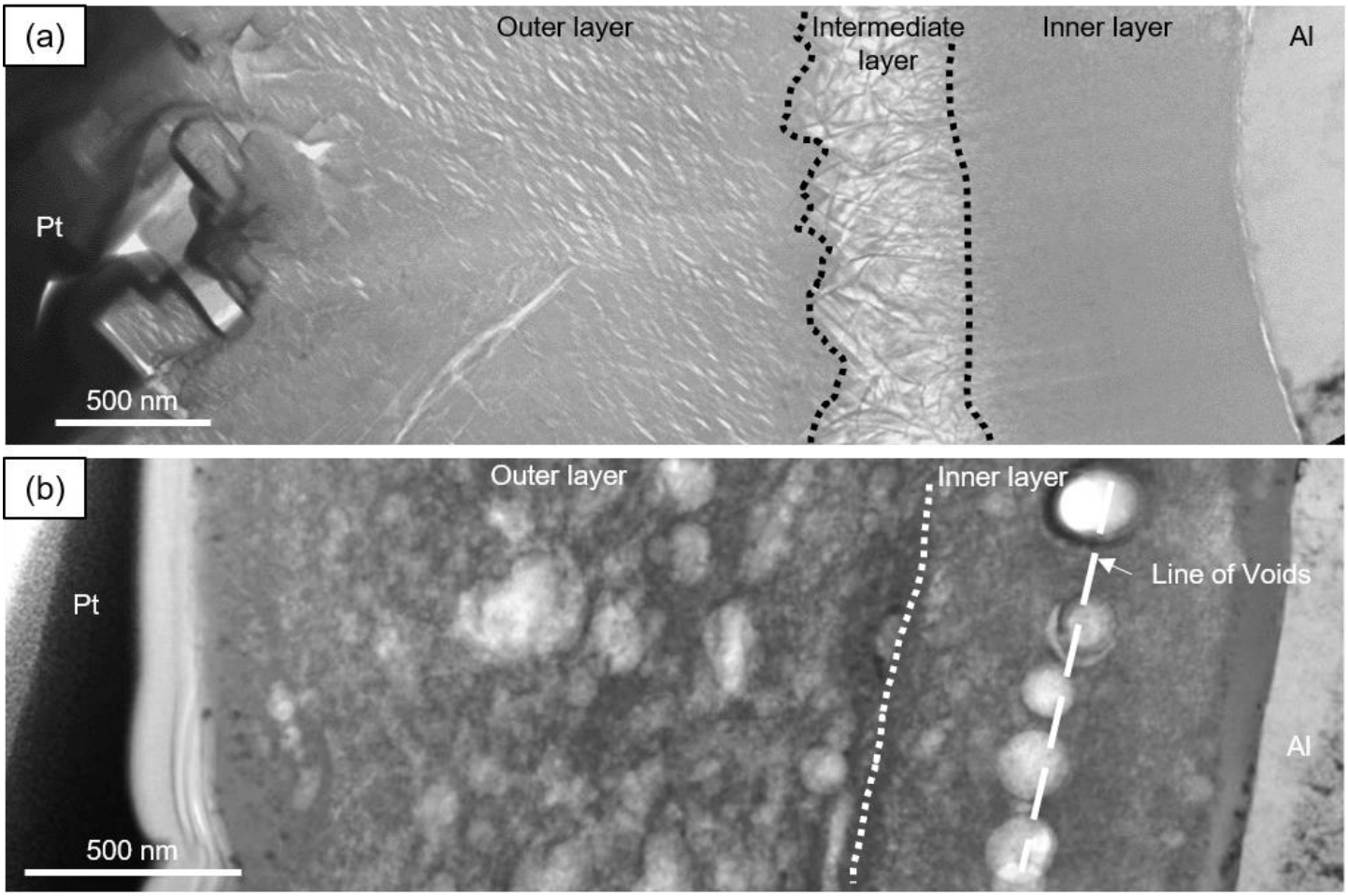

Figure 3: TEM micrographs of (a) a unirradiated film of aluminium hydroxide (obtained on samples corroded at 70°C, in 2.8L of demineralised water and for 7 days), (b) a film irradiated with Al ions of successive energies 5 MeV then 1.2 MeV.

After corrosion experiment, the aluminium hydroxide film is irradiated with Al ions of energies 5 MeV and 1.2 MeV, the two energies are used in order to irradiate the two main layers of the film. The damages are at most 2.5 dpa and 1.5 dpa on average (Fig. 2.a). Fig. 3.b presents a TEM micrograph of the irradiated film. The aluminium hydroxide is between the Pt deposit and the aluminium matrix. After ion irradiation, the distinction between the two former layers (inner and outer layers) is difficult to make and the thin intermediate layer cannot be observed as seen in Fig. 3.b. Voids are present in all the irradiated film. In particular, a line of voids is observed in the middle of the former inner layer. This line likely corresponds to the peak damage done by the Al ions in the inner layer. The presence of voids in ion irradiated oxides at room temperature was already observed [43] : the zirconia film present on ZrNb FIB samples presents some voids after irradiation at 1 and 10 dpa. In addition, a change of microstructure is observed in the hydroxide outer layer of our samples. After ion irradiation, cuboid microcrystals are not observed on the samples surface: as illustrated in Fig. 4.b, the former microcrystal are globular. This change of microstructure is similar to the observations done by Nabhan [10]: a film of boehmite (γ-AlOOH) was obtained during corrosion tests performed with samples in AlFeNi aluminium

alloy in 0.065L of solution at pH 5.2 for 11 days and at 140°C. The samples were then irradiated with Al ions of 1.6 MeV for 36 dpa. Before irradiation, needle-like nanocrystallites (size inferior to 0.5 µm) were observed on the samples surface. After ion irradiation, only spheroids were present on the samples surface (SEM observation).

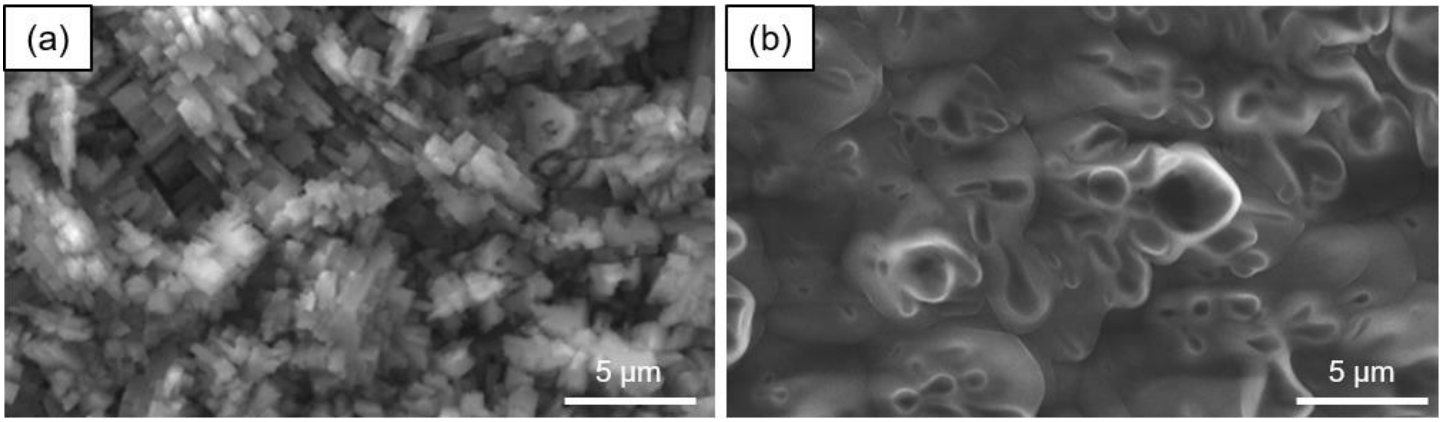

Figure 4: SEM micrographs of the samples surface: (a) unirradiated (obtained on samples corroded at 70°C, in 2.8L of demineralised water and for 7 days) and (b) irradiated with Al ions of successive energies 5 MeV then 1.2 MeV.

Selected Area Electron Diffractions (SAED) are performed on the inner layer and on the outer layer of the irradiated film. Similar diffraction patterns are observed in all the irradiated film, one of these patterns is presented in Fig. 5.a. Rings observed in Fig. 5.a indicate the presence of nanocrystallites. A dark field performed on a part of the ring of 1.40 Å is presented in Fig. 5.b: the nanocrystallites that have diffracted are in white. The electron diffraction pattern on Fig. 5.a can be attributed to a nanometric η-Al_2O_3 phase [28,29]. In the literature [29], this oxide phase comes from the thermal decomposition of bayerite and pseudo-boehmite at 200-650°C in vacuum. During irradiation, the thermal flux is low (0.2W/cm² for 1.2 MeV Al^+ and 0,8 W/cm² for 5 MeV Al^{2+}) and the maximal measured temperature of samples is 20°C. Considering the low oxide thickness (4 µm) on the 1mm thick alloy samples, even with the low thermal conductivity of the oxide, the temperature in the oxide is close to 20°C : this is confirmed by the 2°C thermocouple variation when switching off the ion beam. As a result, the presence of η-Al_2O_3 cannot be attributed to a high temperature. In addition, analyses are performed on the aluminium hydroxide exposed to the vacuum but protected from the irradiation: µ-Raman analyses and electron diffraction indicates the aluminium hydroxide is not dehydrated (traces of η-Al_2O_3 are not observed). As a result, the dehydration is not due to the vacuum but to the ion irradiation. In addition, when the irradiation starts, the pressure of the vacuum in the accelerator increases immediately from $133*10^{-8}$ Pa to $133*10^{-7}$ Pa: due to the ion beam, the former aluminium hydroxide is possibly decomposed into η-Al_2O_3 by releasing water. Unfortunately, the presence of η-Al_2O_3 could not be confirmed by a µ-Raman analysis: after irradiation, the laser light is strongly diffused by the oxide, which makes impossible to realize an accurate measurement. This type of problem is common with this aluminium oxide [30]. Also, phase

transitions in zirconium oxides under ion flux were already observed at room temperature on FIB samples taken in a corroded ZrNb alloy [43]. Therefore, the identified damages created by ion irradiation in the aluminium hydroxide are: creation of voids, change of microstructure and formation of η-Al_2O_3 nanocrystallites.

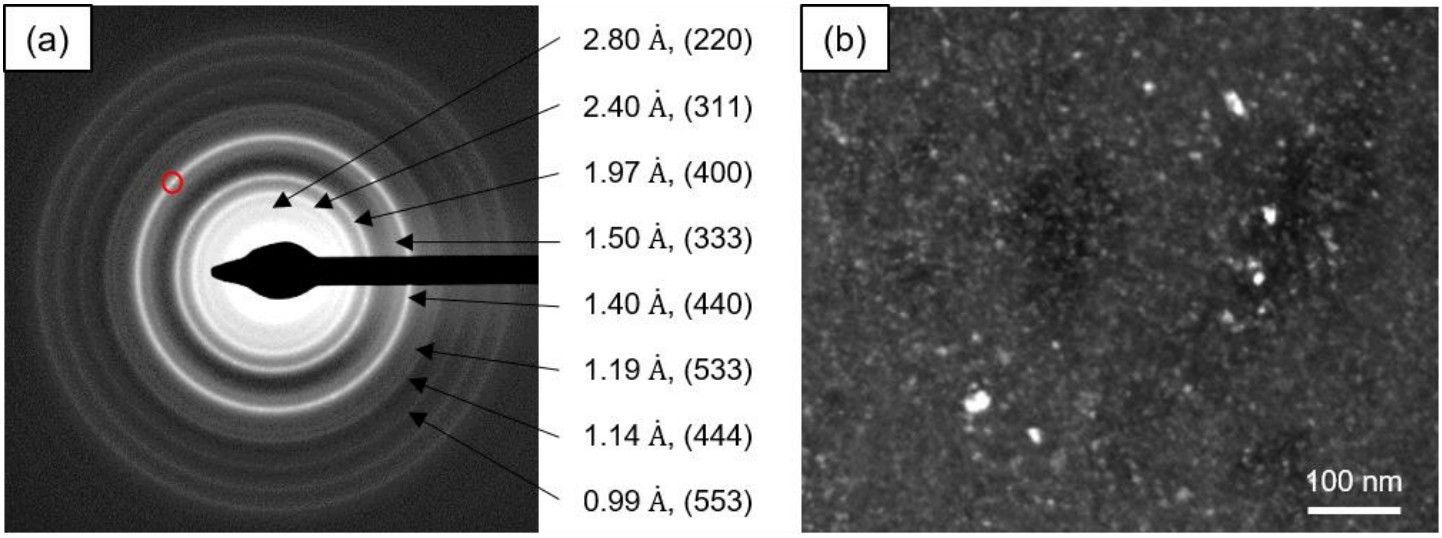

Figure 5: (a) SAED pattern obtained on the film irradiated with Al ions of successive energies 5 MeV then 1.2 MeV (the planes corresponding to the d-spacing come from [28,29]) and (b) Dark Field micrograph of the nanocrystallites which have diffracted in the red circle in Fig 5.a(TEM).

Irradiated samples are re-corroded at 70°C, for 4 days and in 2.8L of demineralised water in order to follow the evolution of the damage in an aqueous medium. After ion irradiation and re-corrosion, the aluminium hydroxide film has the same microstructure than the unirradiated film presented in Fig. 3.a: it is composed of a compact inner layer of boehmite and an outer layer of cuboid microcrystals (similar to the ones observed in Fig. 4.a). A thin intermediate layer of needle-like nanocrystallites is present between these two main layers and voids are not observed (TEM observation). The crystalline structure, analysed by µ-Raman, is also the same for the unirradiated samples and for the irradiated and re-corroded samples: the inner layer is composed of boehmite (γ-AlOOH) and the outer layer, of bayerite (α-$Al(OH)_3$, ~~the crystalline structure is analysed by µ-Raman~~). Traces of η-Al_2O_3 are not detected by SAED. As a result, the film is fully rehydrated and the damage due to ion irradiation is not still present in the aluminium hydroxide film. However, ion irradiation has an influence on the thickness of the film. Fig. 6.a presents the thickness of the inner and outer layers and Fig. 6.b is about the mass gain of samples. The points on the curves represent the average of measurements performed on the three samples. For 11 days (which is the total corrosion time, 7 days before irradiation and 4 days after), the total average thickness of the film and the average mass gain are the most important on irradiated samples: ion irradiation increases aluminium corrosion. In addition, for 11 days, the inner layer composed of boehmite is thicker and the outer layer composed of bayerite is thinner on irradiated samples than on un-irradiated samples. Thus, ion irradiation facilitates the formation of boehmite (γ-AlOOH) to the detriment of bayerite (α-$Al(OH)_3$). This

observation is due to the process of rehydration of the irradiated aluminium hydroxide: according to Aad [31], at a temperature above 50°C (this is 70°C in this study), alumina obtained from dehydrated aluminium hydroxide is rehydrated in water to form boehmite. As a result, after irradiation and re-corrosion, the new inner layer contains, in part, the two former layers. In order to compete this study on the effect of ion irradiation on aluminium corrosion, the metal aluminium matrix is irradiated and then corroded as described in the following section.

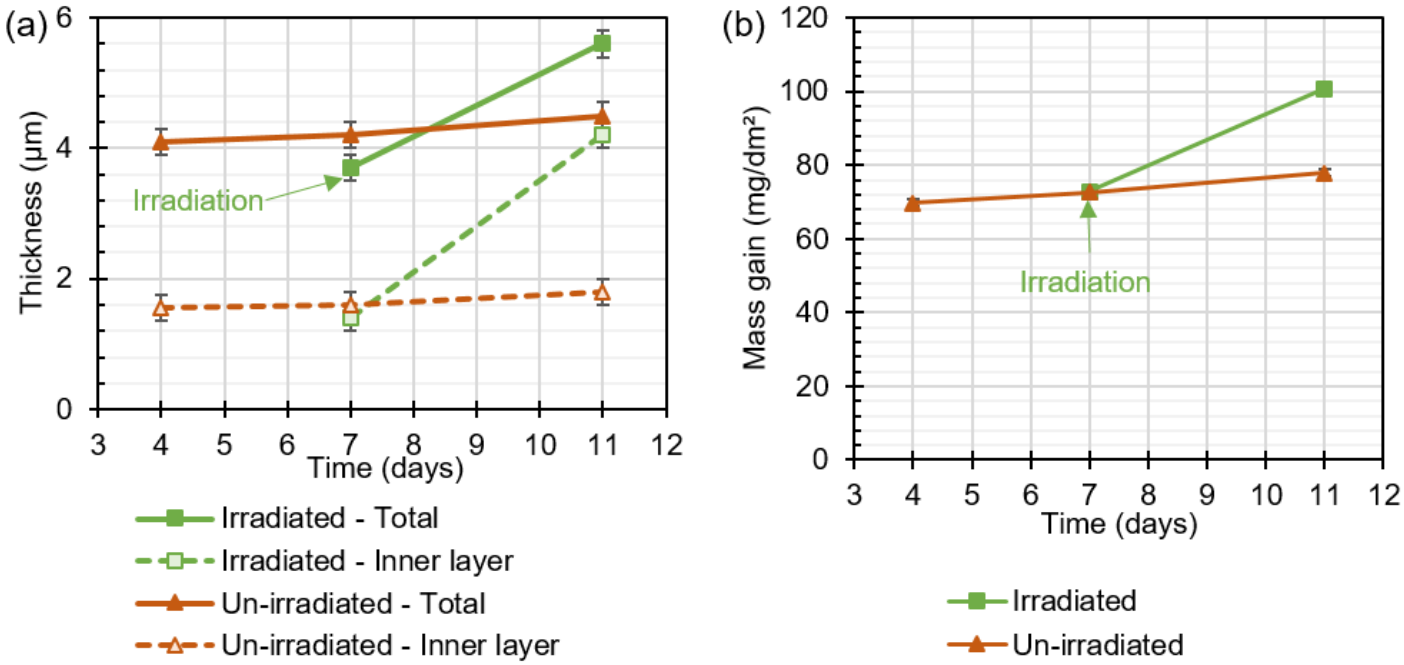

Figure 6: (a) Average thickness of the aluminium hydroxide film and (b) average mass gain of the samples unirradiated and irradiated with Al ions of successive energies 5 MeV then 1.2 MeV (the term “irradiation” on the graphics indicates when the ion irradiation occurs).

3.2 ION IRRADIATION OF THE ALUMINIUM MATRIX

Uncorroded samples in 6061-T6 aluminium alloy are irradiated with Al ions of an energy 1.8 MeV. Samples are then corroded in order to evaluate the impact of the damage created in the aluminium matrix on its corrosion behaviour. Fig. 7 presents two micrographs of un-irradiated matrix (Fig. 7.a) and irradiated matrix (Fig. 7.b). In the unirradiated matrix (Fig. 7.a), the grain size is between 100 and 200 nm on average, the minimum size is ~50 nm and the maximal is ~300 nm. In the irradiated matrix (Fig. 7.b), two areas are observed. The boundary between area 1 and area 2 is placed from SRIM calculations (as described in Fig. 2) as the start of the implantation peak. ~~depending on the grain size.~~ In area ❶, where the damage is between 1 dpa and 5 dpa, the grain boundaries are well defined and the grain size is the same than in the unirradiated matrix presented in Fig. 7.a. In area ❷, at the maximum damage zone of 8 dpa, it is difficult to discern one grain from another and the grain size cannot be measured. This

observation is due to a high dislocation density: the ion irradiation increases the number of dislocations in the material. This observation has already been described in the literature [10]: samples in AlFeNi aluminium alloy were irradiated with Al ions at 18 dpa, the number of dislocations increased in the irradiated zone of the aluminium alloy. In addition, using the defocus technique (large defocus in both under and over focus ranges) with a high magnitude, voids are not observed in the irradiated matrix. This observation agrees with the literature for ~~similar~~ ion irradiations on 6061-T6 alloy up to ~~at 10~~ 30 dpa [~~10,~~32].

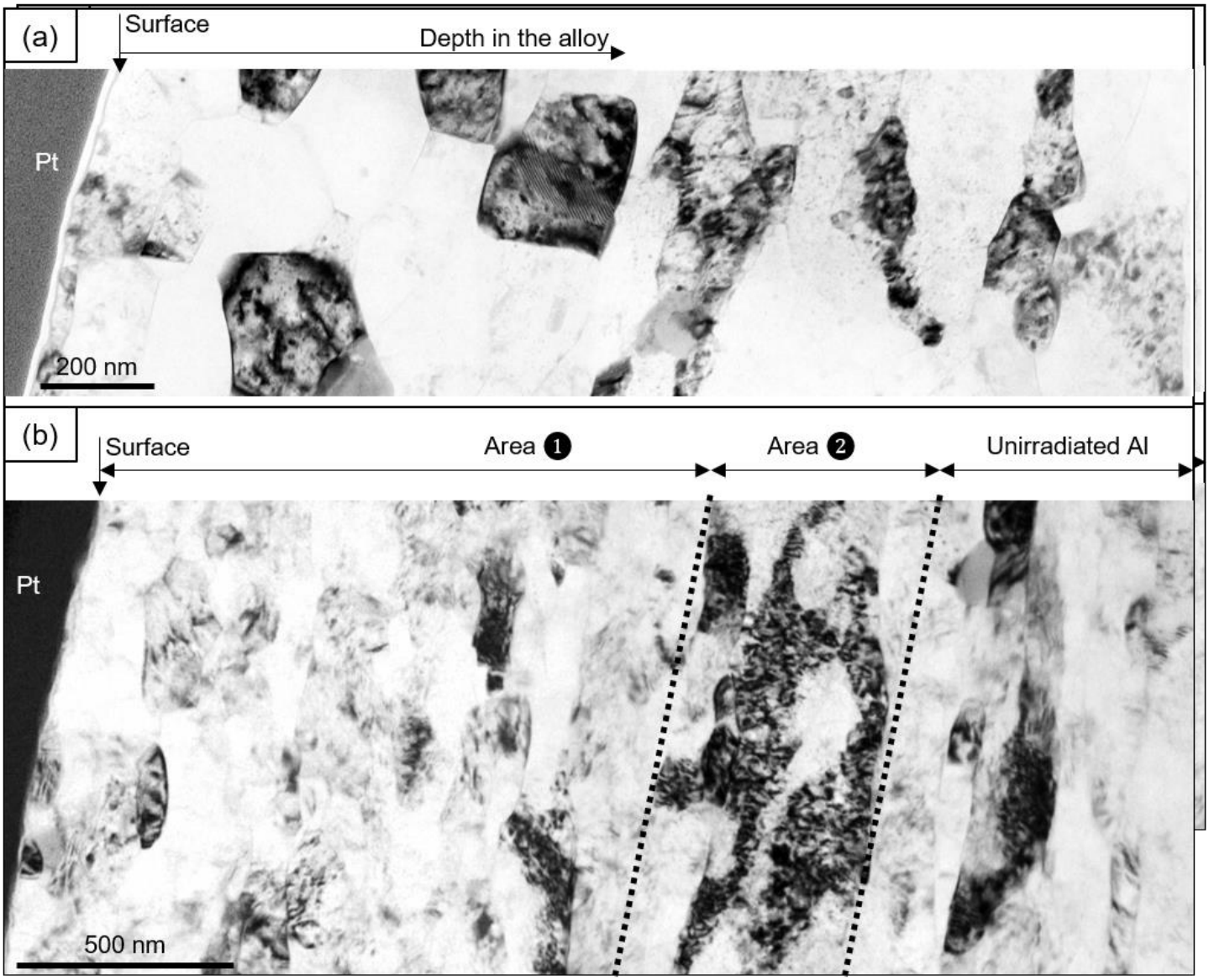

Figure 7: TEM micrographs of (a) an unirradiated matrix of 6061-T6 aluminium alloy and (b) irradiated matrix with Al ions of 1.8 MeV. The areas ❶ and ❷ correspond respectively to the area irradiated at 1-5 dpa (displacement per atom) and to the most irradiated area at 8 dpa. The boundary between area 1 and 2 is the start of the implantation peak (peak calculated with SRIM in Fig. 2.b).

Additional TEM observations are performed on the dispersoids present in the 6061-T6 aluminium alloy. The dispersoids size is between 50 and 200 nm. There are two families of dispersoids depending on their chemical composition: the first one is composed of iron, manganese and chromium, the second is composed of silicon and magnesium (chemical analyses performed with an EDX during the TEM observations). These two types of dispersoids are common in 6061-T6 aluminium alloy: they are Mg_2Si and Al(Cr,Mn,Fe)Si [33,34]. Fig. 8 presents a dispersoid observed from two angles in the unirradiated matrix (Fig. 8.a and b) and two dispersoids observed from different angles in the matrix irradiated at 14 dpa (Fig. 8.c and b, dispersoids located in the area ❷ in Fig. 7.b). In the unirradiated matrix, the contrast of the dispersoid changes with the tilt angle: the dispersoid is transparent with an observation angle of α=0° (Fig. 8.a) and it is grey/black with α=10° (Fig. 8.b). This contrast variation indicates the dispersoid is crystalline. In the matrix irradiated at 14 dpa, the contrast of the dispersoids does not change with the observation angle (Fig. 8.c and d, the dispersoids are observed from several angles between 0 and 20° and variation of contrast is not observed with any angle). The absence of variation of contrast indicates the dispersoids are amorphous [35]. Ion irradiation thus causes an amorphisation of the dispersoids for the conditions used in this study. This observation agrees with the literature for similar ion irradiations [32]: an amorphisation of dispersoids is observed during ion irradiation performed on 6061-T6 aluminium alloy with W ions for 10-30 dpa at 20°C. In addition to the dispersoids, other nanometric phases are present in the 6061-T6 aluminium alloy, the influence of ion irradiation on these phases are the subjects for several studies [32,36] and are not studied during this work.

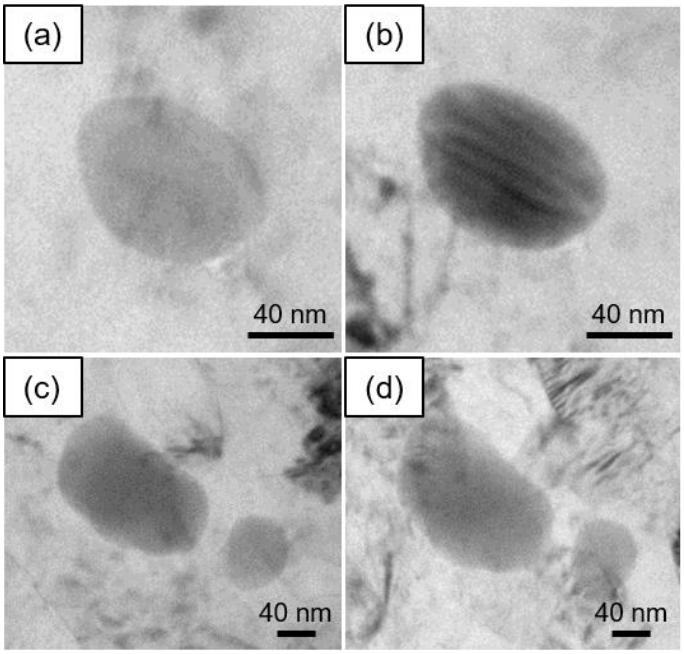

Figure 8: TEM micrographs: dispersoid observed in the unirradiated matrix from two different tilt angles: (a) α=0° and (b) α=10°, and two dispersoids observed in the matrix irradiated at 14 dpa from two different tilt angles: (c) α=0° and (d) α=10°.

After the ion irradiation, the samples are corroded at 70°C, for 4 days and in 2.8L of demineralised water. A film of aluminium hydroxide is present on the corroded samples. Microstructure of the film is the same on unirradiated samples and on irradiated samples: the film is composed of two main layers, an inner and an outer, similar to the ones described in Fig. 3.a and in Section 3.1. The film has also the same crystalline composition on un-irradiated and irradiated samples (mix of bayerite and boehmite, analyses performed by XRD). Thicknesses of the inner layer and the outer layer of the film are respectively 1.63 ± 0.2 µm and 2.65 ± 0.2 µm on average on un-irradiated samples, and 1.98 ± 0.2 µm and 3.06 ± 0.2 µm on average on irradiated samples. Ion irradiation causes thus an increase of thickness of the aluminium hydroxide film: the irradiated samples are more corroded than the unirradiated ones. This increase of aluminium corrosion could be due to the amorphisation of dispersoids and to the increase of dislocation density. Similar observations have been made in corroded irradiated AlFeNi aluminium alloy [10]: uncorroded samples were irradiated with Al ions for 18 dpa and were then corroded at 140°C, for 16 days in 0.065L of solution at pH 5.2. The irradiated samples were more corroded. In order to compete this study about the effect of irradiation on aluminium corrosion, samples are corroded in a MTR under neutron irradiation.

3.3 Corrosion of the 6061-T6 aluminium alloy in Materials Testing Reactor

Samples in 6061-T6 aluminium alloy have been irradiated and corroded in the Osiris nuclear reactor of the French Atomic Energy Commission (CEA) in Saclay, in France. After irradiation experiments in the Osiris reactor, the film obtained on the samples surface is characterised in hot cells. Fig. 9.a presents an SEM observation of the film. For this observation, a sample is broken in two pieces and the film is observed on the fractured side of the sample in order to highlight the layered microstructure of the film. The film is composed of three layers. The inner layer is brittle (Fig. 9.a and c): numerous cracks are present in all the layer. The thickness of this layer is ~5 µm. The intermediate layer is the thickest of the three, its thickness is ~13 µm. This layer looks micro-porous (Fig. 9.a, b and c). The outer layer is composed of cuboid microcrystals (Fig. 9.a and b). These microcrystals are similar to the ones observed on the samples surface during unirradiated corrosion tests (Fig. 4.a). The outer layer is not observed on all the samples surface: desquamations of the hydroxide film are observed (SEM observation of the film surface).

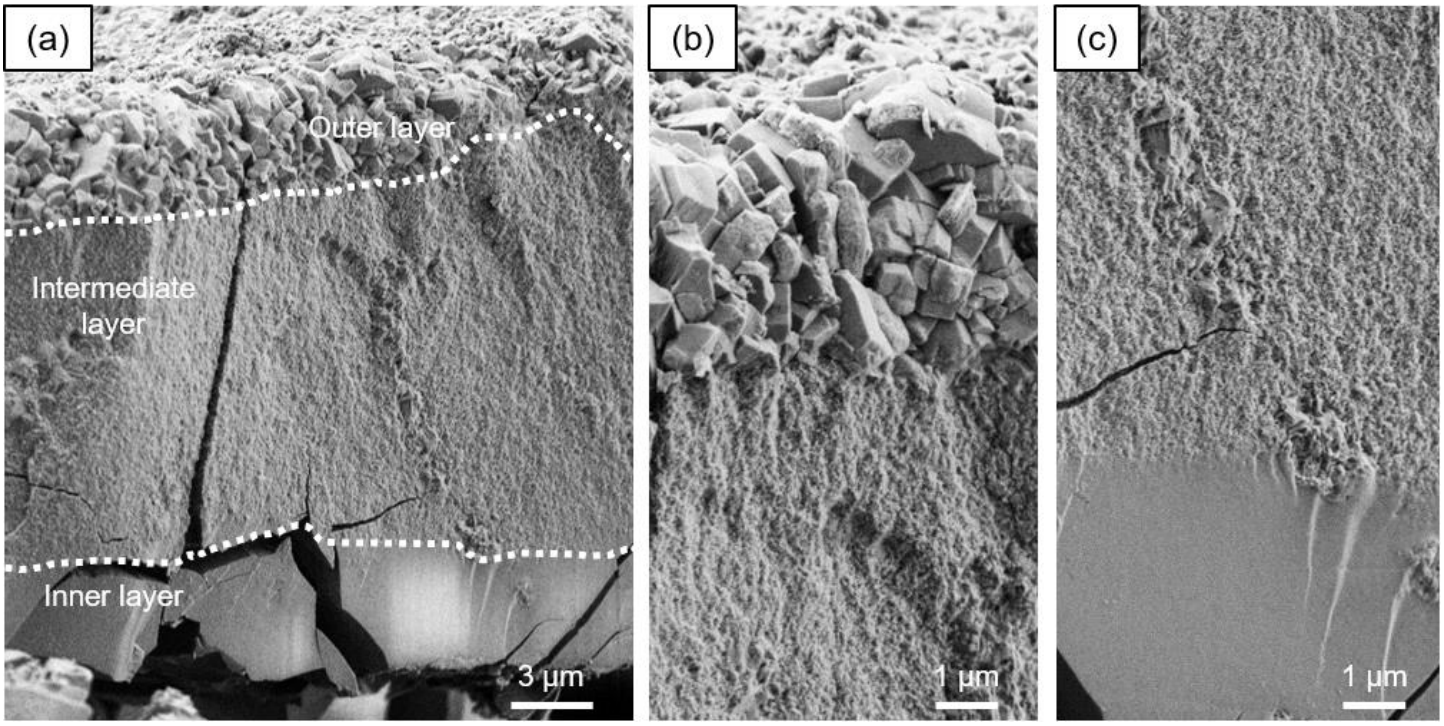

Figure 9: SEM micrographs of (a) the film obtained on sample corroded for 560 days at pH 6 and at 42°C in the reactor Osiris and zoom on (b) the outer and intermediate layers and on (c) the intermediate and inner layers.

The chemical composition of the film is analysed by EPMA. For this analysis, a sample is embedded in a tin-bismuth mixture and then polished down to a 1 µm finish with diamond past. The film is composed on average of 50-55 wt. % of aluminium and 40-45 wt. % of oxygen. Silicon and magnesium are also observed in the film (Fig. 10). In particular, the film is enriched in silicon on a depth of 5/6 µm near the aluminium matrix. This depth corresponds to the thickness of the inner layer: this indicates that only the inner layer of the film is enriched with silicon. Silicon enrichment is not observed for unirradiated samples. This enrichment could be due to the transmutation of aluminium in silicon due to thermal neutrons following the reactions (2) and (3) [37,38]:

$$^{27}_{13}Al + {}^{1}_{0}n \xrightarrow{(n,\gamma)} {}^{28}_{13}Al \quad (2)$$

$$^{28}_{13}Al \rightarrow {}^{28}_{14}Si + e^{-} \quad (3)$$

Silicon enrichment of the film had already been observed during corrosion tests performed in MTR [10,39]. Magnesium content decreases from 0.9 wt. % in the alloy to 0.1 wt. % from a depth of 5/6 µm in the film. Magnesium is thus present only in the inner layer of the film and the decreasing profile of magnesium content indicates a release of this chemical element in solution after a diffusion through the film. This profile agrees with the literature: during corrosion of Mg-containing aluminium alloy, a magnesium release in solution had already been observed during unirradiated corrosion tests [3,20,39] and in an aqueous medium at a pH of 6, the stable form of

the oxidised magnesium is the aqueous ion Mg^{2+} according to the corresponding Pourbaix diagram [40].

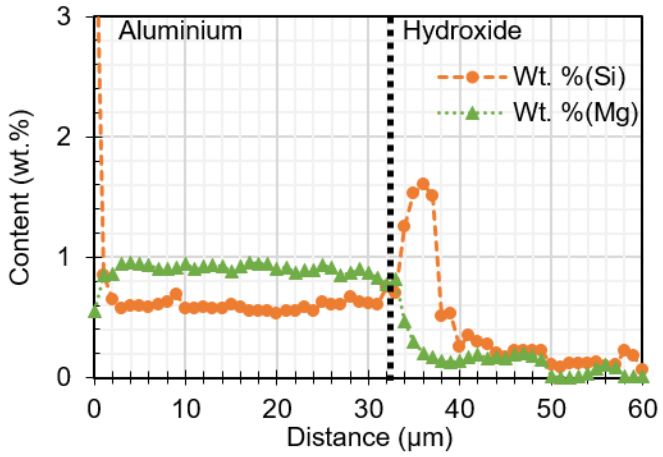

Figure 10: Chemical evolution of magnesium and silicon by EMPA in the aluminium matrix and in the aluminium hydroxide film obtained on a sample corroded for 560 days at pH 6 and at 42°C in the Osiris reactor.

In order to follow the thickness of the film during corrosion test in the Osiris reactor, samples are embedded in an epoxy resin and then polished down to a 1 µm finish with diamond past. The thickness of the film is measured on a cross section of the samples observed with an Optical Microscope. Table 3 summarizes the results of this examination performed on two samples (the displacements per atom due to the fast neutrons flux in the aluminium matrix are calculated based on the formula and the observation of Farrell et al. [6]). In addition, in order to highlight the effect of neutron irradiation on aluminium corrosion, these results are compared to samples corroded in a corrosion loop with recirculating water [41]. The loop allowed a renewal of the aqueous solution: after a passage in front of the sample at very low flow rate, the water was cleaned by filters and then reinjected in the loop. The film is five time thicker on samples corroded in the Osiris reactor than in the corrosion loop: neutron irradiation increases aluminium corrosion. The effect of neutron irradiation on aluminium corrosion is thus very strong. The observations performed on samples corroded in the Osiris rector (layered microstructure of the film, silicon enrichment and increase of aluminium corrosion) allows us to compare neutron and ion irradiations.

Table 3: Thickness of the film measured on samples corroded in the reactor Osiris and in a corrosion loop [41]

Sample id	Corroded in	Time	Temperature	pH	Flow rate	Dose of fast neutrons	Displacement per atom in the aluminium matrix	Dose of thermal neutrons	Thickness of the film

		days	°C		m/s	n/cm² (E > 1 MeV)	Dpa	n/cm² (E = 0.025 eV)	µm
N°1-Osi	Osiris reactor	272	42	6	0.9	$4.65*10^{21}$	6.7	$3.2*10^{22}$	13.5 ± 2.0
N°2-Osi	Osiris reactor	383	42	6	0.9	$6.8*10^{21}$	10	$4.0*10^{22}$	14.0 ± 1.4
N°1-Loop [41]	Corrosion loop	279	50	5.7	-	-	-	-	2.1 ± 0.3
N°2-Loop [41]	Corrosion loop	346	50	5.7	-	-	-	-	2.5 ± 0.3

4. DISCUSSION

Corrosion tests coupled with ion irradiations and corrosion experimentations performed in nuclear reactor are compared in this section. In addition, the observations performed on the ion irradiated samples allow us to propose corrosion mechanisms associated to ion irradiation.

4.1 COMPARISON BETWEEN ION IRRADIATION AND NEUTRON IRRADIATION

Some similarities are observed between ion and neutron irradiations. Films formed in nuclear reactor and obtained after ion irradiation and re-corrosion have similar crystalline structure. Indeed, at 70°C, the aluminium hydroxide film irradiated with Al ions and then re-corroded is composed of a mix of boehmite (γ-AlOOH) and bayerite (α-$Al(OH)_3$), and the main crystalline phase is boehmite. For a similar temperature (70/90°C), the film obtained in Materials Testing Reactors (MTRs) has the same crystalline structure (i.e. the main crystalline phase in the XRD patterns is boehmite with traces of bayerite) [5,9,39]. In addition, the film has a similar layered microstructure after ion irradiation and re-corrosion (cf. Section 3.1), and during corrosion tests with neutron irradiation (Fig. 9). The two types of irradiation increase aluminium corrosion and accelerate the aluminium hydroxide growth on the samples surface (cf. Fig. 6 and Section 3.3). Because of these similarities, ion irradiation can be used during un-activated corrosion tests in corrosion loops or in autoclave in order to be closer to the conditions found in MTRs. However, silicon enrichment is observed in the film obtained in nuclear reactor (cf. Fig. 10), this enrichment is not observed during unirradiated corrosion tests. Silicon ions can be used during ion irradiation in order to simulate the silicon enrichment in the film.

Nevertheless, in this study, we can observe some limitations to the use of ion irradiation to simulate the damage created by the fast neutron flux in reactor. Ion irradiation leads to a dehydration of the aluminium hydroxide. The damage due to this dehydration (nanocrystallites of η-Al_2O_3) may not be observed in aluminium hydroxide irradiated in a nuclear core (SAED should be performed in the samples corroded in the Osiris reactor to answer to this incertitude). In addition, to irradiate the aluminium hydroxide film, the corrosion tests are interrupted, the samples are exposed to air during the break of corrosion tests. Wintergerst observed an effect of breaks during corrosion test: the hydroxide thickness is less important during corrosion tests with breaks than without break [3]. It means the thickness measured in this study may be underestimated because of the interruptions to irradiate the aluminium hydroxide (cf. Section 3.1).

4.2 GROWTH MECHANISMS OF ALUMINIUM HYDROXIDE DURING CORROSION TESTS COUPLED TO ION IRRADIATION (IRRADIATION OF THE ALUMINIUM HYDROXIDE FILM)

Mechanisms of aluminium corrosion have been studied in the literature without irradiation [39,42]. Based on these mechanisms and with the observations done in Section 3.1, the following mechanisms associated with ion irradiation ~~can be~~are proposed below and summarized in ~~(~~Fig. 11~~)~~. It should be noted that the proposed mechanisms apply to ion irradiation and not to neutron irradiation or to in-core irradiation in general. ~~:~~

1. Before ion irradiation, due to corrosion tests, aluminium matrix is oxidised at the interface hydroxide-metal, this oxidation reaction is accompanied by the reduction of water and dioxygen, and the production of OH hydroxide groups. A part of this oxidised aluminium reacts with the OH hydroxide groups to form boehmite (γ-AlOOH), the inner layer, at the hydroxide-metal interface (internal growth). The rest of the oxidised aluminium diffuses through the film and is released as ions Al(III) in the corrosive solution. These ions then precipitate on the samples surface to form bayerite (α-$Al(OH)_3$), the outer layer (external growth). (Fig. 11.a).
2. During ion irradiation, the former aluminium hydroxide is dehydrated and change of microstructure is observed (Fig. 11.b).
3. After irradiation, during the re-corrosion of the samples, the irradiated film is a part of the new inner layer: at 70°C, alumina obtained from dehydrated aluminium hydroxide is rehydrated by water to form boehmite [31], the crystalline phase of the inner layer. Due to the non protective quality of this irradiated film, the matrix is oxidised and aluminium is released in solution. A new outer layer is formed by the precipitation of aluminium ions in solution on the samples surface (Fig. 11.c). The proposed global reactions are :

   $2AlO(OH) \rightarrow Al_2O_3 + H_2O$ and

   $2Al(OH)_3 \rightarrow Al_2O_3 + 3H_2O$

   When the samples are reintroduced in the autoclave containing water for the corrosion test after irradiation, the Al_2O_3 layer is firstly hydrated to AlO(OH) (formation of boehmite, the most thermodynamically stable specie) and the corrosion is observed

again with the formation of $Al(OH)_3$ at the interface AlO(OH)/solution following the mechanism previously described (Figure 11).

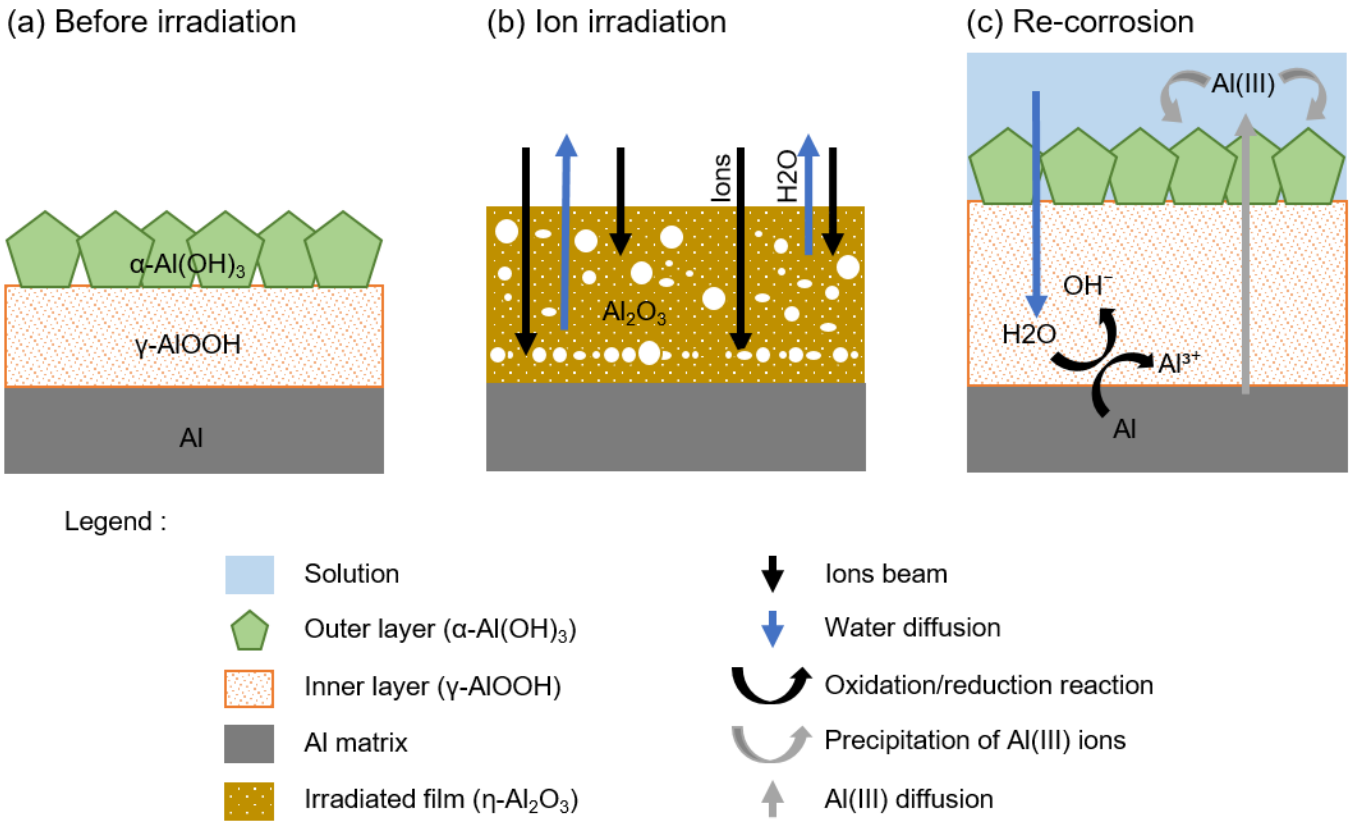

Figure 11: Schematic of the three steps of the proposed mechanisms of aluminium corrosion during corrosion tests coupled with ion irradiation.

5. CONCLUSIONS

In this study, two ion irradiations are performed in order to highlight the effect of ion irradiation on aluminium corrosion. Ion irradiation is performed on an aluminium hydroxide film Before irradiation, this film is composed of three layers: an compact inner layer of boehmite (γ-AlOOH), a thin intermediate layer of needle-like nanocristallites and an outer layer of parallelepiped microcrystals composed of bayerite (α-$Al(OH)_3$). After irradiation, voids are present in the film and a change of microstructure is observed: former cuboid microcrystals become spheroids on the samples surface and the thin intermediate layer is not observed. In addition, ion irradiation causes dehydration of the aluminium hydroxide: nanocrystallites of η-Al_2O_3 are present in all the film. The irradiated samples are then re-corroded. Damage is not observed in the new aluminium hydroxide film and this film is fully rehydrated. However, an effect of ion irradiation persists: ion irradiation increases aluminium corrosion. This observation is attributed to the damages observed in the irradiated film which possibly decrease the passivation properties of the film.

A second ion irradiation is performed on aluminium matrix, on uncorroded samples in 6061-T6 aluminium alloy (Al ions with an energy of 1.8 MeV in order to create at most 14 dpa in the

matrix). This irradiation increases the dislocation density and amorphizes the dispersoids. After irradiation, the samples are corroded. The ion irradiation increases aluminium corrosion. Samples are corroded in the Osiris nuclear reactor (located in CEA Saclay in France), at 42 °C, at a pH of 6 and for 18 months in total. The film has a layered microstructure on the samples surface composed of a brittle inner layer, a thick intermediate layer and an outer layer of cuboid microcrystals. Silicon enrichment is observed in the inner layer, this enrichment is possibly due to the transmutation of aluminium in silicon due to thermal neutron irradiation. Similarities are observed between ion and neutron irradiations: the film has a similar crystalline structure and a similar layered microstructure for the two types of irradiation. In addition, ion and neutron irradiations increase aluminium corrosion and accelerate the aluminium hydroxide growth on the samples surface. Because of these similarities, ion irradiation can be used for corrosion tests in corrosion loops or in autoclave in order to perform parametric studies and ~~still remain relevant~~bring some relevant information on corrosion ~~to the conditions found~~ in MTRs. However, the corrosion mechanisms proposed in this paper apply specifically to ion-irradiation. In particular, ~~However,~~ ion irradiation dehydrates the aluminium hydroxide. This dehydration is one of the limitation of the use of ion irradiation as well a~~i~~s damage flux. As a result, in further studies, ion irradiation coupled to corrosion tests in corrosion loop could be performed in order to increase the application range of the empirical models used in the literature to estimate the thickness of the film depending on the nominal operating conditions of MTRs. Finally, conducting fine TEM characterizations on neutron irradiated samples would be very interesting to observe the particular oxide phases created during irradiation. These studies could be envisioned in future work on this subject.

ACKNOWLEDMENTS

This work received assistance from the “Agence Nationale de la Recherche” program GENESIS referenced as ANR-11-EQPX-0020. The ion irradiation experiments were performed at JANNuS-Saclay (Joint Accelerators for Nanoscience and Nuclear Simulation), CEA Paris-Saclay, France. The nuclear corrosion experiments were performed in the Materials Testing Reactor Osiris, CEA Paris-Saclay, France.

DATA AVAILABILITY STATEMENT

The raw/processed data required to reproduce these findings cannot be shared at this time as the data also forms part of an ongoing study.

REFERENCES

[1] S.J. Pawel, G.L. Yoder, C.D. West, B.H. Montgomery, The development of a preliminary correlation of data on oxide groth on 6061 aluminium under ANS thermal-hydraulic conditions, ORNLTM-11517. (1990).

[2] J.C. Griess, H.C. Savage, T.H. Mauney, J.L. English, Effect of heat flux on the corrosion of aluminium by water. Part I : Experimental equipment and preliminary results, Oak Ridge, TN, USA, 1960.

[3] M. Wintergerst, N. Dacheux, F. Datcharry, E. Herms, B. Kapusta, Corrosion of the AlFeNi alloy used for the fuel cladding in the Jules Horowitz research reactor, J. Nucl. Mater. 393 (2009) 369–380. https://doi.org/10.1016/j.jnucmat.2009.06.003.
[4] C. Vargel, Corrosion de l'aluminium, Dunod, 1999.
[5] A.E. Richt, R.W. Knight, G.M. Adamson, Postirradiation examination and evalution of the performance of HFIR fuel elements, 1971. https://doi.org/10.2172/4698779.
[6] K. Farrell, R.T. King, A. Jostsons, Examination of the irradiated 6061 aluminum HFIR target holder, 1973. https://doi.org/10.2172/4490342.
[7] G.H. Hanson, G.W. Gribson, J.C. Griess, Report of the ANS aluminium cladding corrosion workshop, in: Oak Ridge National Laboratory, Idaho, 1988.
[8] S. Gosmain, Examens par diffraction des rayons X d'échantillons en alliage d'aluminium 6061-T6 provenant du réacteur BR2 de Mol, CEA Saclay, 2005.
[9] B. Kapusta, Synthèse des caractérisations du casier aléolé en AG3-NET irradié de 1966 à 1996 dans Osiris, CEA Saclay, 2006.
[10] D. Nabhan, Etude de la corrosion aqueuse de l'alliage d'aluminium AlFeNi utilisé comme gainage de combustible nucléaire : effet de l'état de surface, du pH et d'une irradiation aux ions, Thèse de doctorat, Collège Doctoral du Languedoc-Rousillon, Université Montpellier 2, 2014.
[11] Y.S. Kim, H.T. Chae, S.V. den Berghe, A. Leenaers, V. Kuzminov, A.M. Yacout, Aluminum cladding oxide growth prediction for high flux research reactors, J. Nucl. Mater. 529 (2020) 151926. https://doi.org/https://doi.org/10.1016/j.jnucmat.2019.151926.
[12] Y.S. Kim, G.L. Hofman, A.B. Robinson, J.L. Snelgrove, N. Hanan, Oxidation of aluminum alloy cladding for research and test reactor fuel, J. Nucl. Mater. 378 (2008) 220–228. https://doi.org/10.1016/j.jnucmat.2008.06.032.
[13] J.C. Griess, H.C. Savage, T.H. Mauney, J.L. English, J.G. Rainwater, Effect of heat flux on the corrosion of aluminium by water. Part II : Influence of water temperature, velocity and pH on corrosion-product formation, Oak Ridge, TN, USA, 1961.
[14] J.C. Griess, H.C. Savage, T.H. Mauney, J.L. English, J.G. Rainwater, Effect of heat flux on the corrosion of aluminium by water. Part III : Final report on tests relative ot the high-flux isotop reactor, Oak Ridge, TN, USA, 1961.
[15] S.J. Pawel, G.L. Yoder, D.K. Felde, B.H. Montgomery, M.T. McFee, The corrosion of 6061 aluminium under heat transfer conditions in the ANS corrosion test loop, Oxid. Met. 36 (1991) 175–194.
[16] S.J. Pawel, D.K. Felde, R.E. Pawel, Influence of coolant pH on corrosion of 6061 aluminium under reactor heat transfer conditions, Oak Ridge, TN, USA, 1995.
[17] J.C. Griess, H.C. Savage, J.L. English, Effect of heat flux on the corrosion of alumnium by water. Part IV : Tests relative to the advanced test reactor and correlation with previous results, Oak Ridge, TN, USA, 1964.
[18] T. Petit, J. Besson, C. Ritter, K. Colas, L. Helfen, T.F. Morgeneyer, Effect of hardening on toughness captured by stress-based damage nucleation in 6061 aluminum alloy, Acta Mater. 180 (2019) 349–365. https://doi.org/10.1016/j.actamat.2019.08.055.
[19] D. Nabhan, B. Kapusta, P. Billaud, K. Colas, D. Hamon, N. Dacheux, Effects of pH, surface finish and thermal treatment on the corrosion of AlFeNi aluminum alloy. Characterization of oxide layers, J. Nucl. Mater. 457 (2015) 196–204. https://doi.org/10.1016/j.jnucmat.2014.10.023.
[20] S. L'Haridon-Quaireau, M. Laot, K. Colas, B. Kapusta, S. Delpech, D. Gosset, Effects of temperature and pH on uniform and pitting corrosion of aluminium alloy 6061-T6 and characterisation of the hydroxide layers, J. Alloys Compd. (2020) 155146. https://doi.org/10.1016/j.jallcom.2020.155146.
[21] J.F. Ziegler, M.D. Ziegler, J.P. Biersack, SRIM – The stopping and range of ions in matter (2010), 19th Int. Conf. Ion Beam Anal. 268 (2010) 1818–1823. https://doi.org/10.1016/j.nimb.2010.02.091.
[22] S.. Zinkle, G.. Pells, Microstructure of Al2O3 and MgAl2O4 irradiated at low temperatures, J. Nucl. Mater. 253 (1998) 120–132. https://doi.org/10.1016/S0022-3115(97)00323-1.
[23] H.H. Neely, W. Bauer, Electron-Irradiation Damage-Rate Measurements in Aluminum, Phys Rev. 149 (1966) 535–539. https://doi.org/10.1103/PhysRev.149.535.
[24] P. Jung, Average atomic-displacement energies of cubic metals, Phys Rev B. 23 (1981) 664–670. https://doi.org/10.1103/PhysRevB.23.664.
[25] F. Rozeblum, Floréal : Résultats et interprétation des mesures obtenues par intégrateurs de dose, CEA Saclay, 2006.

[26] C.J. Doss, R. Zallen, Raman studies of sol-gel alumina: Finite-size effects in nanocrystalliine AlO(OH), Phys Rev B. 48 (1993) 626–637.
[27] H.D. Ruan, R.L. Frost, J.T. Kloprogge, Comparison of Raman spectra in characterizing gibbsite, bayerite, diaspore and boehmite, J. Raman Spectrosc. 32 (2001) 745–750. https://doi.org/10.1002/jrs.736.
[28] D.B. Tilley, R.A. Eggleton, The Natural Occurrence of Eta-Alumina (eta-Al2O3) in Bauxite, Clays Clay Miner. 44 (1996). http://explore.bl.uk/primo_library/libweb/action/display.do?tabs=detailsTab&gathStatTab=true&ct=display&fn=search&doc=ETOCRN613373549&indx=1&recIds=ETOCRN017880329 (accessed January 14, 2019).
[29] K. Wefers, C. Misra, Oxides and hydroxides of aluminium, ALCOA Laboratories, 1987.
[30] Y. Chen, J. Hyldtoft, C.J.. Jacobsen, O.F. Nielsen, NIR FT Raman spectroscopic studies of η-Al2O3 and Mo/η-Al2O3 catalysts, Spectrochim. Acta. A. Mol. Biomol. Spectrosc. 51 (1995) 2161–2169. https://doi.org/10.1016/0584-8539(95)01495-4.
[31] J. Aad, Dégradation chimique et mécanique de l'alumine en phase aqueuse : mécanisme et inhibition en conditions ambiantes et hydrothermales, Thèse de doctorat, Université pierre et Marie Curie - Paris VI, 2016. https://tel.archives-ouvertes.fr/tel-01913067/document.
[32] V. Garric, Etude du gonflement par cavités d'un alliage d'aluminium irradié sous faiseau d'ions, Thèse de doctorat, Université Grenoble Alpes, 2019.
[33] C. Flament, J. Ribis, J. Garnier, T. Vandenberghe, J. Henry, A. Deschamps, Electron irradiation-enhanced core/shell organization of Al(Cr, Fe, Mn)Si dispersoids in Al–Mg–Si alloys, Philos. Mag. 95 (2015) 1–12. https://doi.org/10.1080/14786435.2015.1009959.
[34] Y. Shen, Comportement et endommagement des alliages d'aluminium 6061-T6 : approche micrométrique, Thèse de doctorat, Ecole Nationale Supérieure des Mines de Paris, 2012.
[35] M. Tupin, R. Verlet, K. Colas, M. Jublot, G. Baldacchino, K. Wolski, Effect of ion irradiation of the metal matrix on the oxidation rate of Zircaloy-4, Corros. Sci. 136 (2018) 28–37. https://doi.org/ ~~https://doi.org/~~10.1016/j.corsci.2018.02.023.
[36] C. Flament, J. Ribis, J. Garnier, Y. Serruys, F. Leprêtre, A. Gentils, C. Baumier, M. Descoins, D. Mangelinck, A. Lopez, K. Colas, K. Buchanan, P. Donnadieu, A. Deschamps, Stability of β″ nano-phases in Al-Mg-Si(-Cu) alloy under high dose ion irradiation, Acta Mater. 128 (2017) 64–76. https://doi.org/10.1016/j.actamat.2017.01.044.
[37] D. Zuili, Comportement en corrosion des alliages d'aluminium des séries 5000 et 6000 sous flux de neutrons, CEA Saclay, Saclay, 2000.
[38] B. Kapusta, RCC-MX - Annexe X3.1A et X3.2A, CEA Saclay, Saclay, 2005.
[39] M. Wintergerst, Etude des mécanismes et des cinétiques de corrosion aqueuse de l'alliage d'aluminium AlFeNi utilisé comme gainage du combustible nucléaire de réacteurs expérimentaux., Thèse de doctorat, Université Paris XI, U.F.R Scientifique d'orsay, 2010.
[40] M. Pourbaix, Atlas d'équilibres électrochimiques, Villars, 1963.
[41] S. Cathalau, R. Mombellet, A. Vivet, P. Schindler, Programme expérimental erosion/corrosion de l'aluminium 6061-T6 pour le RJH, résultats de la 3ème et 4ème phase de 2000 heures et synthèse de l'essai 6, CEA Cadarache, 2009.
[42] R.K. Hart, The formation of films on aluminium immersed in water, Trans Faraday Soc. 53 (1956) 1020–1025.
[43] J. Liu, A.H. Mir, G. He, M. Danaye, J. Hinks, S. Donnelly, H. Nordin, S. Lozano-Perez, C. R.M. Grovenor, In-situ TEM study of irradiation-induced damage-mechanisms in monoclinic ZrO_2, Acta Materialia 199 (2020) 429-442 https://doi.org/10.1016/j.actamat.2020.08.064.

Figure captions:

Fig. 1: Purpose, step and conditions of irradiation of the three studies performed in this paper.

Fig. 2: Damage profiles (dpa: displacement per atom) created by (a) Al ions with successive energies of 5 MeV and then 1.2 MeV irradiating the aluminium hydroxide film and by (b) Al ions with an energy of 1.8 MeV irradiating the aluminium matrix, profiles calculated by SRIM with the mode "full damage cascade" [21].

Fig. 3: TEM micrographs of (a) a unirradiated film of aluminium hydroxide (obtained on samples corroded at 70°C, in 2.8L of demineralised water and for 7 days), (b) a film irradiated with Al ions of successive energies 5 MeV then 1.2 MeV.

Fig. 4: SEM micrographs of the samples surface: (a) unirradiated (obtained on samples corroded at 70°C, in 2.8L of demineralised water and for 7 days) and (b) irradiated with Al ions of successive energies 5 MeV then 1.2 MeV.

Fig. 5: (a) SAED pattern obtained on the film irradiated with Al ions of successive energies 5 MeV then 1.2 MeV (the planes corresponding to the d-spacing come from [28,29]) and (b) Dark Field micrograph of the nanocrystallites which have diffracted in the red circle in Fig 5.a(TEM).

Fig. 6: (a) Average thickness of the aluminium hydroxide film and (b) average mass gain of the samples unirradiated and irradiated with Al ions of successive energies 5 MeV then 1.2 MeV (the term “irradiation” on the graphics indicates when the ion irradiation occurs).

Fig. 7: TEM micrographs of (a) an unirradiated matrix of 6061-T6 aluminium alloy and (b) irradiated matrix with Al ions of 1.8 MeV. The areas ❶ and ❷ correspond respectively to the area irradiated at 1-5 dpa (displacement per atom) and to the most irradiated area at 8 dpa.

Fig. 8: TEM micrographs: dispersoid observed in the unirradiated matrix from two different tilt angles: (a) α=0° and (b) α=10°, and two dispersoids observed in the matrix irradiated at 14 dpa from two different tilt angles: (c) α=0° and (d) α=10°.

Fig. 9: SEM micrographs of (a) the film obtained on sample corroded for 560 days at pH 6 and at 42°C in the reactor Osiris and zoom on (b) the outer and intermediate layers and on (c) the intermediate and inner layers.

Fig. 10: Chemical evolution of magnesium and silicon by EMPA in the aluminium matrix and in the aluminium hydroxide film obtained on a sample corroded for 560 days at pH 6 and at 42°C in the Osiris reactor.

Fig. 11: Schematic of the three steps of the proposed mechanisms of aluminium corrosion during corrosion tests coupled with ion irradiation.

Figure 1

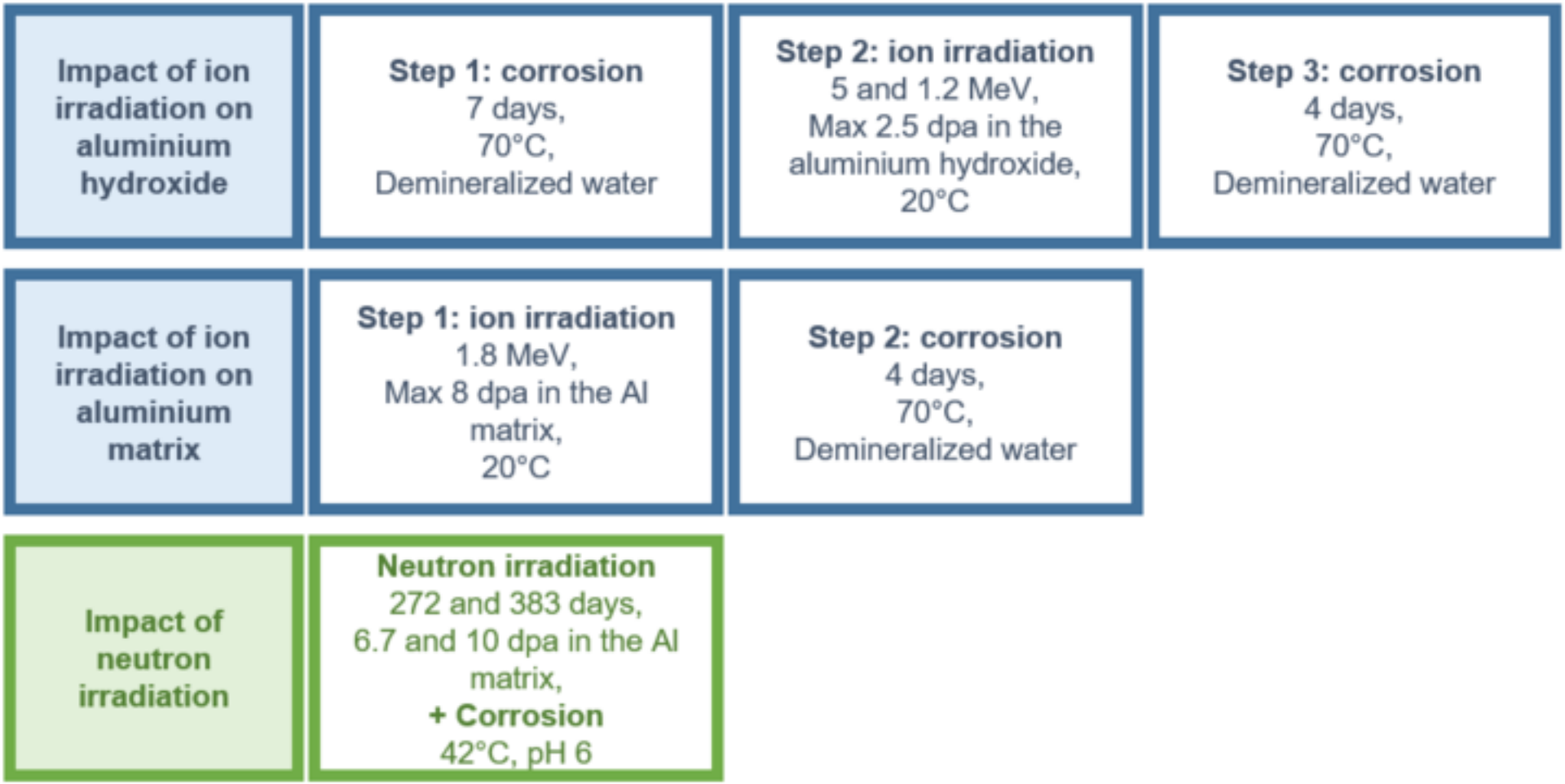

Figure 2

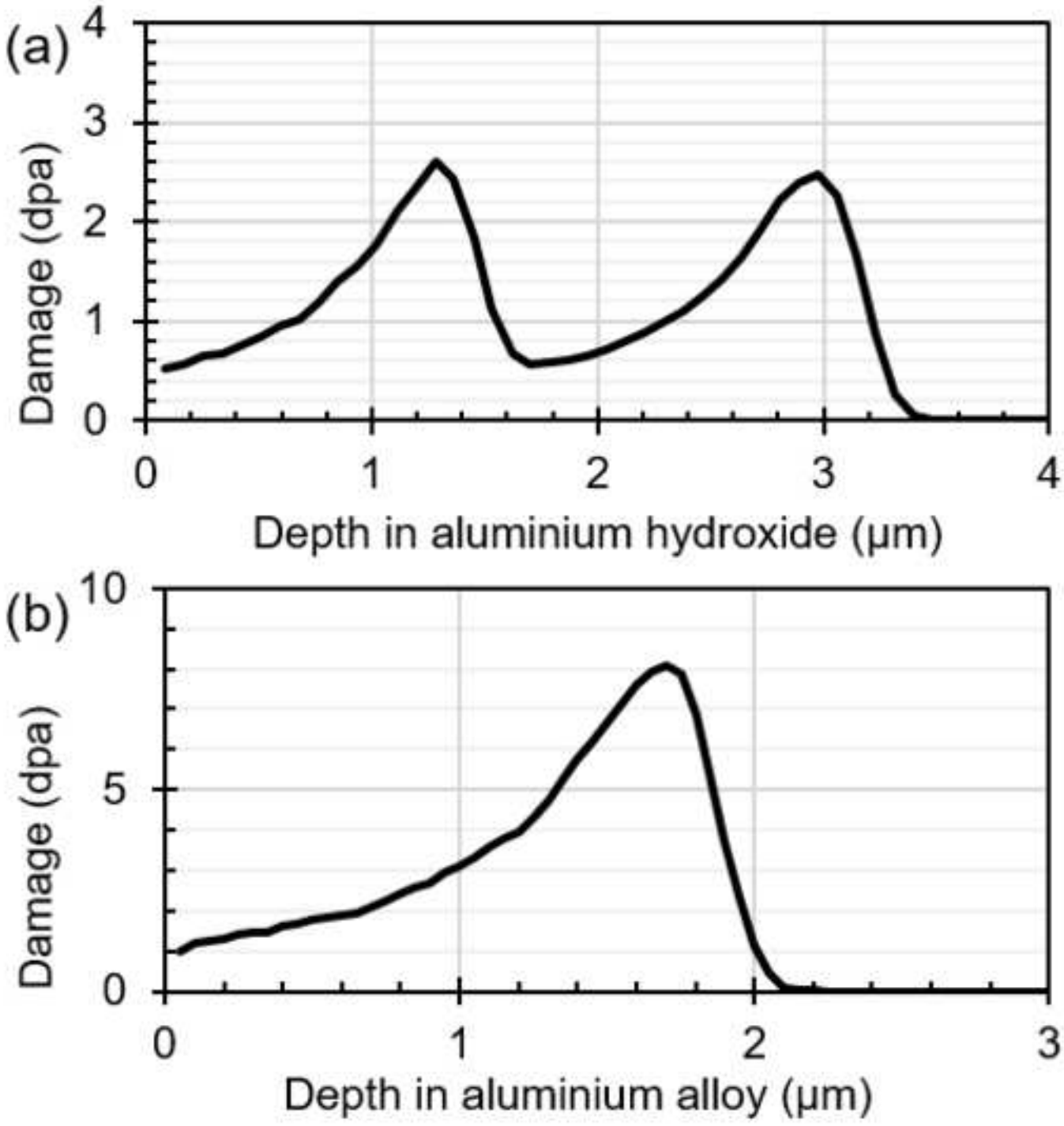

Figure 3

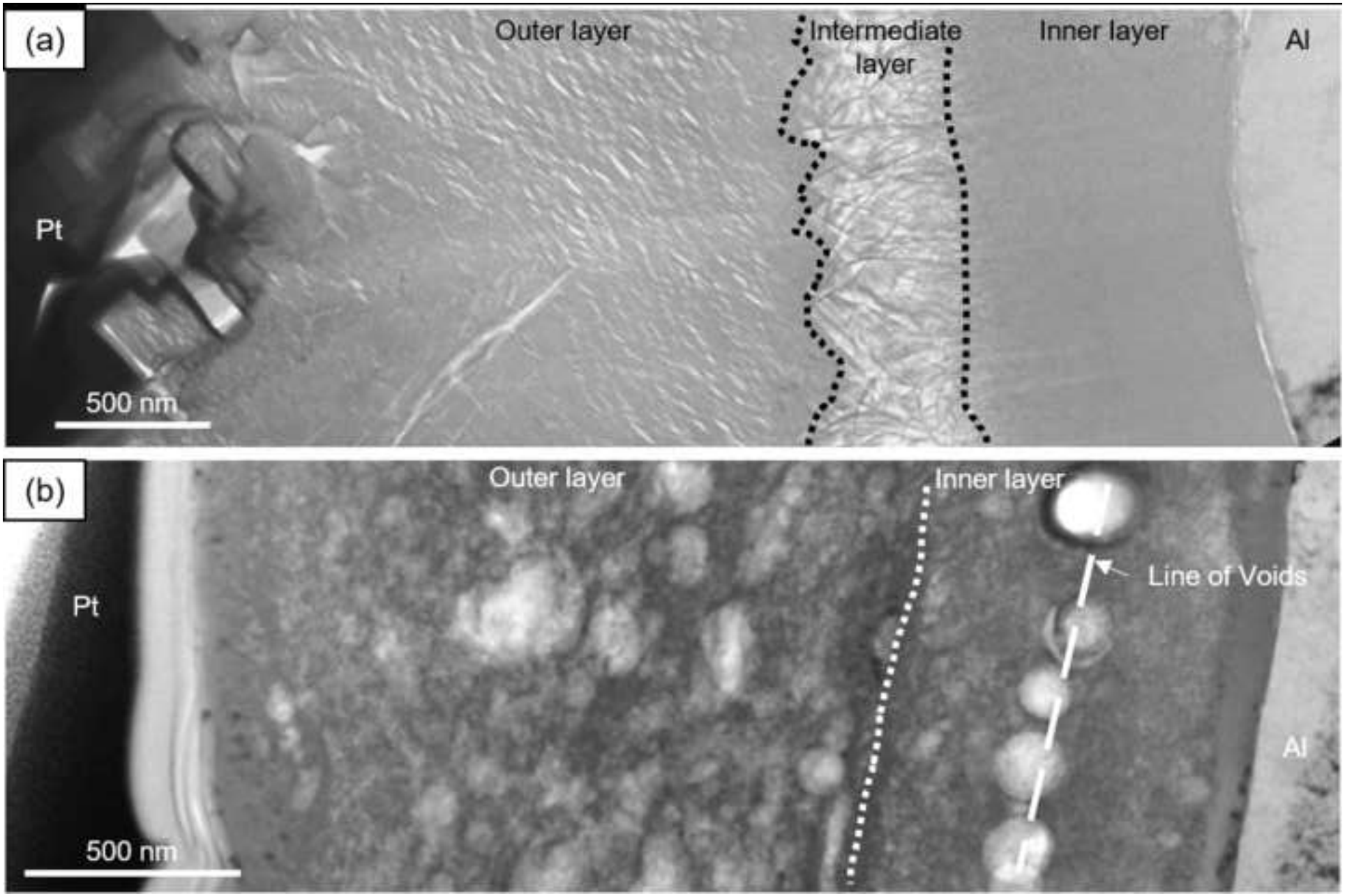

Figure 4

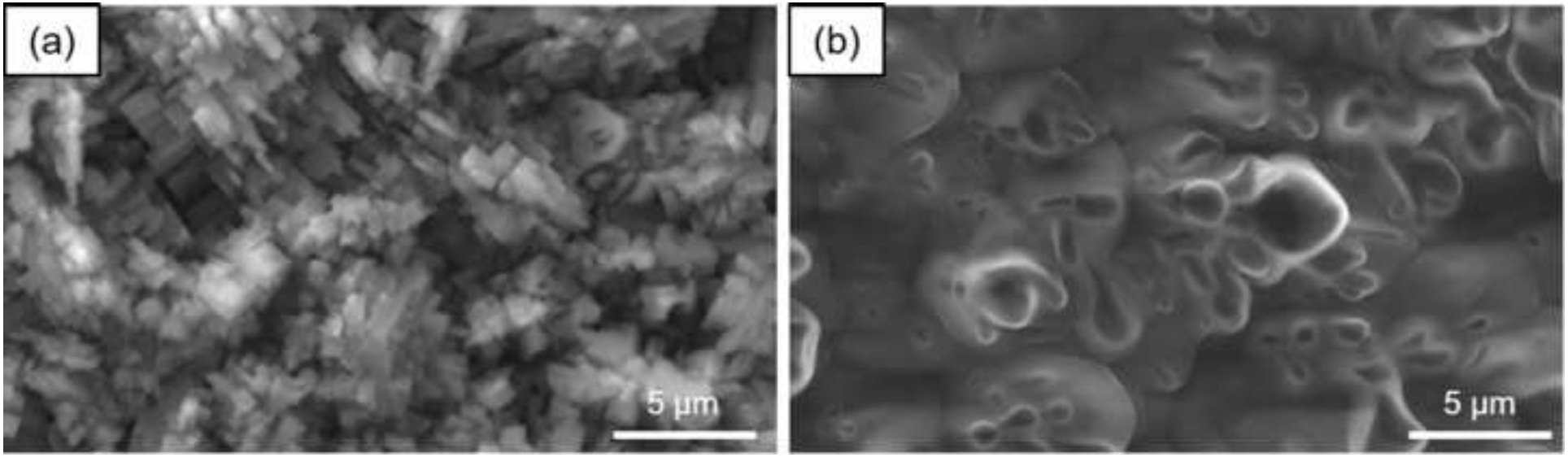

Figure 5

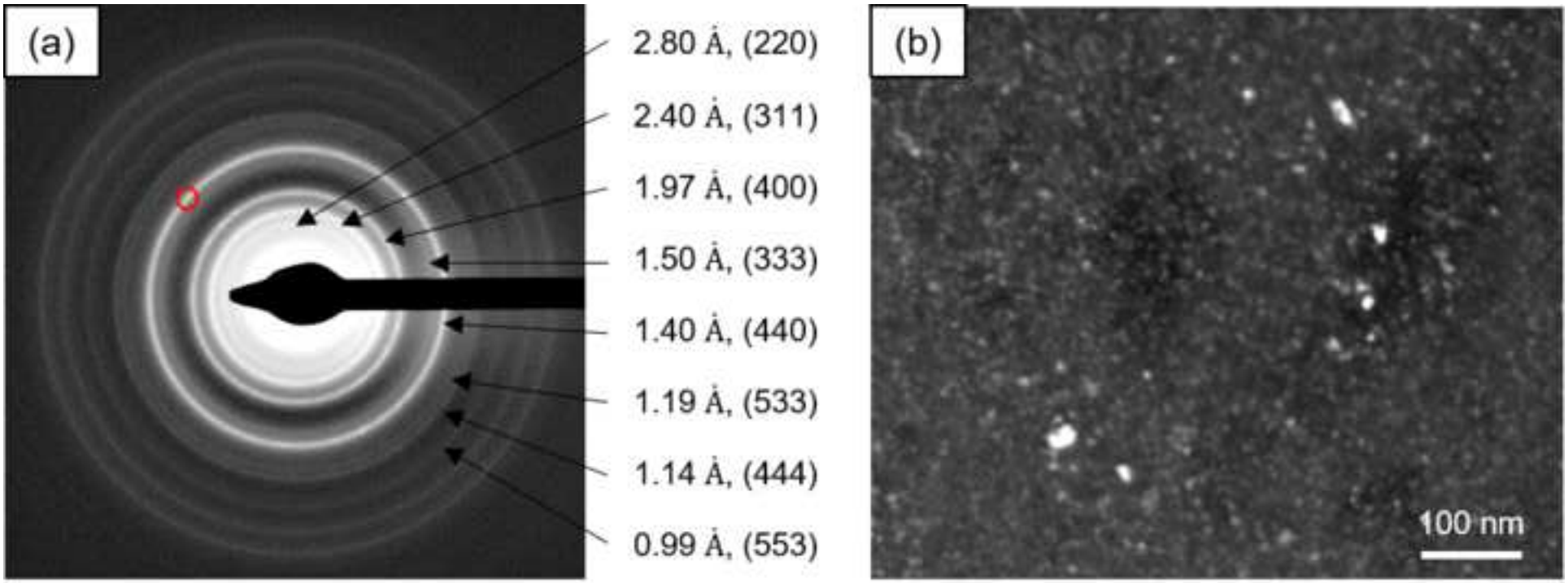

Figure 6

Click here to access/download;Figure;FIG6.tif

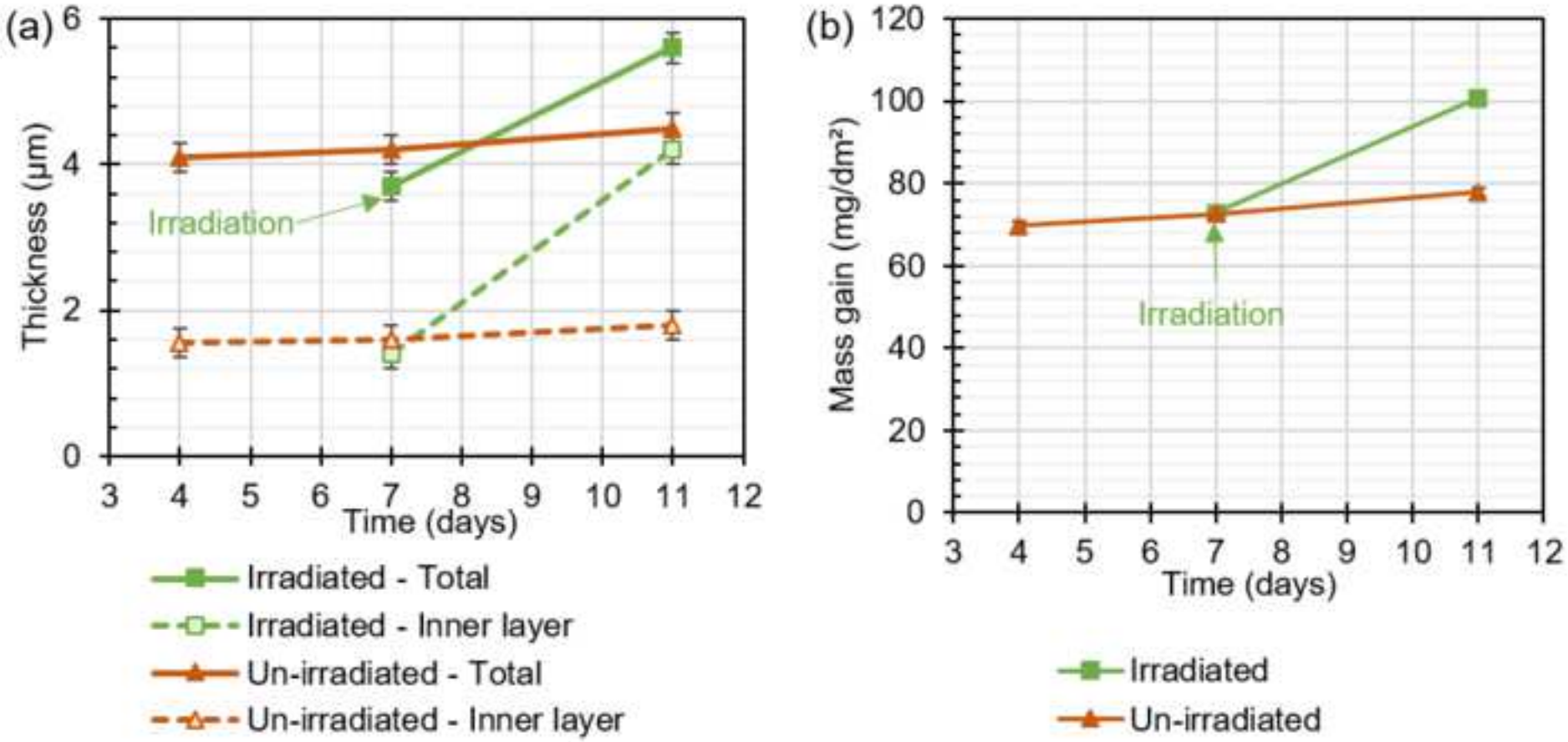

Figure 7

Click here to access/download;Figure;FIG7.tif

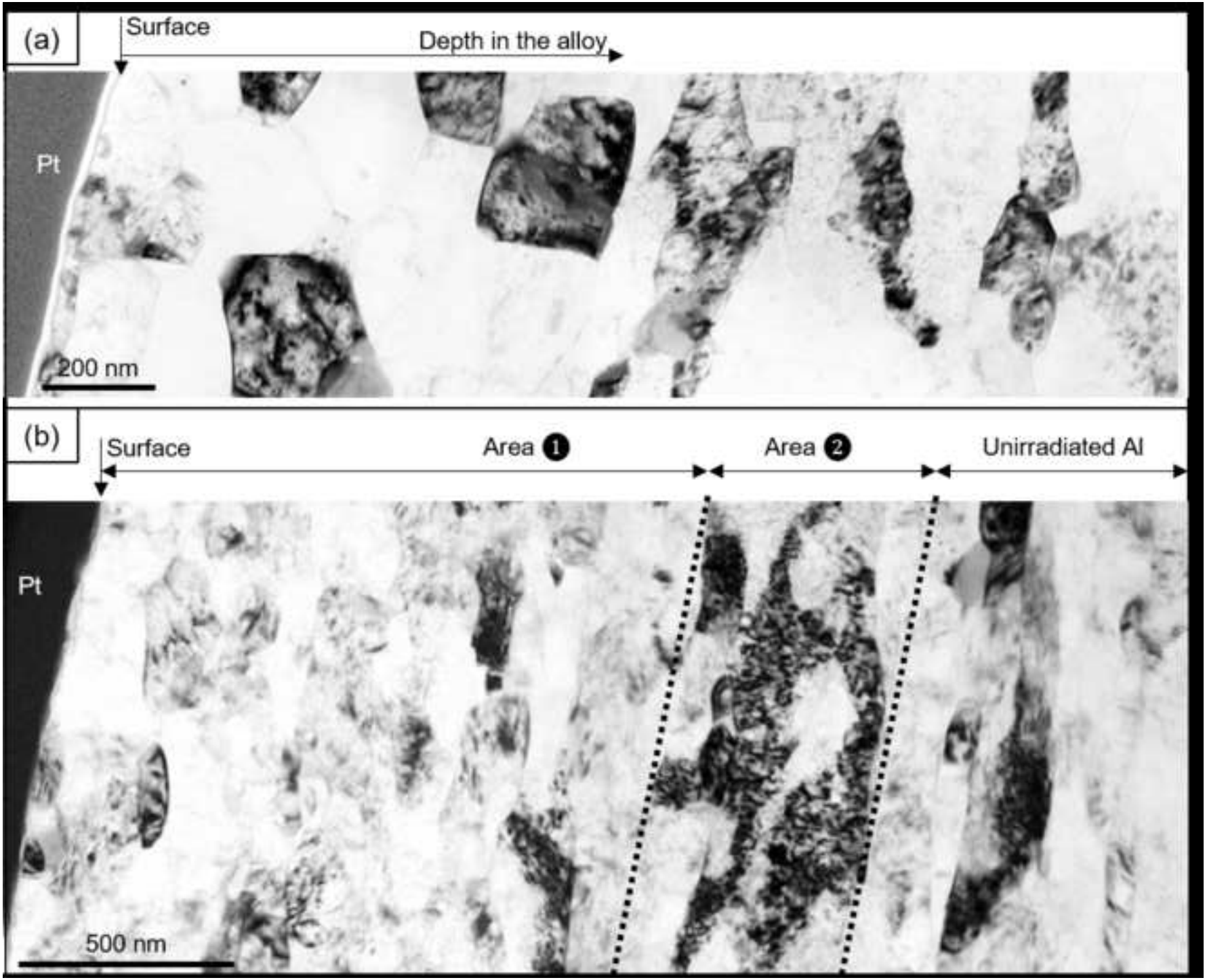

Figure 8

Click here to access/download;Figure;FIG8.tif

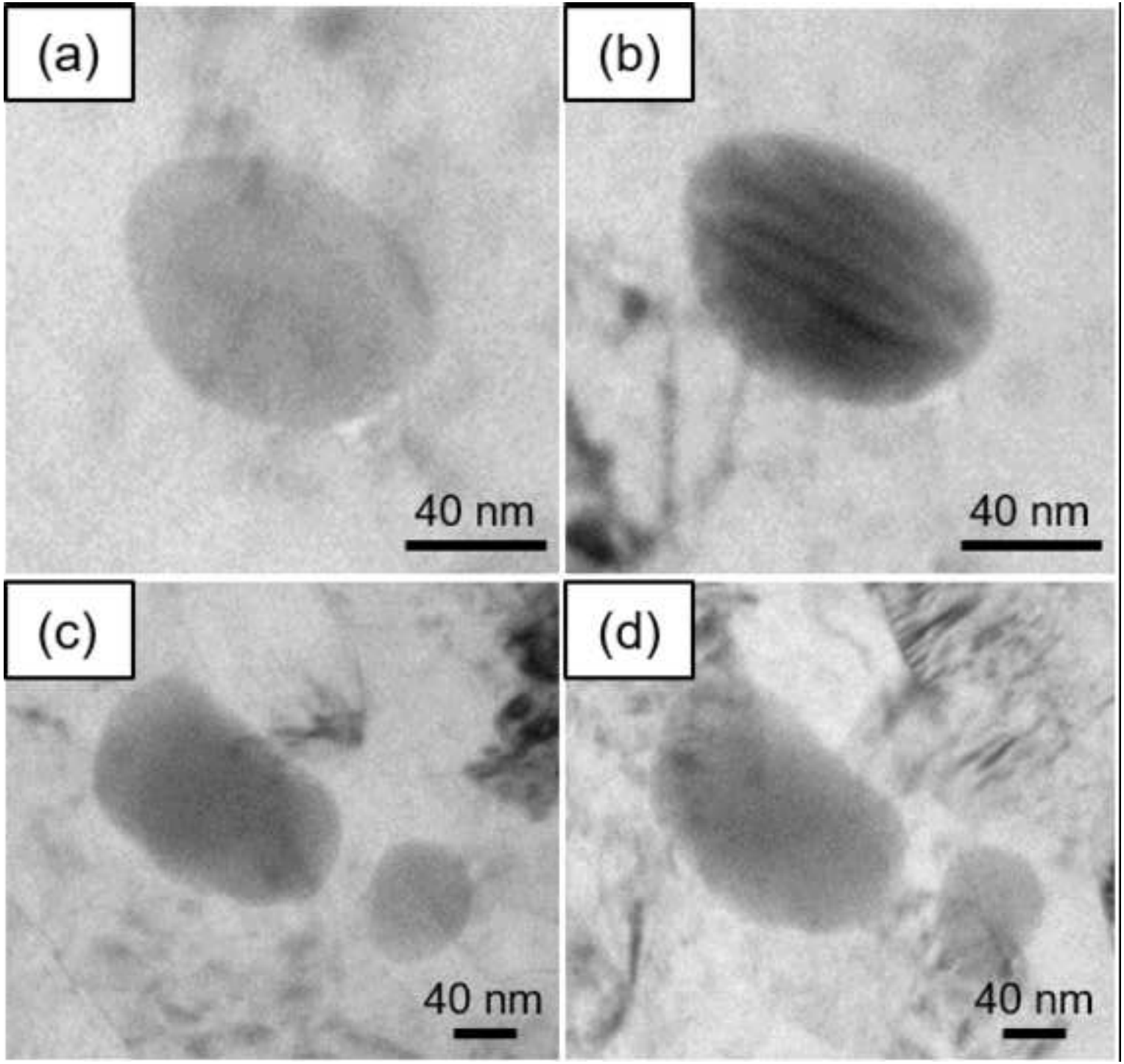

Figure 9

Click here to access/download;Figure;FIG9.tif

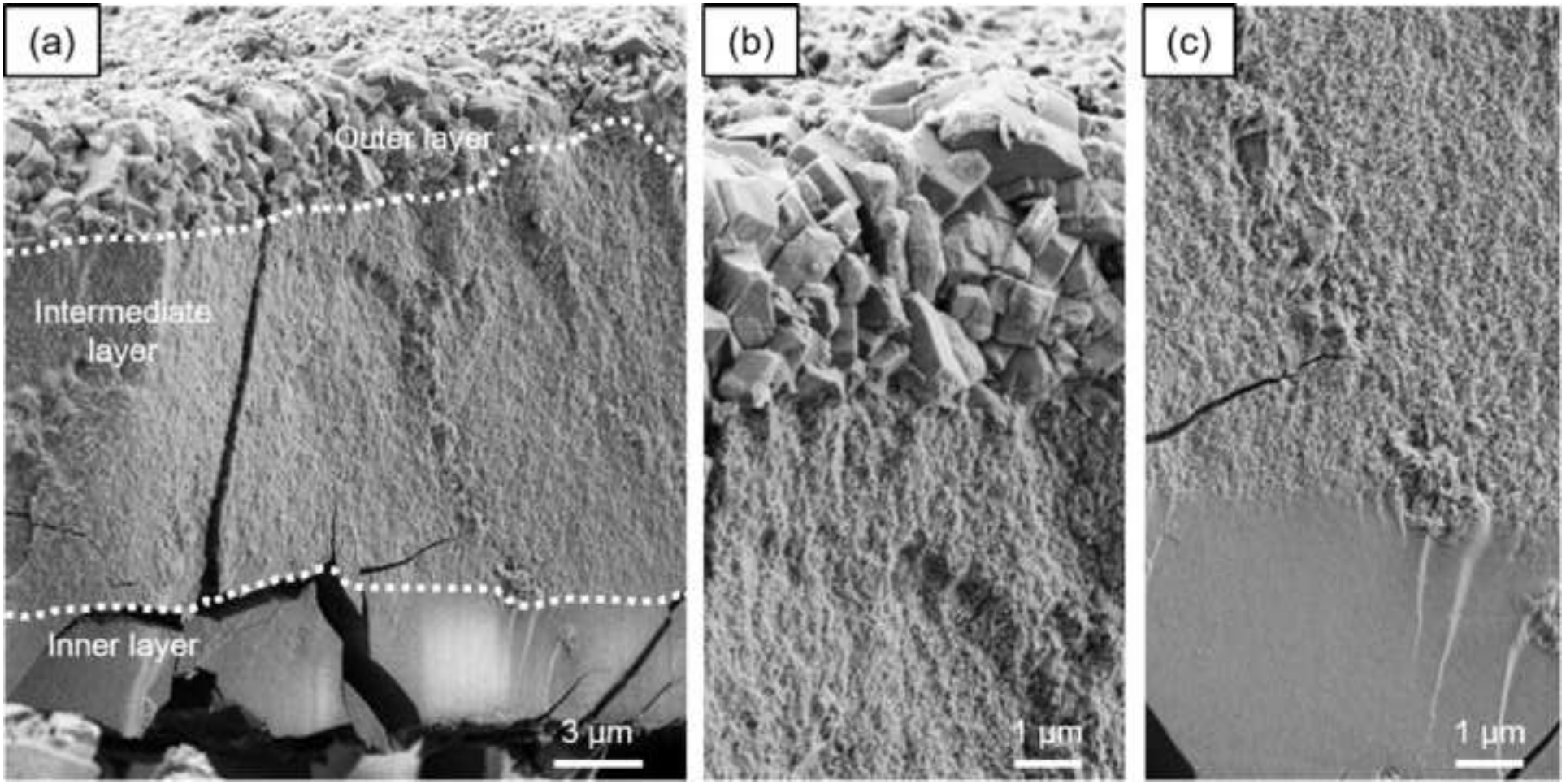

Figure 10

Click here to access/download;Figure;FIG10.tif

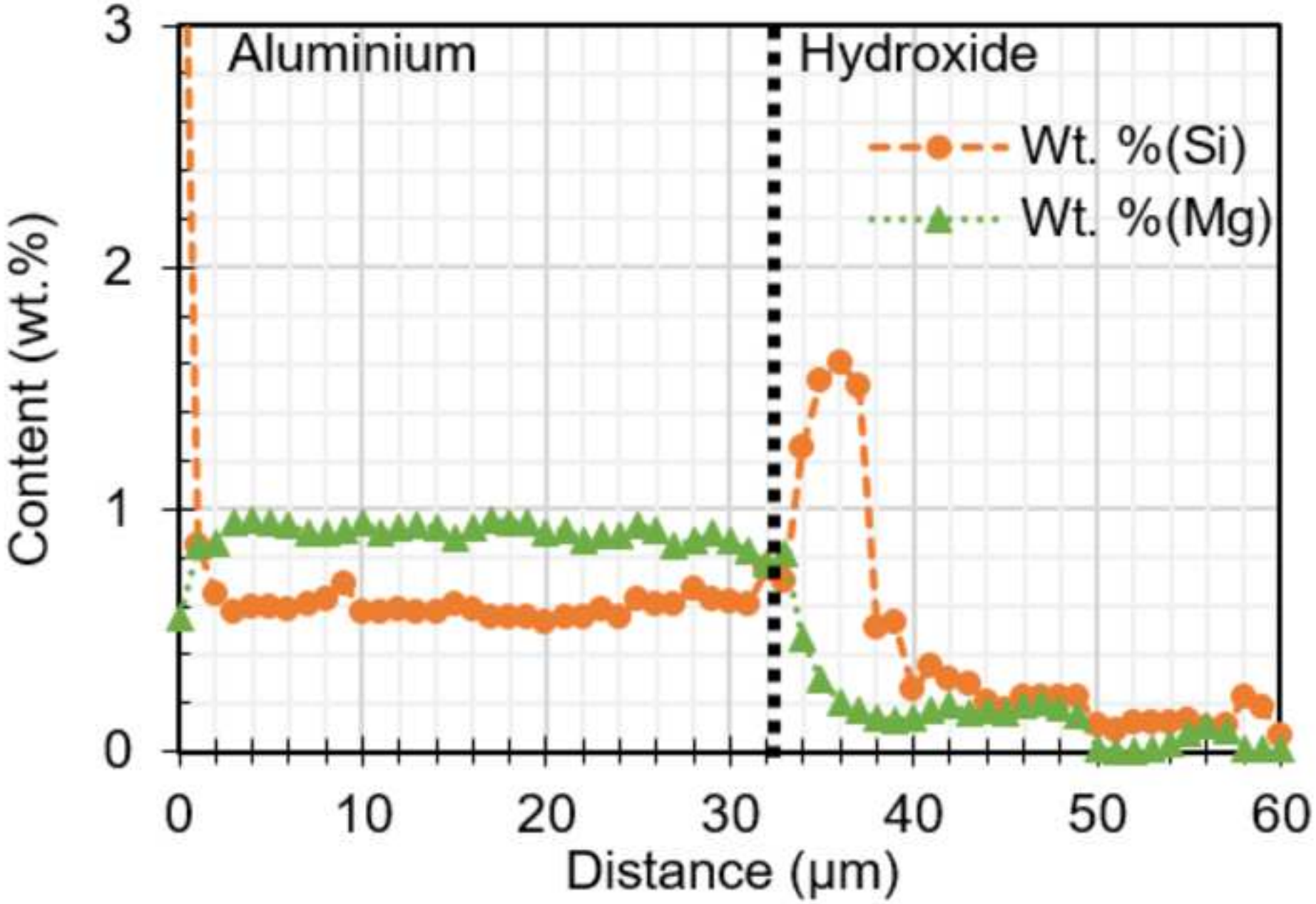

Figure 11

Click here to access/download;Figure;FIG11.tif

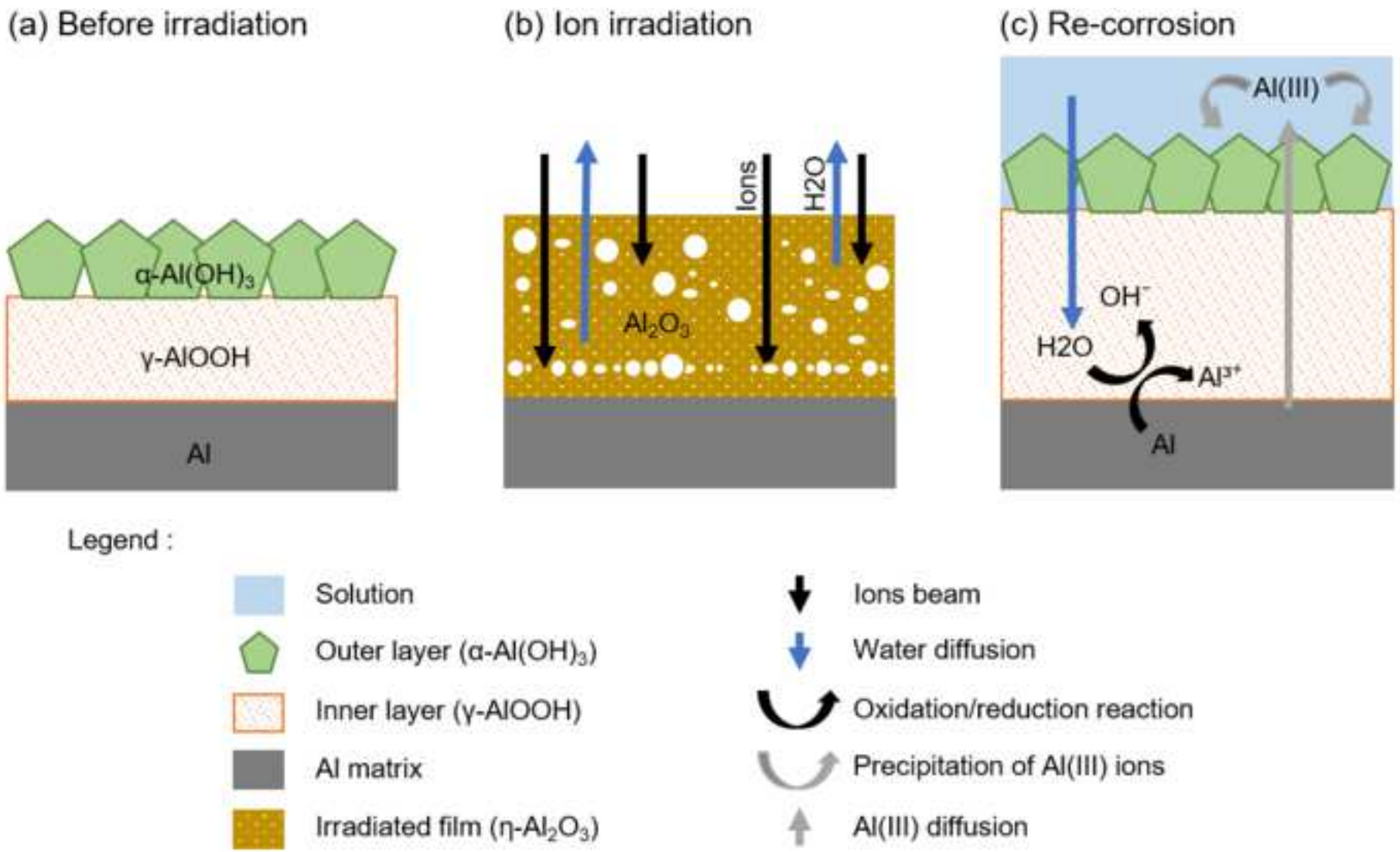

Credit Author Statement

Sarah L'HARIDON-QUAIREAU: Investigation, Methodology, Conceptualization, Writing – original draft, Review and editing

Kimberly COLAS : Supervision, Methodology, Conceptualization, Validation, Review and editing

Bénédicte KAPUSTA: Supervision, Funding acquisition, Project administration, Review and editing

Dominique GOSSET, Bénédicte VERHAEGHE, Marie LOYER-PROST and Gaëlle GUTIERREZ: Methodology,

Sylvie DELPECH: Supervision, Validation, Conceptualization, Review and editing

Declaration of interests

☒ The authors declare that they have no known competing financial interests or personal relationships that could have appeared to influence the work reported in this paper.

☐The authors declare the following financial interests/personal relationships which may be considered as potential competing interests:

Click here to access/download

Supplementary File

Supplementary_data.docx